Lattice Gauge Theoretic Analysis of Topological Ordering in the Majorana Toric Code

Master's Thesis

Submitted to the Faculty of Mathematics, Computer Science
and Natural Sciences at RWTH Aachen University

presented by

Alexander Ziesen

under the supervision of

Prof. Dr. Fabian Hassler
and
Prof. Dr. David DiVincenzo
JARA Institute for Quantum Information, RWTH Aachen University

March, 2019

Abstract

In this thesis, we consider a two dimensional square lattice of mesoscopic superconducting islands carrying four Majorana zero modes (MZM), each. We consider the islands to form an array of Josephson junctions, where the MZM allow for additional inter-island single electron transfer. This model is known to realise topological order in the form of Kitaev's toric code. With a calculation of the effective Hamiltonian, we prove that the presence of charge-2e Josephson tunnelling has a stabilising effect on the toric code gap. In previous works, the charge signatures of the phase diagram as well as the types of transition lines were investigated. The goal of this thesis is to investigate the signatures of topological ordering. To this end, we introduce a duality mapping of the MZM to spins yielding a lattice gauge theory of $U(1)$ matter parity coupled to an emergent $\mathbb{Z}_2$ gauge field and shift the focus from the matter to the gauge perspective. In this form, we can utilise the equal time formulation of the Fredenhagen-Marcu order parameter, a generalised Wilson loop, to detect the topological signatures and give an intuitive picture of (open) loop condensation to understand the topological phase transition.

Contents

List of Figures

Chapter 1

Introduction

Quantum information is a relatively young field of not only physics, which gained a lot of interest since 1994, when an integer factorisation algorithm was proposed by Shor [1]. This algorithm, if run on a working quantum computer, could solve the prime factoring of large integers in polynomial time. The fact that the latter is impossible to achieve on a classical computer, however, is a central assumption to the RSA (Rivest-Shamir-Adleman) scheme for public key encryption, which is nowadays widely used for secure communication [2]. In other words, a working quantum computer could render the current encryption standards obsolete.

To this day, a commercially usable quantum computer has yet to be built. The elementary building blocks are the qubits, purely quantum mechanical two-level systems. The increased computational power of qubits stems from their abilities to be in a superposition state and entangle with each other. These states are extremely fragile. Therefore, additionally to noise, they suffer from quantum decoherence. The latter phenomenon is completely absent for their classical counterparts, the bits. In attempts to overcome this issue various different qubit platforms, for example spin [3] and superconducting qubits [4, 5], have been proposed over the years as well as quantum error correction schemes as stabiliser codes [6] have been developed. In this thesis, we concern ourselves with the system called Majorana toric code. A stabiliser code based on Majorana qubits, where the logical qubit states are topologically different. An experimentally more practical version, the surface code, has potential applications as quantum memory [7]. Therefore, gaining deep physical understanding of this specific code might take us one step closer to the realisation of quantum computers.

To this end, Chapter 2 provides an introduction to the basic concepts involved in this thesis. We start with a discussion of the toric code, proposed by Kitaev in 1997 [8], and in particular construct the topologically protected ground states, the logical qubit states. We will learn that there are many physical qubits needed to encode a logical qubit. The

chosen realisation for physical qubits is based on Majorana zero modes. As one of many instances validating Anderson's famous remark „More Is Different" [9], the Majorana zero modes are found to be quasi particles arising from the collective behaviour of a many-electron system. A physical qubit is then encoded through the occupancy of such a mode.

In Chapter 3 we follow an idea originating in Ref. [10] to realise the toric code using a two dimensional lattice of Majorana qubits, the so called Majorana toric code. The phase diagram of the system is discussed, for which the charge signatures and phase transitions are already well established [10–13]. Additionally, the aforementioned toric code was found in certain limiting regimes of the phases [11, 14], indicating additional topological ordering. In this thesis, we thus want to gain insight into the topological signatures of the different phases. Therefore, we perform a duality mapping of the microscopic model onto a lattice gauge theory of U(1) matter and emergent $\mathbb{Z}_2$ gauge fields, thereby enabling the use of lattice gauge order parameters to detect the desired signatures.

The ordering is then finally analysed in Chapter 4. We show the emergence of the toric code in an effective Hamiltonian calculation, in which we furthermore investigate mechanisms stabilising the topological properties in the presence of Josephson tunnelling. Afterwards, we work our way through basic lattice gauge models and their order parameters. We discuss a pure gauge theory with the non-local Wilson loop order parameter [15] linked to the potential of external static matter charges. The findings are then generalised to the Fredenhagen-Marcu order parameter [16] probing the existence of free charges in a system containing also dynamical matter. The latter is then proven to be a proper order parameter in the lattice gauge theory derived in Chapter 3.

With the evaluation of the Fredenhagen-Marcu order parameter, we are then in a position to interpret the topological ordering with the condensation of open loops in the system. Thus, we provide an order parameter that can diagnose the topological signatures throughout the phase diagram and furthermore give an intuitive picture for the underlying mechanisms. The thesis then ends with a brief conclusion and outlook on possible future directions of research following up on the presented work.

Chapter 2

Basic Concepts

Before we start investigating the model of the Majorana toric code (MTC), we first have to understand the two core concepts involved. On one hand this is the Majorana zero mode and on the other hand Kitaev's toric code. This chapter is devoted to provide a brief introduction to both topics to the degree that is necessary for the remainder of the thesis.

2.1 Toric code

One essential step to achieve the goal of scalable quantum computation is to develop a scheme that prohibits errors from corrupting the logical information of the processor. In classical computation, the simplest idea to protect against logical errors is based on redundant coding. As an example, a logical bit 0 can be copied and encoded into three physical bits as (000). If a bit-flip error occurs on one of the three physical bits, resulting e.g. in (010), one can measure all physical bits and correct the bit-flip according to the outcome of a majority voting. This idea cannot be transferred to quantum computation. The linearity constraint contradicts the existence of a perfect cloning operator on a Hilbert space. This is known as the No-Cloning theorem of quantum information [17,18]. Thus, there is the need for alternative concepts of error correction. A proposition for such a quantum error correction scheme using the idea of redundant encoding is the toric code [8], a representative of the class of stabiliser codes [6]. To understand the properties of the toric code, we consider a two dimensional square lattice with periodic boundary conditions (PBC) as depicted in Fig. 2.1.

In this setup, spin-1/2 degrees of freedom σ_{ij} are placed in the center of each link of a 2D square lattice. The corresponding measurement operators are the Pauli operators $\sigma^z_{ij}, \sigma^y_{ij}, \sigma^x_{ij}$, where i and j label neighbouring nodes. They square to one, e.g. ${\sigma^z_{ij}}^2 = 1$, satisfy $\left\{\sigma^\alpha_{ij}, \sigma^\beta_{ij}\right\} = 0$ if $\alpha \neq \beta$ and commute otherwise (for $\alpha, \beta \in \{x, y, z\}$). From here on, we take the spins to be the physical qubits. Assuming that the total number of qubits

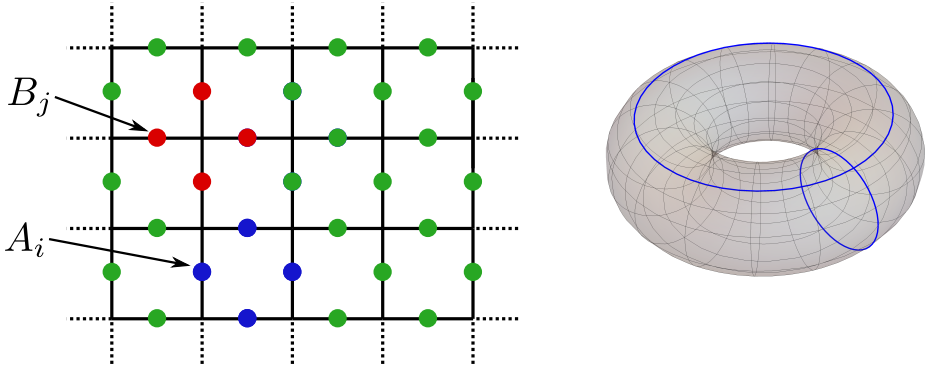

(a) Stabilisers of the toric code (b) Non-contractible loops

Figure 2.1: Schematic of the logicals and stabilisers of the toric code. In (*a*), a two dimensional square lattice is depicted, where a spin-1/2 degree of freedom (green) is placed centrally on each of the links. A representative of each subgroup of stabilisers, A_i (blue) as a plaquette operation and B_j (red) as a star operation, is visualised explicitly. Image (*b*) shows the two dimensional lattice with periodic boundary conditions, a torus. The two non-contractible loops related to the logical states of the toric code are highlighted in blue.

is n this gives a Hilbert space dimension of 2^n. The stabilisers of this code are given by

$$A_i = \prod_{\square_i} \sigma^z \qquad \text{and} \qquad B_j = \prod_{+_j} \sigma^x \,. \tag{2.1}$$

The stabilisers are visualised in Fig. 2.1(a). In the following we will refer to the A_i as plaquette and the B_j as star operators due to their respective geometric shapes. The plaquettes are labelled according to the lower left node, whilst the star index matches the central node. In the 2D square lattice i, j run over all lattice sites. For clarity, the indices at the plaquette and star are omitted in the following. The set of stabilisers commutes and the code space is determined as the $+1$ eigenspace of all independent stabilisers. With the constraints $\prod_i A_i = \prod_i B_i = \mathbf{1}$, as each Pauli operator squares out, we have $2n - 2$ independent stabilisers. Thus, we obtain that the toric code possesses a four $(2^n/2^{n-2})$ dimensional code space [6]. Thus, one can encode two logical qubits. A lot of work has been done regarding error correction schemes involving additional ancilla qubits and the determination of error correction thresholds of the code [19]. In this work, we focus more on the properties of the different states of the code space. To this end, we turn to the Hamiltonian formulation of the toric code [8]. For stabiliser codes this reformulation is achieved with the following recipe: The Hamiltonian is constructed by the linear combination of all stabilisers. Since the code space is the $+1$ eigenspace of the stabilisers, one chooses all coefficients negative. Thus, the code space coincides with the

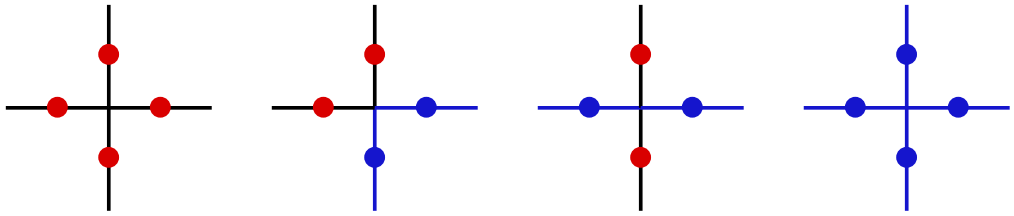

Figure 2.2: Allowed node configurations that satisfy $\prod_+ \sigma^x = 1$. We focus on a specific node, where the adjacent spins are displayed in the x-basis. The colors red/blue indicate the spin σ_{ij} to be in the $+1/-1$ eigenstate of σ^x_{ij}. To be valid, the configuration needs to contain an even number of -1 eigenstates. To obtain the complete set, the four (two) possible rotations of the second (third) graph have to be considered as well.

ground state space of that Hamiltonian. Through this, one obtains

$$H_{TC} = -\sum_i A_i - \sum_i B_i = -\sum_i \prod_{\square} \sigma^z - \sum_i \prod_{+} \sigma^x \,, \tag{2.2}$$

which has a four-fold degenerate ground state. To get an intuitive understanding of the ground states, we follow an idea laid out in Ref. [20]. A ground state has to satisfy $\prod_+ \sigma^x = 1$ at each node of the lattice. In the x-basis all the valid configurations are given in Fig. 2.2.

We see that all spins could be in the $+1$ eigenstate of σ^x or an even number of spins is in the -1 eigenstate. By coloring the links associated with spins of the latter eigenvalue in blue, we can see that if we consider the lattice as a whole, those blue lines have to form closed loops in order to result in a valid configuration. We can therefore write the allowed states as superposition of closed loops

$$|\tilde{G}\rangle = \sum_{s\in\mathcal{S}} w_s \, |s\rangle \ , \tag{2.3}$$

with arbitrary weights w_s. The set $\mathcal{S}$ denotes all allowed loop configurations. If we apply a plaquette operator A_i in the x-basis, it flips all the spins around that plaquette. In the ground state, we need $|\tilde{G}\rangle$ to also be in the $+1$ eigenstate of all individual A_i, which can only be achieved by taking the equal weight superposition

$$|G\rangle = \sum_{s\in\mathcal{S}} w \, |s\rangle \ . \tag{2.4}$$

Therefore, we can intuitively picture that the ground states of the toric code are loop condensates, where all loop configurations are equally likely [20]. An explicit way of writing the ground states is

$$|G\rangle = \prod_i \frac{1}{\sqrt{2}} \left(\mathbf{1} + A_i\right) |0\rangle \ , \tag{2.5}$$

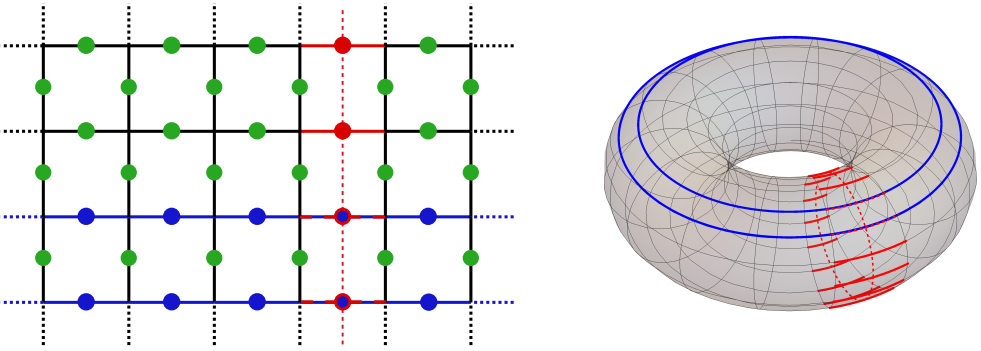

(a) (b)

Figure 2.3: Pair of logical operators of the toric code. In panel (a), we see that in a product of adjacent plaquette operators A_i the shared spins are unaffected as the Pauli operators square out. This leaves two parallel lines of σ^z operators (blue). If such a chain of plaquette operators is wrapped around the torus, we end up with two parallel non-contractible loops of σ^zs as shown in (b). A single one of those is a logical Z operator. The respective logical X (red) is given by a product of σ^x along a NC curve on the dual lattice.

where $|0\rangle$ is the state where all spins are in the $\sigma^x = 1$ eigenstate and $\sqrt{2}$ is the normalisation factor. The construction above holds for all states in the ground state space. In order to distinguish the ground states, we have to look at the non-contractible (NC) loops exemplary shown in Fig. 2.1(b). If we consider the product of plaquette operators A_i wrapping once around the torus, this results in two parallel loops of σ^z operators as shown in Fig. 2.3.

So being in the x-basis, we can only add or remove an even number of NC loops of $\sigma^x = -1$ eigenvalued spins by applying plaquette operators. Revisiting the above construction of $|G\rangle$, we realise that it keeps the parity of the number of NC loops invariant. Thus, the ground state $|G\rangle$ inherits the number of NC loops from the initial state $|0\rangle$. As a consequence, we can write the four ground states as

$$|G_{p_1,p_2}\rangle \;=\; \sum_{s\in\mathcal{S}} w\,|s;p_1,p_2\rangle \;=\; \prod_i \frac{1}{\sqrt{2}}\,(\mathbf{1}+A_i)\,|0;p_i,p_2\rangle\;, \tag{2.6}$$

with $p_1, p_2 \in \{0,1\}$ encoding the parities of the number of the NC loops in both directions. The state $|0\rangle$ is redefined as containing no contractible loops. Therefore, we find that the four ground states and thereby the logical qubit states differ in their topological properties.

Additionally, we construct the logical operators of the toric code, *i.e.*, operators that map the different code states, or in our case ground states, onto each other. In order to

switch between the states in Eq. (2.6), we need to add/remove single NC loops in the system, which is done by applying

$$Z_{\Gamma_{1/2}} = \prod_{(i,j)\in\Gamma_{1/2}} \sigma_{ij}^{z}\,, \tag{2.7}$$

where $\Gamma_{1/2}$ are the two different NC curves in Fig. 2.1(b). To measure the parity of those loops, we take the product of all σ^x operators along the NC curves $\tilde{\Gamma}_{1/2}$ of the dual lattice

$$X_{\tilde{\Gamma}_{1/2}} = \prod_{(i,j)\in\tilde{\Gamma}_{1/2}} \sigma_{ij}^{x}\,. \tag{2.8}$$

This way, we can count the parity of NC loops in the direct lattice as each of them shares one link with this operator. A pair of logical operators is visualised in Fig. 2.3. Note that the two dimensional square lattice is self-dual [21]. These intuitively constructed operators satisfy the formal requirements of logicals in stabiliser codes [8].
To show that the logical qubit states are protected against local errors, those can be incorporated into the Hamiltonian formulation as perturbations [22]. Assuming that g is the rate of a local qubit flip error, we write

$$V = -g \sum_{<i,j>} \sigma_{ij}^{z}\,. \tag{2.9}$$

This construction works analogously for other errors as long as those are strictly locally bounded. In perturbation theory, the logical states can only mix at $\mathcal{O}(L)$ in g, where L is the length of the smallest non-contractible curve. Therefore, mixing is exponentially suppressed for $L \to \infty$. Lastly, we have to prove that the ground states remain degenerate even in the perturbed case. To do this, we take two ground states $|G\rangle$ and $|G'\rangle = Z_{\Gamma_1}|G\rangle$. Then we show that

$$\langle G|\, V P_+ G_0 \ldots P_+ V\, |G\rangle = \langle G'|\, V P_+ G_0 \ldots P_+ V\, |G'\rangle \tag{2.10}$$

by expressing $|G'\rangle$ in terms of $|G\rangle$ and commuting the latter Z_{Γ_1} to the front such that it squares out. The P_+ project away from the ground space and $G_0 = 1/(E_0 - H_0)$ are the Greens functions, for details see Sec. 4.1.1. Thus, the perturbative corrections to the eigen energies are identical for all ground states, keeping them degenerate. This makes the toric code particularly interesting as a platform for quantum memory as the logical information is protected on the physical level and in theory no specific error correction scheme is necessary [8].

We will revisit this construction of the ground states again for the case of additional degrees of freedom on the links of the square lattice. In conclusion, the toric code is based on the redundant coding approach, where a lattice of physical qubits encodes two

topologically protected logical qubits, which can be useful as quantum memory. In the following section, we study a promising platform for those physical qubits.

2.2 Majorana zero modes in condensed matter physics

The idea of Majorana fermions (MF) was introduced by Majorana in 1937 in the context of particle physics. He found a symmetric formulation of electron and positron quantum theory by splitting the fermionic operators into their Hermitian and anti-Hermitian parts, which led him to the conclusion that neutral spin-1/2 particles potentially are their own anti-particles [23]. Anti-particle is meant in the sense that a MF with momentum $\boldsymbol{p}_1 = \boldsymbol{p}$ can annihilate a MF with $\boldsymbol{p}_2 = -\boldsymbol{p}$. The search for a so-called Majorana particle as an elementary particle, for example in measuring a neutrino-less double β-decay, has not been successful to this day, but a similar idea gains increasing interest in the condensed matter physics community. In many-body systems, so-called Majorana zero modes (MZMs) are predicted as emergent quasi-particles rather than elementary ones, in multiple solid state models [24]. The similar naming in honor of Majorana is due to the fact that these quasi-particles are their own anti-particles. Within recent years, the experimental quest for these quasi-particles intensified, although, also in this case, a conclusive verification of their existence is still to be made [25]. Those Majorana zero modes will be of interest in this thesis. We begin to work our way through the model of a Kitaev chain [26] to familiarise ourselves with the notation around MZMs and see their emergence with non-local properties.

We introduce the Majorana modes into the language of second quantisation by splitting the fermionic annihilation and creation operators for electrons into their "real" ($\gamma_{j,2}$) and "imaginary" parts ($\gamma_{j,1}$), where we suppress the spin index,

$$c_j = \frac{1}{2}(\gamma_{j,2} + i\gamma_{j,1}^\dagger) \qquad \text{and} \qquad c_j^\dagger = \frac{1}{2}(\gamma_{j,2} - i\gamma_{j,1}^\dagger)\,. \tag{2.11}$$

By doing so, the Majorana modes are associated with half a fermionic degree of freedom (DOF) and thus can only appear in even numbers in a physical system. For the inverse relations, we find

$$\gamma_{j,2} = c_j + c_j^\dagger \qquad \text{and} \qquad \gamma_{j,1} = i(c_j^\dagger - c_j)\,. \tag{2.12}$$

Making use of the fermionic algebra of $c_i, c_i^\dagger$, we obtain that $\gamma_{j,a}^\dagger = \gamma_{j,a}$, *i.e.*, they are Hermitian meaning that particles are their own holes as expected. They furthermore square to identity ($\gamma_{j,a}^2 = \mathbf{1}$) and satisfy the Clifford algebra $\{\gamma_{i,a}, \gamma_{j,b}\} = 2\delta_{ij}\delta_{ab}$, for $a, b \in \{1, 2\}$ [27]. To show the importance of these modes, we apply this reformulation of the electronic creation and annihilation operators to the toy model introduced by Kitaev in 2001 [26]. The Kitaev chain is a finite 1D tight-binding chain with additional p-wave

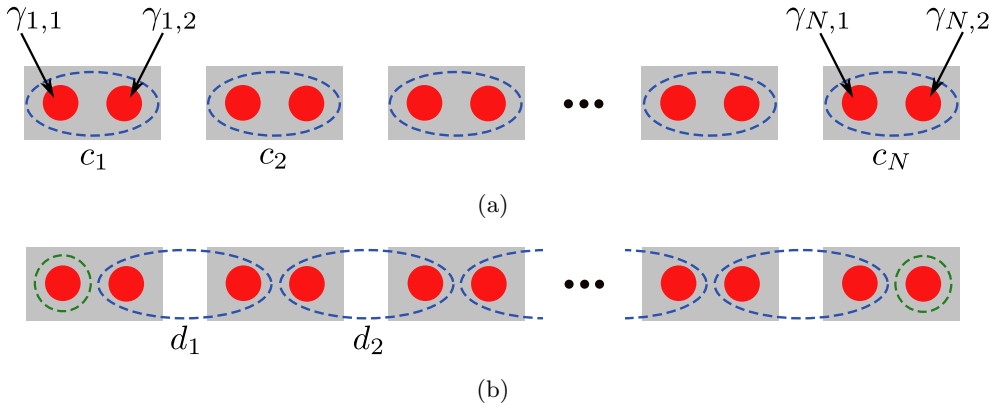

Figure 2.4: Schematic of the N-site Kitaev chain. In (a), we see the tight binding chain of electrons (grey), with their decomposition into two Majorana modes (red). Panel (b) displays the topological phase of the chain, where in the bulk the Majorana modes from adjacent electrons are paired into fermionic modes (blue dashed lines) such that two modes $\gamma_{1,1}$,$\gamma_{N,2}$ (green dashed lines) at the boundaries are paired to a non-local fermionic mode at zero energy. The graphic is inspired by Ref. [24].

superconducting pairing. The Hamiltonian for a chain of N sites is given by

$$H_{KC} = -\sum_{i=1}^{N-1}\left(tc_i^\dagger c_{i+1} + \Delta c_i c_{i+1} + \text{H.c.}\right) - \mu\sum_{j=1}^{N} n_j\,. \tag{2.13}$$

The first term describes nearest neighbour hopping along the chain with a rate t and the second one spin-less superconducting pairing with the superconducting gap Δ. This Hamiltonian describes a spin-polarised system, where Cooper pairs can only be formed by electrons on different sites. We introduced H.c., for Hermitian conjugate in order to compactify the expression. The last term contains the chemical potential μ and the electron number operator $n_j = c_j^\dagger c_j$ and is introduced due to the lack of particle number conservation in the superconducting pairing. Considering the parameter choice of $\Delta = t$ and $\mu = 0$ and inserting Eq. (2.12), we obtain from Eq. (2.13)

$$H_{KC} = -it\sum_{i=1}^{N-1}\gamma_{i,2}^\dagger\gamma_{i+1,1} = 2t\sum_{i=1}^{N-1}\left(d_i^\dagger d_i - \frac{1}{2}\right)\,, \tag{2.14}$$

with new bulk fermionic modes $d_i = \frac{1}{2}\left(\gamma_{i+1,1} + i\gamma_{i,2}\right)$. Under this parameter choice, the chain is effectively described by the coupling of Majoranas from electrons at adjacent sites. This can best be understood from the schematic in Fig. 2.4.

Through the reformulation of the Hamiltonian, we essentially regard each electron as a superposition of Majorana modes located at the position of the electron, which is depicted in Fig. 2.4(a). For the specific parameter choice however, the system can effectively be described by pairing the Majorana modes from adjacent electrons within the

bulk to new fermionic modes d_i, which are gapped by $2t$, thereby forming a non-local fermionic mode $d_{\mathrm{nl}} = \frac{1}{2}(\gamma_{N,2} + i\gamma_{1,1})$ at the boundaries of the system. This situation is displayed in Fig. 2.4(b). From its absence in Eq. (2.14), we can infer that the occupation of this mode costs zero energy, making the ground state two-fold degenerate. Thus, one can encode a topologically protected qubit into this two dimensional ground state space, since a simultaneous non-local operation on both bounding Majorana zero modes is necessary to go from qubit state $|0\rangle$, where the occupation of d_{nl} is $n_{\mathrm{nl}}|0\rangle = d_{\mathrm{nl}}^{\dagger} d_{\mathrm{nl}}|0\rangle = 0$, to qubit state $|1\rangle$, with $n_{\mathrm{nl}}|1\rangle = |1\rangle$ [28]. Additionally, the MZMs have non-Abelian exchange statistics [29], distinguishing them from the original fermionic Majorana particles. These exotic statistics allow the implementation of a considerable amount of computational gates on this qubit through braiding operations, see Refs. [8, 24, 28]. The analysis of the toy model, the Kitaev chain, suffices as an introduction to the properties and notation around the MZMs for the purpose of this thesis. It should be noted that Hamiltonians of a more realistic system can in an appropriate limit be effectively mapped onto Eq. (2.13). For example a semiconducting nanowire in proximity to an s-wave superconductor with an externally applied magnetic field can effectively describe a spin-polarised system similar to the Kitaev chain [28].

We have seen that with Majorana zero modes we could encode topologically protected qubits, where gate operations would be done with braiding, which makes them particularly interesting for the realisation of quantum computation. Those MZM are the physical qubits in the Majorana toric code. This concludes the discussion of the basic concepts and we will put them to use in the following introduction of the Majorana toric code.

Chapter 3

The Majorana Toric Code

In this chapter, we introduce the Majorana toric code (MTC). We start from the microscopic Hamiltonian of a system of superconducting islands carrying Majorana zero modes. We continue by investigating its symmetries and the phase diagram from a charge perspective. Then, we perform a mapping onto a lattice gauge theory of U(1) matter coupled to $\mathbb{Z}_2$ gauge fields, enabling the analysis of topological order. This chapter consists of multiple smaller sections that introduce the main features of the MTC and therefore lays the foundation for the subsequent more in-depth considerations.

3.1 The model

The underlying microscopic system is a two dimensional square lattice of Majorana box qubits (MBQ). Each of these boxes is a mesoscopic superconducting island, which due to its finite size possesses a charging energy $4E_C = 2e^2/C$ per Cooper pair. The C denotes the capacitance with respect to ground and e the elementary charge. We assume to have four Majorana zero modes per island. This model was first studied in Ref. [10]. Throughout this thesis, we consider the MZMs independent of their specific realisation. Experimentally pursued settings are for example semiconducting nanowires placed on superconductors [30], briefly mentioned above, and superconductors deposited onto topological insulators [31]. The islands are interacting in a way that allows for charge transfer. Besides the Josephson tunnelling of Cooper pairs H_J, Majorana assisted single electron tunnelling H_M between nearest neighbour islands can occur, see Fig. 3.1.

Generally, the single electron tunnelling H_M for a link (k, l) in $\hat{e}_1$-direction contains the operator pair $i\gamma^k_{a,1}\gamma^l_{b,1}$, but as each link can be associated with a unique Majorana zero mode at each endpoint, we will suppress additional indices in the following and write

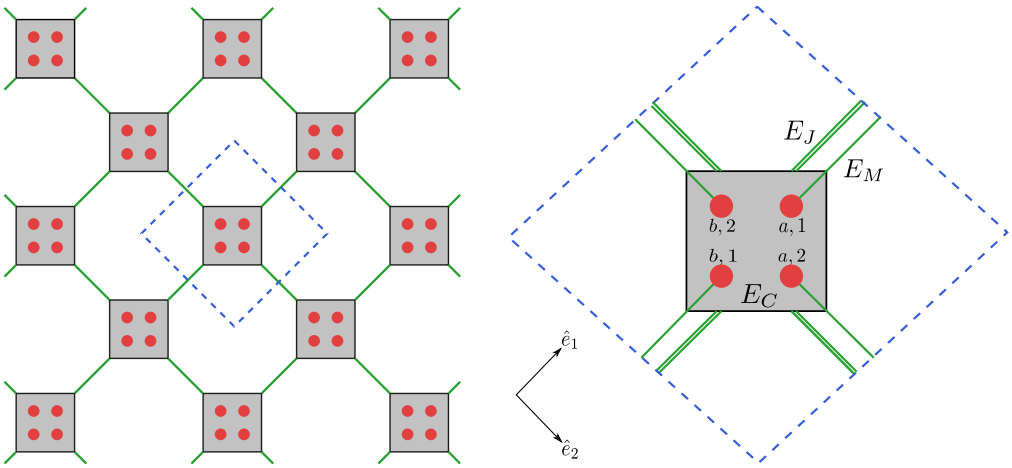

(a) 2D lattice (b) Unit cell

Figure 3.1: Schematic of the Majorana toric code. In (a) one can see mesoscopic superconducting islands (grey) organised in a two dimensional square lattice with nearest neighbour interaction (green). Panel (b) depicts a unit cell of this lattice. On each island there are four Majorana zero modes (red) and it possesses a finite charging energy $4E_C = 2e^2/C$ per Cooper pair. The nearest neighbour interactions are comprised of Cooper pair tunnelling at rate E_J and Majorana assisted single electron tunnelling at rate E_M.

$i\gamma^k\gamma^l$. The Hamiltonian for this system is then given by [10]

$$H = H_C + H_J + H_M\,, \tag{3.1a}$$

$$H_C = 4E_C \sum_i n_i^2\,, \tag{3.1b}$$

$$H_J = -E_J \sum_{<k,l>} \cos\left(\phi_k - \phi_l\right), \tag{3.1c}$$

$$H_M = -E_M \sum_{<k,l>} i\gamma^k\gamma^l \cos\left(\frac{\phi_k - \phi_l}{2}\right), \tag{3.1d}$$

where the space of physical states $|\text{phys}\rangle$ is subject to the gauge redundancy

$$Q_j\,|\text{phys}\rangle = |\text{phys}\rangle\ , \qquad \text{with} \qquad Q_j = -\gamma^j_{a,1}\gamma^j_{a,2}\gamma^j_{b,1}\gamma^j_{b,2}\ \mathrm{e}^{2\pi i n_j}\,. \tag{3.2}$$

The charging and Josephson term, $H_C + H_J$, comprise the Cooper pair box Hamiltonian [4, 5], where we treat the special case of zero offset charge. The number of Cooper pairs per island n_i and the superconducting phase on the islands ϕ_i are conjugate variables with $[\phi_i, n_j] = i\delta_{ij}$. The MZMs host single electrons, which is captured by H_M [32]. We saw in Section 2.2 that the Majorana operators γ^j are Hermitian and satisfy the Clifford algebra. Even though the model contains emergent Majorana zero modes, we have to keep in mind that the physical particles which can be added and removed are electrons described by the operator $c_j^\dagger = \mathrm{e}^{i\phi_j/2}(\gamma_a^j + i\gamma_b^j)/2$ [33]. Those affect the charge as well as

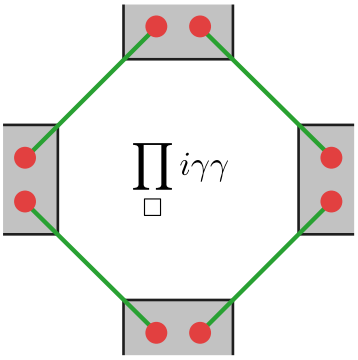

Figure 3.2: Local plaquette symmetry of the Majorana zero modes (red). The product of the MZM around a plaquette on the direct lattice is a conserved quantity.

the Majorana sector since they are split into a charge part $e^{i\phi_j/2}$ and the neutral spin-1/2 fermion $(\gamma_a^j + i\gamma_b^j)/2$ (cf. Sec. 2.2). The gauge constraint Eq. (3.2) therefore parity couples the charges to the MZMs on each island, truncating the tensor product Hilbert space of the charge and Majorana sectors [32], making sure that we restrict ourselves to the physical Hilbert space.

3.2 Symmetries

Before the phase diagram is analysed, it is worthwhile to look at symmetries in the system. Besides the gauge redundancy in Eq. (3.2), which is often referred to as a local gauge symmetry of the system, there is another conserved local quantity. The operator $\tilde{Q}_j = \prod_{\square} i\gamma\gamma$ commutes with H and Q_j given in Eq. (3.1) and (3.2). The product in $\tilde{Q}_j$ includes all links around a smallest cycle on the direct lattice, a plaquette (cf. Fig. 3.2). This means that in particular the product of all Majorana operators along a closed loop in the direct lattice is a conserved quantity. Furthermore, there are global symmetries related to the couplings in the Hamiltonian. If we start with the case of $E_M = 0$, the Hamiltonian is given by the coupled Cooper pair box Hamiltonian

$$H_{(E_M=0)} = 4E_C \sum_i n_i^2 - E_J \sum_{<i,j>} \cos\left(\phi_i - \phi_j\right) . \tag{3.3}$$

In this case, one can introduce a transformation

$$E_J \to -E_J \qquad \text{and} \qquad \phi_k \to \phi_k + \pi\,, \quad \forall k \in K\,, \tag{3.4}$$

where K is a set of indices containing the index of every other node, *i.e.*, next nearest neighbours. This can be achieved by coloring the islands according to a bipartite lattice and taking only one sub-lattice. This is analogous to the construction of the Néel state in an antiferromagnet. We assume here that the number of lattice sites per dimension is even such that with periodic boundary conditions one finds that every node k is

surrounded by non-transformed nodes and vice versa. This transformation leaves the Hamiltonian and therefore its spectrum invariant. Thus, the sign of the Cooper pair tunnelling rate E_J is irrelevant. For the full Hamiltonian

$$H_{MTC} = 4E_C \sum_i n_i^2 - E_M \sum_{<k,l>} i\gamma^k\gamma^l \cos\left(\frac{\phi_k - \phi_l}{2}\right) - E_J \sum_{<k,l>} \cos\left(\phi_k - \phi_l\right) , \quad (3.5)$$

this is not the case. Due to the introduction of H_M the transformation in Eq. (3.4) does not leave the spectrum invariant any more. Instead one can construct a new transformation

$$E_M \to -E_M \qquad \text{and} \qquad \phi_k \to \phi_k + 2\pi\,, \quad \forall k \in K\,, \quad (3.6)$$

which proves the invariance under a sign flip of E_M only. Thus, due to the presence of the single electron tunnelling, the sign of the coupling E_J is of importance in the full Hamiltonian. This can be intuitively understood since the process of two single charge transfers along a link, yields the same result as a single Cooper pair transfer. Therefore, the tunnelling terms can couple with $E_M^2 E_J$. Sec. 4.1.3 will shed more light on the coupling mechanism, where the $E_M \to -E_M$ symmetry has to be respected in an effective Hamiltonian calculation of the system. Furthermore, the symmetry has additional implications for the phase diagram, which we discuss in Sec. 3.4. In particular, the symmetry in E_M forces transition lines to approach the $E_M = 0$ axis in a right angle. For $E_J = 0$ this is not the case any more if single electron tunnelling is included in the model (cf. Fig. 3.3).

3.3 Charge basis formulation

To get a better intuition for the Hamiltonian in Eq. (3.6) from the charge perspective, we rewrite it in the charge basis. This improves our understanding of the subsequently described charge signatures in the phase diagram. First, we note that due to the presence of MZMs not only Cooper pairs but also single electrons exist in the system. Thus, we find that the expectation value of the Cooper pair number operator can take half-integer values, *i.e.*, $n_i \in \mathbb{Z}/2$ for eigenstates of the Hamiltonian. Using that ϕ_i and n_i are canonically conjugate variables, we find that

$$\begin{aligned} \left[n_j, \mathrm{e}^{i\phi_k}\right] &= \underbrace{\left[n_j, \phi_k\right]}_{=\,-i\delta_{jk}} i\mathrm{e}^{i\phi_k} = \mathrm{e}^{i\phi_j}\delta_{jk} \\ \Rightarrow \quad n_j\mathrm{e}^{i\phi_k} &= \mathrm{e}^{i\phi_k} n_j + \delta_{jk}\mathrm{e}^{i\phi_j} = \mathrm{e}^{i\phi_k}(n_j + \delta_{jk})\,. \end{aligned} \quad (3.7)$$

Restricting ourselves to the charge sector for now, we can formulate $|n\rangle = |n_1, n_2, \ldots, n_N\rangle$ as charge basis states for a system of N islands. With Eq. (3.7), the creation operator

of a Cooper pair charge on island i then follows to be

$$\mathrm{e}^{i\phi_j}\,|n\rangle = \alpha\,|n_1, n_2, \ldots, n_j + 1, \ldots, n_N\rangle \qquad \Rightarrow \qquad {d_j^\dagger}^2 = \mathrm{e}^{i\phi_j}\,, \tag{3.8}$$

where α accounts for normalisation. Analogously one obtains

$$\left[n_j, \mathrm{e}^{-i\phi_k}\right] = -\mathrm{e}^{-i\phi_j}\delta_{jk} \qquad \Rightarrow \qquad d_j^2 = \mathrm{e}^{-i\phi_j}\,. \tag{3.9}$$

For $\mathrm{e}^{\pm i\phi_j/2}$ this analysis readily yields

$$d_j^\dagger = \mathrm{e}^{i\phi_j/2}\,, \qquad\qquad d_j = \mathrm{e}^{-i\phi_j/2}\,, \tag{3.10}$$

i.e., $\mathrm{e}^{\pm i\phi_j/2}$ add/remove the charge of a single electron on site j such that the number of Cooper pair charges is raised or lowered by $1/2$ respectively. Of further interest are the relations

$$\left[\mathrm{e}^{2\pi i n_j}, \mathrm{e}^{\pm i\phi_k}\right] = 0\,, \quad \forall j, k\,. \tag{3.11}$$

It follows that a change in the number of Cooper pair charges on an island by one does not affect its parity. This is to be expected as a Cooper pair consists of an even number of electrons. For the single electron raising and lowering operators the situation is different, because

$$\left[\mathrm{e}^{2\pi i n_j}, \mathrm{e}^{\pm i\phi_k/2}\right] = 0\,, \qquad \text{for} \quad j \neq k \tag{3.12}$$

$$\left\{\mathrm{e}^{2\pi i n_j}, \mathrm{e}^{\pm i\phi_k/2}\right\} = 0\,. \tag{3.13}$$

Adding/removing a single charge changes the parity. We also note that the fractional raising and lowering operators fulfil a Pauli algebra with the parity operator. Rewriting the cosines with Euler's formula and inserting the creation and annihilation operators into Eq. (3.1) yields

$$H = H_C + H_J + H_M\,, \tag{3.14a}$$

$$H_C = 4E_C \sum_i n_i^2\,, \tag{3.14b}$$

$$H_J = -\frac{E_J}{2} \sum_{<k,l>} {d_k^\dagger}^2 d_l^2 + d_k^2 {d_l^\dagger}^2\,, \tag{3.14c}$$

$$H_M = -\frac{E_M}{2} \sum_{<k,l>} i\gamma^k\gamma^l \left(d_k^\dagger d_l + d_k d_l^\dagger\right)\,. \tag{3.14d}$$

In this form the effect of the different terms on the charge sector is explicitly indicated. We see that as claimed above, H_J leads to a Cooper pair charge being removed at island l and added at island k or vice versa. With H_M the analogous process is described, but

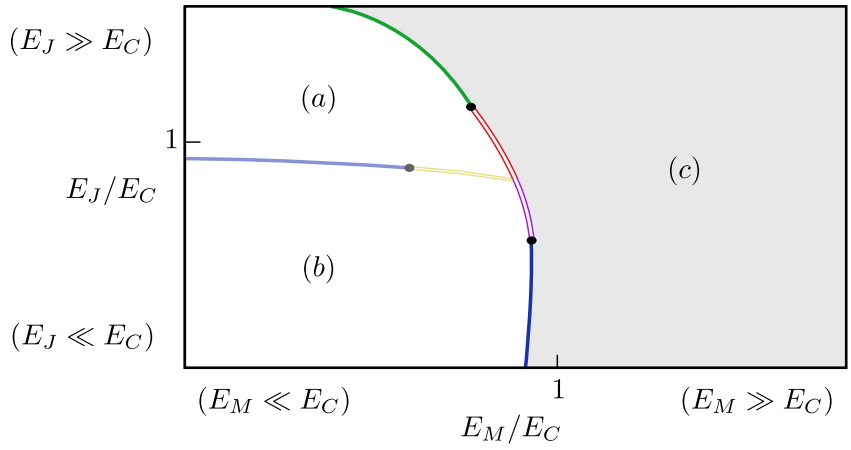

Figure 3.3: Phase diagram of the Majorana toric code (cf. Eq. (3.1)), for constant charging energy E_C. For small enough but finite coupling parameters E_M, E_J the system is in a Mott insulator phase (b). For increasing single electron tunnelling E_M, there is a (2+1)D-XY type transition (blue) into a charge-e superconductor (c). If instead the Cooper pair tunnelling rate E_J is increased, another XY type transition turns the system into a charge-$2e$ superconductor. From there the system reaches the charge-e superconductor by a (2+1)D-Ising type transition. The dots and double lines denote tricritical points and first order transitions, respectively. For detailed information on those, see Refs. [12, 13].

with single charges. The latter also involves the MZMs on the links and we see that crucially those appear independent of the direction in which the charge tunnels.
This brings us in a position to discuss the phase diagram of the Majorana toric code from a charge perspective.

3.4 Phase diagram

The phase diagram of this model has partially been explored in previous works [10–13] and is depicted in Fig. 3.3 for constant charging energy E_C.
The different phases can be distinguished by their charge signature [10]. If both the single electron and the Cooper pair tunnelling rate are small compared to the charging energy, charge transfer is suppressed and the system behaves like a Mott insulator (MI) (b). Upon increase of the Cooper pair tunnelling E_J, the system undergoes a second order continuous symmetry-breaking transition of the (2+1)D-XY universality class into a charge-$2e$ superconductor (a). It is experimentally observed that different physical systems can share the same critical exponents when undergoing a second order phase transition. The correlation length scale hypothesis claims that in the critical region the only relevant scale in the system is the correlation length. Thus, the physics is rendered independent of the microscopic details in the system. Second order transitions can thus be arranged into universality classes, each describing a specific set of critical exponents [21]. Focusing on the limiting case of $E_M = 0$, we see that the Hamiltonian in

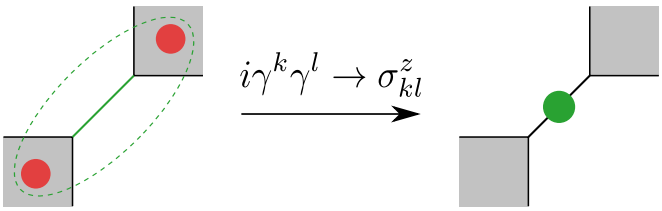

Figure 3.4: Duality mapping from MZMs to spins. The product of MZMs (red dots) at the endpoints of a link, gets mapped to spins centered on the links (green dot).

Eq. (3.1) takes the form of the XY model in accordance to the transition type mentioned above [21]. An increase in the single electron tunnelling rate E_M leads for both, the MI and the $2e$-superconductor phase, to turn into a charge e-superconductor. The transition type depends on the strength of the Josephson energy E_J. For small E_J, the transition is again of the (2+1)D-XY type [10], turning into a discrete symmetry breaking (2+1)D-Ising transition for large E_J [11]. The connection between those asymptotic results is made in Ref. [12]. Proposing a Landau field theory, it is predicted that the (2+1)D-XY type transition turns through a couple of tricritical points and first order transitions into the (2+1)D-Ising class. We can also see the above discussed symmetry features respected in the diagram. The XY transition approaches the $E_M = 0$ axis in a right angle, while this is not the case at the $E_J = 0$ axis. In order to verify the transition types in future experiments, Ref. [13] uses the Landau field theory, where the Majorana sector is gauge fixed, to predict the universal conductivities at the different phase transitions, which is an experimentally measurable quantity. To be precise, it is the spin fields that get fixed in Ref. [13]. Since those are obtained from coarse-grained spins, which in turn are the duality mapped MZMs, this distinction is not important for the statement under consideration. The mapping between the MZMs and spins is presented in the following.

3.5 Mapping to lattice gauge theory

Besides the charge signatures discussed thus far, the model was found to realise Kitaev's toric code [8, 34] in both phase (a) [11] and (b) [10, 14]. As described in Sec. 1, this means those phases possess topological order. To analyse the topological signatures of the phases, we shift the focus from the charge to the Majorana sector. To this end, we map the microscopic Hamiltonian in Eq. (3.1) onto a lattice gauge theory. The transformation

$$i\gamma^k\gamma^l \;\to\; \sigma^z_{kl} \quad \text{and} \quad -\gamma^j_{a,1}\gamma^j_{a,2}\gamma^j_{b,1}\gamma^j_{b,2} \;\to\; \prod_{+}\sigma^x\,, \tag{3.15}$$

is obtained with the bond algebraic approach [35, 36], see Appendix A for details.
The product of the MZMs located at the endpoints of a link gets transformed into a spin,

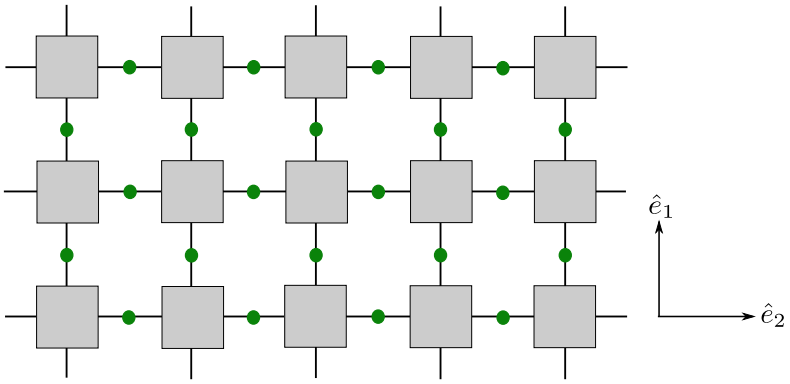

Figure 3.5: Sketch of the two dimensional square lattice, with U(1) matter degrees of freedom $e^{i\phi}$ (grey squares) located at the nodes of the lattice and $\mathbb{Z}_2$ gauge DOF σ_{ij} (green dots) placed centrally on the links connecting nearest neighbouring nodes. This system can realise a $\mathbb{Z}_2$ lattice gauge theory with U(1) matter (Higgs) fields.

that is placed centrally on it (cf. Fig. 3.4). The spins are denoted by the Pauli operators σ^x_{ij} and σ^z_{ij}. This transformation keeps the number of degrees of freedom invariant. Initially a combination of two MZMs is a fermionic mode that can be occupied or not and afterwards we have a single spin, which can be in the up or down state.
The system after the transformation is visualised in Fig. 3.5, where the lattice is rotated by $\pi/4$ compared to Fig. 3.1. The Hamiltonian description of the model reads

$$\begin{aligned} H_{MTC} &= H_C + H_J + H_M \\ &= 4E_C \sum_i n_i^2 - E_J \sum_{<i,j>} \cos\left(\phi_i - \phi_j\right) - E_M \sum_{<i,j>} \sigma^z_{ij} \cos\left(\frac{\phi_i - \phi_j}{2}\right) , \end{aligned} \tag{3.16}$$

$$\text{with} \quad Q_i = e^{2\pi i n_i} \prod_+ \sigma^x \, . \tag{3.17}$$

The form of Eq. (3.17) can be associated with a Gauss' law, comparable to a discrete version of the one from electrodynamics [21]. In this case it couples a U(1) matter field by its parity to the $\mathbb{Z}_2$ gauge field surrounding it. Thus, we will in the following refer to the node and link variables also as matter and gauge fields, respectively. Notably, the gauge field does not obtain direct dynamics via the Hamiltonian in Eq. (3.16), but rather indirectly mediated through the matter field (cf. Eq. (3.17)).

In the next chapter we study different lattice gauge theories and their respective order parameters. Afterwards, we will be able to pinpoint decisive properties of the model at hand. Finally, we analyse topological ordering in this system with a $\mathbb{Z}_2$ gauge field coupled to the parity of the U(1) matter field.

Chapter 4

Topological Ordering

In this chapter, we verify the existence of topological ordering in the Majorana toric code and study different order parameters for lattice gauge theories. Starting from the Wilson loop as diagnostic of different phases in pure gauge theories, we construct the Fredenhagen-Marcu order parameter as a generalisation. The latter is a diagnostic for theories containing dynamical gauge as well as matter fields. Subsequently, we evaluate the Fredenhagen-Marcu order parameter in the Majorana toric code model and proof that it detects the topological ordering in the system.

4.1 The toric code limit

To see the emergence of topological ordering in the model in Eq. (3.16), we focus on the regime where the charging energy is dominant $E_C \gg E_M, E_J$. From a charge point of view, we discussed that the system is in a Mott insulator phase. In the following, we use a perturbative analysis to determine the effective Hamiltonian to leading order in the tunnelling rates E_J, E_M.

4.1.1 Formalism

The unperturbed Hamiltonian is given by

$$H_0 = 4E_C \sum_i n_i^2 \,. \tag{4.1}$$

In light of the perturbation in Eq. (4.6), we already apply the gauge constraint

$$Q_j \,|\text{phys}\rangle = |\text{phys}\rangle \;, \qquad \text{where} \quad Q_j = \mathrm{e}^{2\pi i n_j} \prod_+ \sigma^x \,, \tag{4.2}$$

at this stage of the calculation. Thereby, we restrict the unperturbed ground state space considerably without altering the final result. The respective ground state has to fulfil

$$n_i^2 \left|G\right\rangle = 0\,, \qquad \forall\, i\,, \tag{4.3}$$

for the matter sector. Using the gauge constraint on that ground state, we have

$$Q_j \left|G\right\rangle = \prod_{+} \sigma^x \left|G\right\rangle = \left|G\right\rangle\ . \tag{4.4}$$

This means that all closed loops of $\sigma_i^x = -1$ on the direct lattice are allowed for the gauge invariant formulation of the ground state. In fact, any linear combinations of those basis states is valid, yielding the superposition of all those closed loops (cf. Eq. (2.3))

$$\left|G\right\rangle = \sum_{s\in\mathcal{S}} w_s \left|s, n_i = 0\right\rangle \ = \ \sum_{s\in\mathcal{S}} w_s \left|s\right\rangle\ . \tag{4.5}$$

Note that this ground state is highly degenerate as the weights w_s for the superposition are arbitrary as long as only H_0 is considered. In the original picture this situation corresponds to a macroscopic number of uncoupled superconducting islands. In that case, the two fermionic modes (four MZMs) on each island can be both occupied or both empty resulting in an even parity. Since in the regime under consideration the number of charges per island is well-defined, we focus on the charge representation in Eq. (3.14).

We consider the Josephson and Majorana terms of the full Hamiltonian in Eq. (3.16) as a perturbation to the dominant charge term in Eq. (4.1). After the transformation from MZMs to spins the perturbation can be written as

$$V = E_J V_J + E_M V_M = -\frac{E_J}{2} \sum_{<i,j>} \left({d_i^\dagger}^2 d_j^2 + d_i^2 {d_j^\dagger}^2 \right) - \frac{E_M}{2} \sum_{<i,j>} \sigma_{ij}^z \left(d_i^\dagger d_j + d_i d_j^\dagger \right)\ . \tag{4.6}$$

For $E_M \neq 0$ we will see that the fourth order effective Hamiltonian describes the toric code. So most of the ground state degeneracy is lifted in the presence of the perturbation and the equal weight superposition yields the lowest energy.
To set up the formalism of the perturbation theory, we define the projectors

$$P_- = \sum_G \left|G\right\rangle\!\left\langle G\right| \qquad \text{and} \qquad P_+ = 1 - P_-\,. \tag{4.7}$$

The P_- is the projector on the ground state space and P_+ projects onto the orthogonal space. From an energy perspective these spaces are separated on a scale of $\mathcal{O}(E_C) \gg \mathcal{O}(E_M, E_J) = \mathcal{O}(V)$. Applying Brillouin-Wigner perturbation theory [37], the effective

low-energy Hamiltonian is given by

$$H_{\text{eff}}(E) = P_-\Big(H_0 + V + VP_+ \underbrace{\frac{1}{E - H_0 - V}P_+}_{= \frac{1}{E-H_0}\sum_{k=0}^{\infty}\left(V\frac{1}{E-H_0}P_+\right)^k} V\Big)P_- \,. \tag{4.8}$$

The E denotes the eigen energies of the full Hamiltonian. The self-consistency of the above equation is highlighted by the E dependence on the left hand side. This dependence is in the following suppressed. The effective Hamiltonian lives in the ground state space of H_0 where the gauge constraint is applied.

Furthermore, we define the projections of the terms in the Hamiltonian to

$$V_{\pm\mp} = P_\pm V P_\mp \qquad \text{and} \qquad H_{0+} = P_+ H_0 P_+ \,. \tag{4.9}$$

Here, H_0 is diagonal in both the ground state space and the perturbed states ($V\,|G_0\rangle$), since all of them have a well defined charge number. This leaves us with

$$H_{\text{eff}} = E_0 + V_{--} + V_{-+}\frac{1}{E - H_{0+}}\sum_{k=0}^{\infty}\left(V_{++}\frac{1}{E - H_{0+}}\right)^k V_{+-} \,, \tag{4.10}$$

where E_0 is the ground state energy. There are some important things to note for the case under consideration. First, to comply with the condition that the perturbation is much smaller than the unperturbed Hamiltonian, the Green's function has to be negative for E close to the ground state energy.

$$\frac{1}{E - H_{0+}} < 0 \,, \qquad \text{as} \quad E = E_0 + \underbrace{\delta E}_{\mathcal{O}(V)} \,, \quad H_{0+} = E_0 + \underbrace{\delta H}_{\mathcal{O}(E_C)} \quad \text{and} \quad \delta H > 0 \,. \tag{4.11}$$

If we now redefine the potential $\tilde{V} = -V$ we obtain that

$$H_{\text{eff}} = E_0 - \tilde{V}_{--} - \tilde{V}_{-+}\tilde{G}_0(E)\sum_{k=0}^{\infty}\left(\tilde{V}_{++}\tilde{G}_0(E)\right)^k \tilde{V}_{+-} \,, \tag{4.12}$$

with $\tilde{G}_0(E) = 1/(H_{0+} - E)$. This is a self-consistent equation for the effective Hamiltonian in Brillouin-Wigner perturbation theory. The Hamiltonian H_{eff} can now be determined to arbitrary order by considering more and more terms of the sum over k and expanding $\tilde{G}_0(E)$ around the ground state energy (see Appendix B). If we would approximate $E = E_0$, then only negative corrections to the ground state energy can occur. In other words, positive corrections are only generated by the energy expansion of the Green's function. For convenience, we will drop the tilde in $\tilde{G}, \tilde{V}$ in the following.

To obtain an intuitive understanding of the different virtual processes that yield contributions to the effective Hamiltonian, we have to look at the effect of the different terms in the perturbation. Those are depicted in Fig. 4.1 on the direct lattice.
The application of one perturbation leads to tunnelling of a single electron or a Cooper pair between adjacent nodes. Both generate the respective charge transfer, but for single electrons a flip of the gauge variable on the link connecting the nodes occurs additionally. Revisiting Eq. (4.12), we know that every valid contribution to H_{eff} is given by a process that starts and ends in a charge-less state due to the projectors P_-. Therefore, we visualise all valid contributions using the notation of the perturbative terms in Fig. 4.1 by requesting that the generated diagram fulfils flow conservation in every node. This is similar to Kirchhoff's laws for circuits. Two candidate diagrams are displayed in Fig. 4.2. In the diagram (a) three charges flow from the bottom right node to the top left. Two of them flow by the bottom left node, while one passes through the top right. The latter one flips two gauge fields. This process does not satisfy the required charge conservation in the top left and bottom right node, so it does not describe a valid contribution to the effective Hamiltonian in Eq. (4.12). Contrarily, diagram (b) only involves back and forth hopping on the same links. Therefore, the resulting state is again charge-less. With the effective Hamiltonian and the diagrams at hand, we subsequently analyse the leading order contributions.

4.1.2 Emerging toric code

To determine the lowest order contribution to the effective Hamiltonian that is not a constant, we have to go as high as fourth order in the perturbation [11, 14]. This contribution is depicted in Fig. 4.3.
As only single charge tunnelling involves the gauge DOF on the links, one has to find a valid process that contains a fractional number of charges transferred per link to yield a non-constant term. To leading order, this is given by the smallest cycle in the system, a plaquette, where charges can flow around and return to the charge-less ground state space. The only non-constant contribution to fourth order is then given by a single electron flowing around a plaquette. The depicted process is a representative as analogous terms are obtained independent of the starting point or the orientation (clock-wise/ counter clock-wise) of the charge flow. The respective fourth order term in the expansion of Eq. (4.12) is given by (cf. Appendix B)

$$H_{\text{eff}}^{(4)} = -V_{-+}G_0(0)V_{++}G_0(0)V_{++}G_0(0)V_{+-} = const - \frac{5}{16}\frac{E_M^4}{E_C^3}\sum_i \prod_{\square} \sigma^z \,. \tag{4.13}$$

Here, we used $E_0 = 0$. So the leading order non-constant correction is obtained as a fourth order process purely in E_M. The negative sign of the prefactor can be seen directly from Eq. (4.12) as this term consists only of contributions with $E = E_0$. The

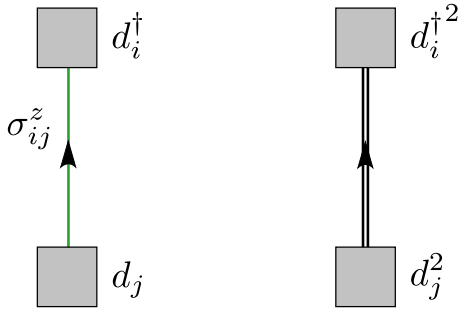

Figure 4.1: Spatial visualisation of single perturbations, where the line indicates a link of the direct lattice. On the left is the tunnelling of a single electron from node j to i, which lowers the charge on island j by $1/2$ (in numbers of Cooper pairs) and adds this charge to node i. Additionally, the gauge field on the link between those nodes flips (colored green). On the right, a Cooper pair tunnels between the nodes. This only involves a charge transfer of one.

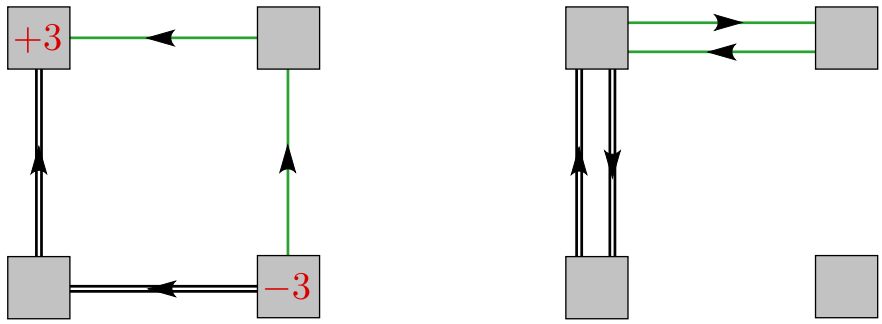

(a) Invalid diagram (b) Valid diagram

Figure 4.2: Visualisation of different virtual processes in the effective Hamiltonian on the direct lattice. Diagram (a) is a fourth order process that is invalid. In two nodes the total charge does not add up to zero. The diagram (b) is also fourth order, but fulfils flow conservation in all nodes and thus gives a valid contribution to the effective Hamiltonian. If no charge transfer occurs, the respective link is not drawn explicitly.

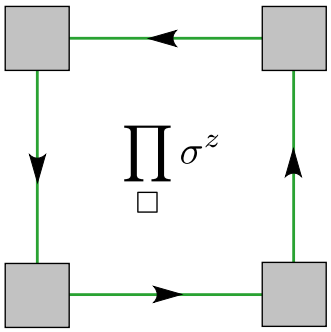

Figure 4.3: Schematic of a fourth order contribution to the effective Hamiltonian. A single charge flows around the smallest cycle on the square lattice. This yields gauge flips around a plaquette.

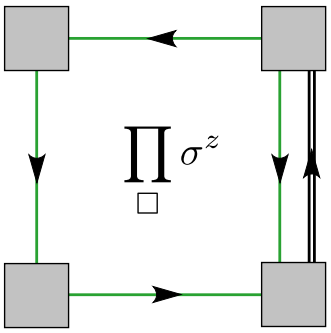

Figure 4.4: Schematic of a fifth order contribution to the effective Hamiltonian. Effectively, a single charge flows around a plaquette, but on one link there is a Cooper pair hopping, which is partially cancelled by a single electron tunnelling against the flow orientation.

Hamiltonian in Eq. (4.13) combined with the gauge constraint in Eq. (4.4) gives the toric code analysed in Sec. 2.1. The prefactor of this plaquette term is related to the gap, *i.e.*, the energy difference between the ground and first exited states, of the toric code by a factor of two. Thus, most of the ground state degeneracy is lifted and we are left with the four-fold topologically degenerate ground state. Moreover, we proved that the Mott insulator phase (b) in the phase diagram in Fig. 3.3 is topologically ordered. Thereby, we obtain the same result as Ref. [14], where the limiting case $V = E_M V_M$ was considered. This is to be expected as the leading order correction should be independent of the inclusion of $E_J V_J$ to the perturbation in Eq. (4.6), since the Cooper pair tunnelling is decoupled from the gauge field and only the latter yields non-constant contributions to the effective Hamiltonian.

In conclusion, we saw the emergence of the toric code in the limit of dominant charging energy E_C, reducing the ground state degeneracy to a four-fold topological one. The question remains what influence the Cooper pair hopping has to leading order in E_J on the gap of the toric code.

4.1.3 Stabilisation of the toric code

To calculate the leading order plaquette corrections in E_J assuming again the full perturbation $V = E_J V_J + E_M V_M$, we will focus on terms of the form $E_M^4 E_J$. There is a plaquette operator generated by single electron hopping combined with an additional Cooper pair hopping from V_J. So we are looking for processes that involve five perturbations before returning to a charge-less state and have a fractional number of charges transferred for at least one link. A representative process is shown in Fig. 4.4.

In order to obtain a non-constant contribution, a single charge has to effectively flow around a plaquette again. From the top right node there is a single charge tunnelling counter clock-wise to the bottom right, analogously to the fourth order diagram in Fig. 4.3. On the remaining link, however, there is a Cooper pair tunnelling event occurring in flow direction. The additional charge on the top left is then transferred back with a single electron hopping. From a charge perspective this is a valid diagram. To see that it also flips all gauge DOF around a plaquette exactly as the fourth order contribution,

we have to acknowledge that the action on the gauge variables is independent of the direction of the single charge tunnelling (cf. Eq. (4.6)). The respective fifth order term in the effective Hamiltonian (cf. Appendix B)

$$H_{\text{eff}}^{(5)} = -V_{-+}G_0(0)\left[V_{++}G_0(0)\right]^3 V_{+-} = const - \frac{61}{144}\frac{E_M^4 E_J}{E_C^4}\sum_i \prod_{\square} \sigma^z \tag{4.14}$$

is calculated by summing all valid permutations of the digram in Fig. 4.4 for each node in the lattice. This contribution does not include any terms from the energy expansion of the Green's function, so it must have a negative prefactor. Comparison to Eq. (4.13) implies that the absolute value of the plaquette term prefactor increases since the prefactors have the same sign. This means that the toric code ground space is additionally stabilised for small Cooper pair hopping rate E_J. Notably, E_J appears in an odd power in the fifth order term, in contrast to E_M. This is in accordance with the symmetry consideration in Sec. 3.2. The effective Hamiltonian respects the symmetry under $E_M \to -E_M$ since the single electron coupling occurs only in even powers. The process in Fig. 4.4 manifestly shows the emergence of an odd number of Cooper pair tunnellings in a valid process due to the additional presence of single electron transfer.

4.1.4 Plaquette interaction

Lastly, we go to sixth order in the effective Hamiltonian. The terms in the expansion are given by (cf. Appendix B)

$$\begin{aligned} H_{\text{eff}}^{(6)} = &-\delta E^{(4)} V_{-+}G_0(0)^2 V_{+-} - \delta E^{(2)} V_{-+}G_0(0)M^2 G_0(0)V_{+-} \\ &- V_{-+}G_0(0)\left[V_{++}G_0(0)\right]^4 V_{+-}\,, \end{aligned} \tag{4.15}$$

where

$$M^2 = 2V_{++}G_0(0)V_{++}G_0(0) + V_{++}G_0(0)^2 V_{++}\,. \tag{4.16}$$

The M^2 only simplifies the notation. The $\delta E^{(2)}$ and $\delta E^{(4)}$ are the second and fourth order corrections to the energy $E = E_0 + \delta E^{(2)} + \delta E^{(4)}$. The detailed calculation of all different contributions is left to Appendix C. One key remark is that the correction from the energy expansion are both found to be negative ($\delta E^{(2)}, \delta E^{(4)} < 0$) meaning that the sixth order term contains competing contributions. In principle it could be positive and reduce the gap of the toric code. Summing up all diagrams that lead to a plaquette term in sixth order yields

$$H_{\text{eff}}^{(6,1)} = -\left[\frac{259}{1728}\frac{E_M^6}{E_C^5} + 0,09556\frac{E_M^4 E_J^2}{E_C^5}\right]\sum_i \prod_{\square} \sigma^z\,, \tag{4.17}$$

where the second contribution is displayed as a floating point number just for clarity. Notably, even though the prefactors are increasingly small, the toric code is further

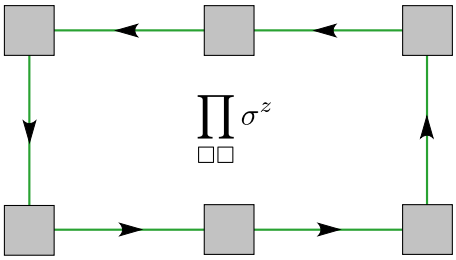

Figure 4.5: Schematic of a sixth order contribution to the effective Hamiltonian. A single charge flows around the second smallest cycle on the square lattice. This yields gauge flips around the perimeter of two adjacent plaquettes.

stabilised. Besides the corrections to the single plaquette term, there is a plaquette interaction emerging in sixth order. The corresponding process is visualised in Fig. 4.5. A single charge can flow around the perimeter of two adjacent plaquettes, which is the second smallest cycle in the square lattice. The gauge fields on the perimeter get thereby flipped. The sum of all relevant diagrams is calculated to be

$$H_{\text{eff}}^{(6,2)} = -\frac{63}{256}\frac{E_M^6}{E_C^5}\sum_i \Big(\prod_{\square\square}\sigma^z + \prod_{\substack{\square\\\square}}\sigma^z\Big)\,. \tag{4.18}$$

The σ^z on the shared link can be added for clarity as they square out to one. This term introduces a nearest neighbour interaction between adjacent plaquettes. This interaction commutes with the single plaquette term and results in an additional stabilisation of the ground state space [11], not to a phase transition.
Combining the previous results from Equations (4.13), (4.14), (4.17) and (4.18), we obtain for the effective Hamiltonian in Eq. (4.12) up to sixth order

$$\begin{aligned} H_{\text{eff}} = const - \Big[\frac{5}{16}\frac{E_M^4}{E_C^3} + \frac{61}{144}\frac{E_M^4 E_J}{E_C^4} + \frac{259}{1728}\frac{E_M^6}{E_C^5} + 0,09556\frac{E_M^4 E_J^2}{E_C^5}\Big]\sum_i\prod_{\square}\sigma^z \\ - \frac{63}{256}\frac{E_M^6}{E_C^5}\sum_i\Big(\prod_{\square\square}\sigma^z + \prod_{\substack{\square\\\square}}\sigma^z\Big)\,. \end{aligned} \tag{4.19}$$

Note that this Hamiltonian only lives in the ground state space and we omitted the projection operators. The prefactors were calculated analytically and reproduced using a computer algebra program. Besides the previously known leading order plaquette contribution E_M^4, we found the leading order correction in E_J to stabilise the toric code. This means that in the presence of the full perturbation $V = E_J V_J + E_M V_M$, Cooper pair and single electron hopping, the transfer of Cooper pairs increases the gap of the toric code in leading order. In sixth order, we obtained a nearest neighbour plaquette interaction improving the stabilisation further. In the remaining part of the thesis, we investigate lattice gauge order parameters that allow us to distinguish the topological toric code phase from the non-topological ones. Prior to that, we give a quick review of how to reproduce the above Brillouin-Wigner calculation with the method of Schrieffer-Wolff transformation.

4.1.5 Alternative Schrieffer-Wolff transformation

Besides the aforementioned Brillouin-Wigner perturbation, multiple other schemes to perform perturbative calculations exist. A method particularly useful to determine effective Hamiltonians for a subspace of possibly degenerate states is the Schrieffer-Wolff transformation. A comprehensible introduction to the matter is for example given in Appendix B of Ref. [38]. We assume a Hamiltonian $H = H_0 + V$ that decomposes into an unperturbed part H_0 and the perturbation V. If the spectrum of H_0 consists of subspaces that are separated on a scale $\gg \mathcal{O}(V)$, this transformation provides a means to block diagonalise the full Hamiltonian into two separate subspaces to a chosen order in V. With the block off-diagonal generator S this is written as

$$H_{\text{eff}} = \mathrm{e}^{S}\ (H_0 + V_{\text{d}} + V_{\text{od}})\ \mathrm{e}^{-S}\,, \tag{4.20}$$

where H_{eff} is block diagonal and we split the perturbation in a block diagonal part V_{d} and block off-diagonal part V_{od}. Since the generator S is in general not straightforward to calculate, the Taylor series of the exponentials is inserted instead. Eq. (4.20) can then be separated into a block diagonal and off-diagonal equation. Choosing the off-diagonal equation to vanish up to a desired order in V then yields the respective series for the generator. By plugging the result into the equation for the block diagonal part, we obtain the effective Hamiltonian up to the chosen order.

This procedure gets increasingly complicated at high order, for example the sixth order used in our calculations. Therefore, Ref. [39] formulates a diagrammatic technique to identify all necessary terms and translate them to the operator formalism. The effective Hamiltonian then follows to be

$$H_{\text{eff}} = H_0 P_- + P_- V P_- + \sum_{n=2}^{\infty} \sum_{T \in \mathcal{T}(n)} w(T) O(T)\,. \tag{4.21}$$

The first two terms coincide with those in Eq. (4.12), where P_- is again the projection onto the ground state space. For the remaining orders $n > 2$ we have to determine the set of all valid diagrams $\mathcal{T}(n)$ and formulate their operator representation $O(T)$ with the corresponding weight $w(T)$. The considered diagrams are tree diagrams. They are graphs with nodes and edges, where the top node, without superiors, is referred to as root. Edges emanating from this root, the branches, connect it to subsequent nodes, the children. Terminating nodes, *i.e.*, those without children, are called leaves.

The set of allowed trees has to satisfy the two rules:

- The root has an odd number of children.
- Every node that is not the root has either only one child or an even number of children.

In Fig. 4.6 a range of valid tree structures is depicted. Additionally, Ref. [39] gives an inductive definition to obtain the operator formulation of each node bottom up together with the respective tree weights. This, we will not repeat in detail. We rather focus on important remarks for the specific model considered in this thesis. In the course of the calculation, the linear operator mapping $\mathcal{L}(X) = \sum_{i,j} X_{ij}/(E_i - E_j) \, |i\rangle \langle j|$ is introduced, which behaves roughly like the Green's function in the Brillouin-Wigner theory. However, it is defined to be zero for the block-diagonal part of an operator X. This ensures that the energy difference is exclusively taken for states from distinct subspaces and makes this method especially useful in the case of degenerate states.
The separation of the perturbation into V_d and V_od tells us that an even number of V_od has to enter valid contributions. Furthermore, in the model at hand, we are interested in non-constant plaquette contributions so that we only want to keep diagrams that can generate at least one connected fourth order correction. Thus, the block diagonal part V_d needs to enter such a term at least twice. This can be seen since only V_d allows for a process connecting states from within the high energy subspace. The latter in turn is necessary for corrections that generate a charge flow around a plaquette before returning to the charge-less ground state space (cf. Fig. 4.3). In contrast to that, the perturbation V_od necessarily links states from distinct subspaces. With this knowledge, we analyse the rules for the operator formulation in Ref. [39] and observe that only those nodes, which are not a root and have exactly a single child contribute the desired V_d. This enables us to exclude constant terms in the effective Hamiltonian already on the diagrammatic level. Up to sixth order, the tree diagrams yielding plaquette contributions are depicted in Fig. 4.6.

The nodes contributing the block diagonal part V_d are displayed in gray. We find that at fourth and fifth order there is only one allowed tree. In sixth order, counting all possible permutations in the branches of the trees, there are 13 contributions. For comparison, at order $n = 4, 5, 6$ there are in theory $|\mathcal{T}(n)| = 3, 7, 20$ valid diagrams [39] so that we already exclude half of them. Retrieving the operator formulation is still a tedious task, which we do not present explicitly. Instead, we list the translation of the tree contributions to the previous Brillouin-Wigner language.

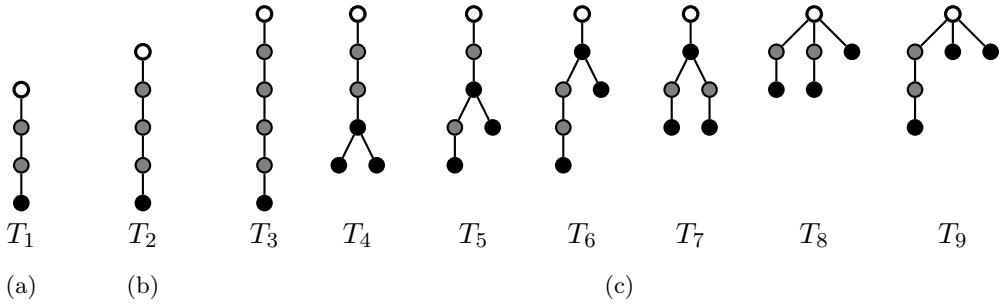

Figure 4.6: Tree diagrams of different orders n contributing to non-constant terms in the effective Hamiltonian calculated with a Schrieffer-Wolff transformation. The roots are depicted in white and all nodes contribution diagonal perturbations V_d are colored in gray. The remaining nodes giving off-diagonal perturbations V_od are black. There is one diagram (a) for order $n = 4$, one (b) for order $n = 5$ and 13 (c) for order $n = 6$, where we also count all permutations of the branches.

Starting with the first three trees and denoting the projections analogously to the previous section, we find

$$w(T_1)O(T_1) = P_-\ V_\mathrm{od}G_0(0)[V_{\mathrm{d}++}G_0(0)]^2V_\mathrm{od}\ P_- \tag{4.22}$$

$$w(T_2)O(T_2) = P_-\ V_\mathrm{od}G_0(0)[V_{\mathrm{d}++}G_0(0)]^3V_\mathrm{od}\ P_- \tag{4.23}$$

$$w(T_3)O(T_3) = P_-\ V_\mathrm{od}G_0(0)[V_{\mathrm{d}++}G_0(0)]^4V_\mathrm{od}\ P_-\,. \tag{4.24}$$

Thus, the single branched trees correspond to the terms in Eq. (4.12) that are obtained without the self consistent energy expansion. The fact that a tree is branched out therefore means that those are contributions from the iterative energy corrections. For the remaining diagrams we then find

$$\begin{aligned}\sum_{\mathcal{P}}\sum_{m=4}^{9} w(T_m)O(T_m) = P_-\ \big[\ & V_\mathrm{od}G_0(0)M^2G_0(0)V_\mathrm{od}\ \cdot\ V_\mathrm{od}G_0(0)V_\mathrm{od} \\ & + V_\mathrm{od}G_0(0)[V_{\mathrm{d}++}G_0(0)]^2V_\mathrm{od}\ \cdot\ V_\mathrm{od}[G_0(0)]^2V_\mathrm{od}\big]\ P_-\,,\end{aligned} \tag{4.25}$$

with
$$M^2 = 2G_0(0)V_{\mathrm{d}++}G_0(0)V_{\mathrm{d}++} + V_{\mathrm{d}++}[G_0(0)]^2V_{\mathrm{d}++}\,. \tag{4.26}$$

The first sum runs over all branch permutation $\mathcal{P}$ of the diagrams. Thus, we met our goal of reproducing the effective Hamiltonian description previously obtained with Brillouin-Wigner perturbation theory. Note that this section should merely pose as a guidance if one is interested to reproduce the results from the previous section using the Schrieffer-Wolff transformation. Detailed calculations do not result in additional physical insight into the analysed topological order.

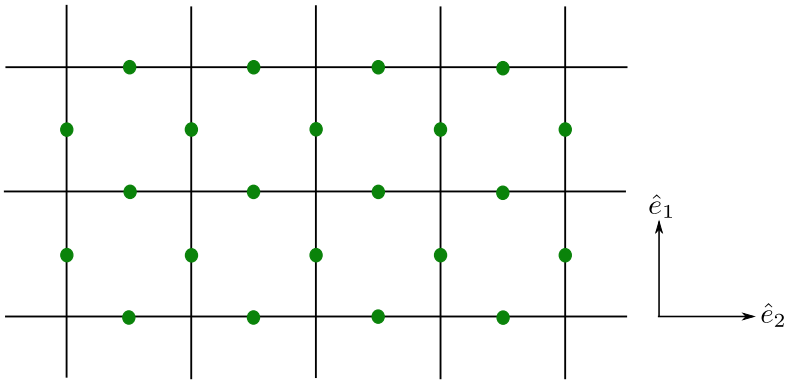

Figure 4.7: Sketch of the two dimensional square lattice, with $\mathbb{Z}_2$ gauge DOF σ_{ij} (green dots) placed centrally on the links. With this system, we can construct a $\mathbb{Z}_2$ lattice gauge theory. Using this setup one can realise the toric code (cf. Sec. 2.1).

This completes our calculations of the effective Hamiltonian and we move on to the study of lattice gauge theories and their respective order parameters.

4.2 Order parameters in lattice gauge theories

In this section, different order parameters of lattice gauge theories are analysed. We start with the Wilson loop order parameter and subsequently construct a generalisation of it, the Fredenhagen-Marcu operator. The Wilson loop diagnostic works in a system with only gauge degrees of freedom, where it can be linked to the potential between static external matter charges. It fails, however, for lattice gauge theories with gauge as well as matter fields, where the matter is dynamical. Under these circumstances, the Fredenhagen-Marcu operator is applicable. The model investigated in the thesis falls into the latter category.

4.2.1 Wilson loops

As we will find local order parameters to fail as diagnostic in the gauge theory analysed in this thesis, we have to get acquainted with the concept of a non-local order parameter. Therefore, we focus on a lattice gauge theory of pure gauge DOF and discuss the Wilson loop. We take the system in Fig. 3.5 and remove the matter DOF such that we are left with the spins on the links of the two dimensional square lattice (cf. Fig. 4.7).
As Hamiltonian we consider

$$H = -\Delta \sum_i \prod_{\square} \sigma^z - \frac{1}{\Delta} \sum_{<i,j>} \sigma^x_{ij} \,, \tag{4.27}$$

$$\text{with} \quad Q_i \left|\text{phys}\right\rangle = \left|\text{phys}\right\rangle \,, \qquad \text{where} \quad Q_i = \prod_{+} \sigma^x \,. \tag{4.28}$$

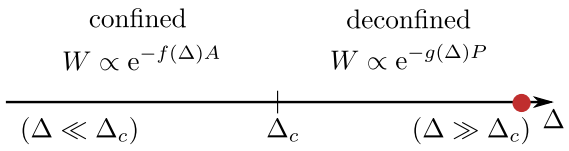

Figure 4.8: Phase diagram of the two dimensional quantum Ising gauge model. The model has a confined and a deconfined phase depending on the value of the coupling Δ relative to the critical value Δ_c. Deep in the deconfined phase we find the toric code (red circle). The order parameter is given by the Wilson loop W which satisfies an area law in the confined, and a perimeter law in the deconfined phase.

This is the two dimensional quantum Ising gauge model [21]. To discuss this system, it is most intuitive to consider the σ^z-basis. The coupling strength of spins around a plaquette is given by Δ, while the term proportional to $\frac{1}{\Delta}$ introduces disorder on each individual spin placed on a link. For $\Delta \gg 1$, this model realises the toric code (cf. Sec. 2.1). The Hamiltonian has a local gauge symmetry Eq. (4.28). Locality refers to the fact that the operators involved in Q_i are contained in a spatially bounded region of the system, which is independent of the lattice size. The goal of this section is to construct an order parameter that can distinguish the two phases of the system,the confined and the deconfined one, as we will find out (cf. Fig. 4.8). We follow the treatment of Ref. [21]. To realise the importance of non-locality, it is worthwhile to initially take a step back to the quantum Ising model

$$H = -\tilde{\Delta} \sum_{\substack{< i,j > \\ < j,k >}} \sigma^z_{ij}\sigma^z_{jk} - \frac{1}{\tilde{\Delta}} \sum_{<i,j>} \sigma^x_{ij}\,. \tag{4.29}$$

The disorder term remains unchanged, but the four point interaction is replaced by nearest neighbouring coupling of two spins. The Hamiltonian in Eq. (4.29) possesses only a global $\mathbb{Z}_2$ symmetry $\mathcal{Q} = \prod_{<ij>} \sigma^x_{ij}$. The model in Eq. (4.29) realises two phases. For dominant nearest neighbour coupling $\tilde{\Delta}$ the spins are aligned, describing a magnetised system (ferromagnet). There, the global symmetry is spontaneously broken. If in turn the transverse magnetic field $1/\tilde{\Delta}$ dominates, the system is completely disordered (paramagnet) with respect to the operator σ^z. The order parameter to distinguish these two phases is the magnetisation m_{ij}. It is calculated as

$$m_{ij} = \langle G|\sigma^z_{ij}|G\rangle = \begin{cases} \neq 0 & \text{magnetised} \\ = 0 & \text{unmagnetised} \end{cases}, \tag{4.30}$$

with the ground state $|G\rangle$. This operator is highly local as it involves only a single spin. Going back to Eq. (4.27), the straightforward expectation is that we analogously find an ordered and disordered phase for the quantum Ising gauge model. Due to the *local* gauge symmetry in Eq. (4.28), however, the construction of a local magnetisation as

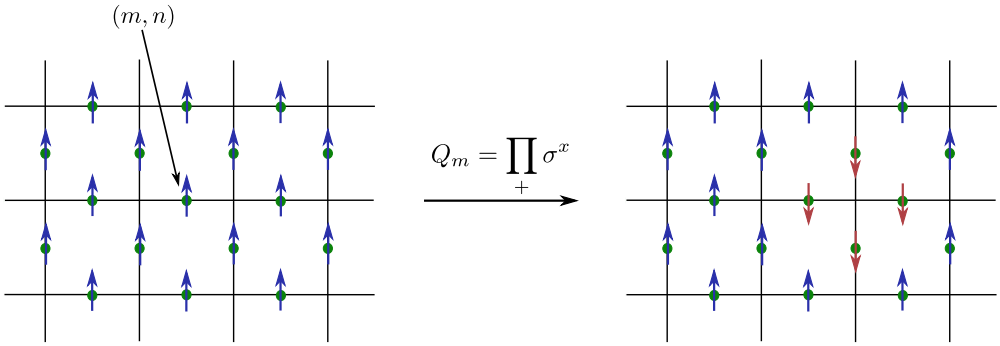

Figure 4.9: On the left there is the two dimensional square lattice without frustrated plaquettes. This is expressly fulfilled as even all individual spins are aligned. After the action of a local gauge transformation on the spins around node m, we see that locally the magnetisation of the individual spins is flipped. The plaquettes, however, remain not frustrated.

order parameter is impossible. To see this, imagine the $\Delta \to \infty$ limit where we for now assume that all spins in the system are in the $+1$ eigenstate of σ^z. This state definitely has a finite local magnetisation on an arbitrary but fixed spin σ_{mn}. Furthermore, we know that the energy of the state is independent of the specific gauge choice. If we apply Q_m on a node m that lies at the endpoint of the fixed link (m, n), the resulting state should describe the state of the system equally well. This transformation is depicted in Fig. 4.9, where we refer to a plaquette with $\prod_\square \sigma^z = -1/1$ as frustrated/ not frustrated. We can see that by applying the local gauge transformation, the magnetisation locally changes, without any energy penalty. The gauge invariant ground state in the $\Delta \to \infty$ limit is given by the equal weight superposition

$$|G\rangle = \sum_i \frac{1}{\sqrt{2}} (1 + Q_i) |0\rangle \ , \tag{4.31}$$

where $|0\rangle$ is the state with all individual spins being in the $+1$ eigenstate of σ^z. Since every gauge choice has the same weight, $|G\rangle$ must have a vanishing local magnetisation $m_{ij} = 0$ regardless of the system in Eq. (4.27) being in the ordered phase. This means that there is no local order parameter for the system with a local gauge symmetry. This statement was proven by Eliztur for Abelian theories and later generalised. His theorem says that a local gauge symmetry cannot be broken [40].[1] As a consequence, only a gauge invariant non-local operator can be a candidate order parameter for the system at hand. The correct order parameter is the Wilson loop [21], which was proven by Wegner [15] originally for the classical isotropic Ising gauge model.

[1] An important application of this theorem is the Anderson-Higgs mechanism. According to the theorem, the mechanism can only be associated with a spontaneous breaking of a global gauge symmetry. Not a local one, which is sometimes stated in the literature. A discussion of this can be found in Appendix D.

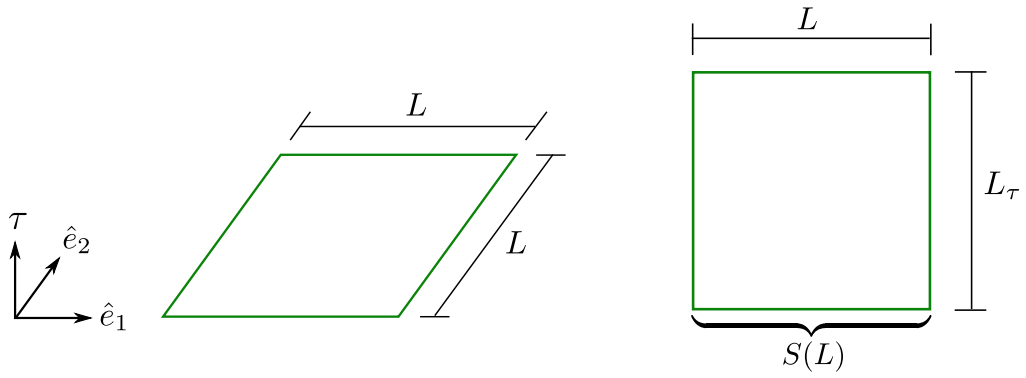

(a) Space-space Wilson loop

(b) Space-time Wilson loop

Figure 4.10: Visualisation of the Wilson loop order parameter. In (*a*) the space-space Wilson loop is displayed. The green line denotes the gauge spins σ_l^z along a square of side length L. In panel (*b*) the space-time Wilson loop is depicted, where one of the directions is the imaginary time direction τ. In this case, we allow a different length L_τ in temporal direction, enabling anisotropy. The strings of gauge spins at a given imaginary time are denoted as $S(L)$.

Space-space formulation

In an isotropic system, the directions in which the loop extends are arbitrary, but in case of the (2+1) dimensional quantum Ising gauge model in Eq. (4.27), we have to distinguish between the space-space and space-time formulation (cf. Fig. 4.10). The latter model is obtained from the classical three dimensional Ising gauge theory, analysed by Wegner, considering the anisotropic limit in the temporal direction. An analogous calculation is performed in Appendix E for the Majorana toric code model. The space-space operator formulation of the Wilson loop is given by

$$W(L) = \langle G| \prod\nolimits_{l\in\mathcal{C}} \sigma_l^z |G\rangle \ . \tag{4.32}$$

The contour C is a square of side length L (cf. Fig. 4.10(a)). Thus, the L dependence on the left hand side of Eq. (4.32) stems from this implicit dependence in $\mathcal{C}$. Therefore, the Wilson loop is given by the product of gauge DOF along the links l of a square on the lattice. This space-space formulation yields the ground state expectation of a square loop of side length L, which is connected to the fluctuation in the gauge field over distance. It is a gauge invariant measure of the correlation between gauge fields, that are a distance L apart.

Space-time formulation

The space-time formulation of the Wilson loop requires additional work. We define the imaginary time dependent gauge spin operators per link l as [22]

$$\sigma_l^z(\tau) = \mathrm{e}^{-H\tau}\ \sigma_l^z\ \mathrm{e}^{H\tau}\,. \tag{4.33}$$

Furthermore, we use the gauge freedom in Eq. (4.28) to fix all time-like links l' to $\sigma_{l'}^z = 1$. This is called the temporal gauge. The length of the loop in imaginary time is given by $L_\tau = v\mathcal{T}$, where we assume the velocity v to be unity. This results in an operator formulation for the space-time loop of

$$W(L,\mathcal{T}) = \langle G|\, S(L,0)\ \ S(L,-\mathcal{T})\,|G\rangle\ . \tag{4.34}$$

This is a gauge dependent formulation and the remaining spatial lines of the loop at different time slices are defined as $S(L,\tau) := \prod_{l\in S_L}\sigma_l^z(\tau)$, where S_L is the curve of links that yields this string (cf. Fig. 4.10(b)). For convenience, we choose the strings to be at times $\tau = -\mathcal{T}$ and $\tau = 0$. This operator can be shown to have implications for the potential between two external static charges. The externality is due to the fact that we only consider the gauge field in our theory so far. Starting from Eq. (4.34) we find

$$\begin{aligned} W(L,\mathcal{T}) &= \langle G|\, S(L)\ \mathrm{e}^{-H\mathcal{T}} S(L)\ \mathrm{e}^{H\mathcal{T}}\,|G\rangle && (4.35)\\ &= \mathrm{e}^{E_G\mathcal{T}}\,\langle G|\, S(L)\ \mathrm{e}^{-H\mathcal{T}} S(L)\,|G\rangle && (4.36)\end{aligned}$$

Shifting the ground state energy E_G to zero and introducing the spectral decomposition of the transfer matrix $\mathrm{e}^{-H\mathcal{T}}$, we obtain

$$\begin{aligned} W(L,\mathcal{T}) &= \sum_n \langle G|\, S(L)\ \mathrm{e}^{-E_n\mathcal{T}}\,|n\rangle\langle n|\, S(L)\,|G\rangle && (4.37)\\ &= \sum_n \mathrm{e}^{-E_n\mathcal{T}}|\langle G|\, S(L)\,|n\rangle|^2\,. && (4.38)\end{aligned}$$

If we consider $\mathcal{T}\to\infty$, we can approximate the sum by the state n' of lowest energy $E_{n'}$ that still has an overlap with the state $S(L)\,|G\rangle$. Assuming we are in a general system, where $S(L)\,|G\rangle$ is not necessarily an eigenstate of H. This yields

$$\lim_{\mathcal{T}\to\infty} W(L,\mathcal{T}) \approx \mathrm{e}^{-E_{n'}\mathcal{T}}|\langle G|\, S(L)\,|n'\rangle|^2\,. \tag{4.39}$$

Making the L dependence of the energy of this intermediate state explicit, we have

$$\lim_{\mathcal{T}\to\infty} W(L,\mathcal{T}) \propto \mathrm{e}^{-E_{n'}(L)\mathcal{T}}\,. \tag{4.40}$$

If two external charges, that couple to the gauge field, were placed at distance L at time τ, this would have exactly the same effect on the gauge DOF as $S(L,\tau)$. The endpoints of the string of gauge fields are fixed. The energy $E_{n'}(L)$ of this state n' thus corresponds to the potential $V(L)$ between two external static charges that are placed a distance L apart. The connection is captured in the formula

$$V(L) \propto -\lim_{\mathcal{T}\to\infty} \frac{1}{\mathcal{T}} \ln\left[W(L,\mathcal{T})\right] . \tag{4.41}$$

With this, we move on to the evaluation of the Wilson loop.

Evaluation

The space-space formulation of the Wilson loop is straightforward as it is independent of time. Thus, we calculate it with time independent perturbation theory. For the Hamiltonian in Eq. (4.27) we obtain

$$W(L) \propto \begin{cases} \exp\left(-\left|\ln\left[\Delta^2\right]\right| L^2\right) & \Delta \ll \Delta_c \\ \exp\left[-\left(\frac{1}{\Delta}\right)^4 L\right] & \Delta \gg \Delta_c \end{cases} \tag{4.42}$$

such that the Wilson loop decays much slower in the ordered phase. For $\Delta \gg \Delta_c$ the gauge DOF around a plaquette are nearly aligned, whereas strong disorder $\Delta \ll \Delta_c$ induces large fluctuations in the gauge DOF, leading to the faster decay of correlation. The detailed calculations are not shown. The general procedure is analogous to the calculations in Sec. 4.3. The result in Eq. (4.42) can be recast in the form

$$W(L) = \begin{cases} \mathrm{e}^{-f(\Delta)A} & \Delta \ll \Delta_c \\ \mathrm{e}^{-g(\Delta)P} & \Delta \gg \Delta_c \end{cases} . \tag{4.43}$$

The prefactors are in general functions f, g depending on the coupling constants in the problem. The area/perimeter of the loop is denoted with A/P, respectively. This so called area and perimeter law is analogously obtained for the isotropic three dimensional Ising gauge model [21]. In the latter case one can use the space-time interpretation which gives

$$V(L) = \begin{cases} \tilde{f}(\Delta)L & \Delta \ll \Delta_c \\ \tilde{g}(\Delta) & \Delta \gg \Delta_c \end{cases} , \tag{4.44}$$

where we use that $A = L \cdot \mathcal{T}$, $P \propto \mathcal{T}$. Note that the coupling Δ in the last expression stems from the three dimensional Ising model. As it qualitatively agrees with the one we used so far, we did not explicitly change the labelling. In the disordered phase there is a linear potential between external static charges indicating a confining phase. In the

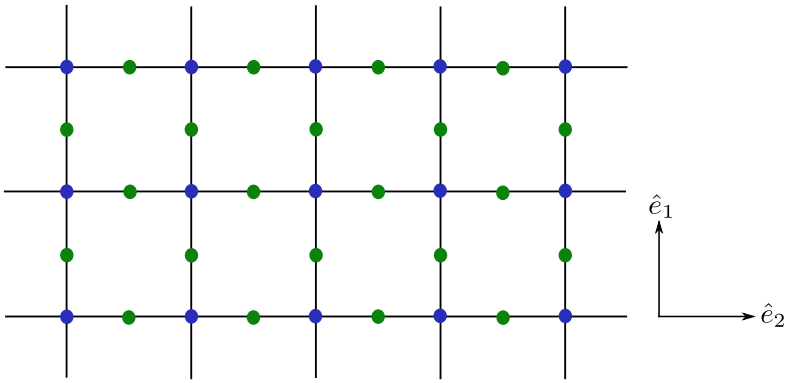

Figure 4.11: Sketch of the two dimensional square lattice, with $\mathbb{Z}_2$ gauge DOF σ_{ij} (green dots) placed centrally on the links and $\mathbb{Z}_2$ matter fields τ_i (blue dots) on the nodes. In other words a $\mathbb{Z}_2$ lattice gauge theory with $\mathbb{Z}_2$ matter.

ordered phase we obtain a constant, *i.e.*, deconfining potential. Thus, we showed that the Wilson loop is a diagnostic for the different phases in Fig. 4.8.

In this section, we saw the necessity of a non-local order parameter for the pure gauge theory in Eq. (4.27) and found the Wilson loop to properly distinguish the phases of the system. Furthermore, we made the connection of the Wilson loop to the potential between external static charges, *i.e.* infinitely heavy matter. The full lattice gauge model of the Majorana toric code in Eq. (3.16) on the other hand contains a light dynamical matter field. The addition of matter DOF on the nodes of the lattice is considered in the following section.

4.2.2 Fredenhagen-Marcu order parameter

Before we can diagnose the signatures of topological in the lattice gauge model of the Majorana toric code, we need to find an order parameter for a system containing dynamical matter. This is necessary since the Wilson loop exhibits a perimeter law everywhere in the presence of dynamical matter [41]. Therefore, we add $\mathbb{Z}_2$ matter DOF on the nodes of the two dimensional square lattice of the previously investigated pure gauge theory (cf. Fig. 4.11). We start with a $\mathbb{Z}_2$ matter field as it couples most naturally to the $\mathbb{Z}_2$ gauge field.

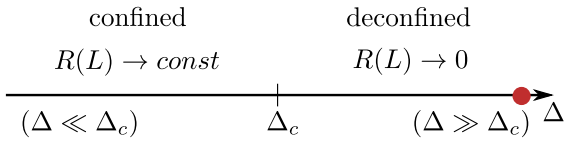

Figure 4.12: Phase diagram of the two dimensional quantum Ising gauge model with Ising matter. The diagram is sketched for a small but finite matter coupling λ, *i.e.*, heavy dynamical matter. The model has a confined and a deconfined phase depending on the value of the coupling Δ between the gauge DOF relative to the critical value Δ_c. Deep in the deconfined phase we find the toric code (red circle). The proper order parameter is the Fredenhagen-Marcu operator $R(L)$. In the large L limit this operator decays to zero in the deconfined and approaches a constant in the confined phase.

The full Hamiltonian of this system is the lattice gauge theory of Ising gauge coupled to Ising matter [20].

$$H = -\Delta \sum_i \prod_{\square} \sigma^z - \frac{1}{\Delta} \sum_{<i,j>} \sigma^x_{ij} - \lambda \sum_{<i,j>} \tau^z_i \sigma^z_{ij} \tau^z_j - \frac{1}{\lambda} \sum_i \tau^x_i \,, \tag{4.45}$$

$$\text{with} \quad Q_i \left|\text{phys}\right\rangle = \left|\text{phys}\right\rangle \,, \qquad \text{where} \quad Q_i = \tau^x_i \prod_{+} \sigma^x \,. \tag{4.46}$$

In addition to the pure gauge field terms in the first line of Eq. (4.45), that we are familiar with from the previous section, there are two matter field terms. The interaction between nearest neighbour matter DOF is not only determined by the coupling strength λ, but also by the value of the gauge DOF on the link between them. Analogous to the gauge field term, there is a disorder term for the matter field, with strength $1/\lambda$. Lastly, the gauge constraint in Eq. (4.46) connects the matter DOF on the node to the gauge spins on the links emanating from it. It is again comparable to a discrete version of Gauss' Law. The phase diagram of this model was investigated in Ref. [41]. For fixed, small but finite λ a confinement/deconfinement transition was found (cf. Fig. 4.12). Thus, similar to the model in the previous section, the phase diagram is non-trivial and a phase transition occurs for a critical coupling Δ.

For small but finite λ this system contains heavy dynamical matter and it was shown that the Wilson loop exhibits perimeter law decay for all parameter choices of Δ

$$W(L) = \begin{cases} \mathrm{e}^{-f(\lambda)P} & \Delta \ll \Delta_c \\ \\ \mathrm{e}^{-g(\Delta)P} & \Delta \gg \Delta_c \end{cases} . \tag{4.47}$$

In other words, after the introduction of dynamical instead of external infinitely heavy matter, the Wilson loop no longer distinguishes the confined from the deconfined phase.

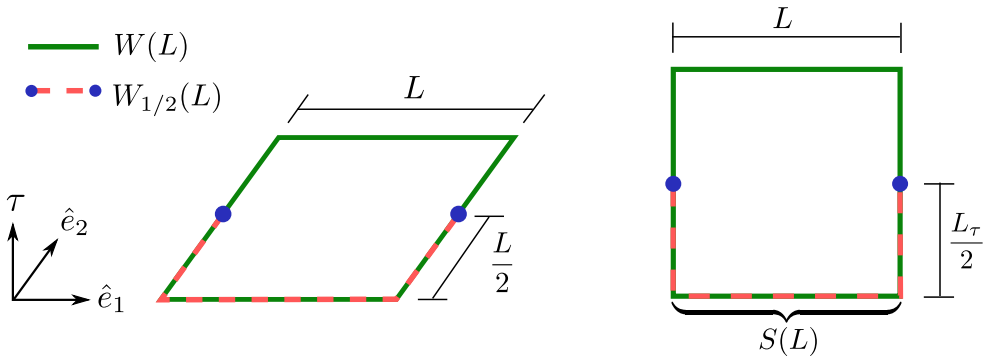

(a) Equal-time version

(b) Fredenhagen-Marcu

Figure 4.13: Visualisation of the Fredenhagen-Marcu order parameter. In (a) there is the equal-time version. The green line denotes the gauge spins σ_l^z along a square of side length L, a space-space Wilson loop. The red dashed line depicts a half Wilson loop, with matter DOF (blue) at the endpoints. In panel (b) the original Fredenhagen-Marcu operator is displayed, where one of the directions is the imaginary time direction τ. The strings of gauge spins at a given imaginary time are denoted as $S(L)$.

Instead, different mechanisms lead to a perimeter law everywhere, which is indicated in Eq. (4.47) already by the different coupling constants Δ and λ in the prefactor of the perimeter decay in the two regimes. In contrast to the area law in the pure gauge theory in the Eq. (4.27), the term propotional to λ (cf. Eq. (4.45)) introduces matter charges that can flow around the perimeter of a loop yielding a perimeter decay even for $\Delta \ll \Delta_c$. Thus, the perimeter decay is purely due to the dynamical matter field, while for $\Delta \gg \Delta_c$ the gauge field pre-dominantly induces it. In conclusion, the Wilson loop is insensitive to the two different mechanisms (gauge and matter dominated) that both induce a perimeter decay depending on the coupling strenght. Therefore, a proper diagnostic should still be non-local due to the gauge constraint but furthermore detect the mechanism leading to the perimeter law. A working order parameter was introduced by Fredenhagen and Marcu [16] as a space-time operator in the context of quark confinement and later adapted in different operator formulations for general lattice gauge models in Ref. [22].

There exist three different operator formulations depending on the space-time orientation of the non-local operators [22], out of which we will discuss two, the equal-time formulation and the original Fredenhagen-Marcu operator.

Equal-time formulation

As for the Wilson loop, we find that the operator formulation of the equal-time version is rather straightforward. We have again a space-space Wilson loop

$$W(L) = \langle G| \prod\nolimits_{l\in\mathcal{C}} \sigma_l^z \, |G\rangle \ , \tag{4.48}$$

where the contour $\mathcal{C}$ is a square of side length L. Additionally, there is a half Wilson loop also in space-space direction, which is terminated with matter DOF at the endpoints of the contour $C_{1/2}$. The matter fields have to be added in order to obtain a gauge invariant quantity. This half Wilson loop is depicted in Fig. 4.13(a) and yields an operator formulation

$$W_{1/2}(L) = \langle G| \, \tau_s^z \prod\nolimits_{l\in\mathcal{C}_{1/2}} \sigma_l^z \ \tau_{s'}^z \, |G\rangle \ . \tag{4.49}$$

The positions of the matter spins at the endpoints of the open gauge strings are labelled s and s', respectively. The equal-time formulation of the operator $R(L)$ is then constructed as the quotient of the half Wilson loop $W_{1/2}$ and the square root of the Wilson loop W as

$$R(L) = \frac{W_{1/2}(L)}{\sqrt{W(L)}} \, . \tag{4.50}$$

The key feature there is the half Wilson loop. In contrast to the closed Wilson loop, it cannot be generated purely using the gauge fields, since first the matter charges have to be annihilated. The quotient R then teases out the leading mechanism that dominates the decay of the Wilson loop. It compares the expectation value $W_{1/2}$ that definitely involves the mechanism of flowing matter to the mechanism insensitive Wilson loop W. That this works most clearly be seen graphically, where we follow the treatment in Ref. [22].

We refer to nearest neighbour hopping of matter DOF (proportional to λ in Eq. (4.45)) as edges and aligned gauge DOF around plaquettes (proportional to Δ in Eq. (4.45)) as surfaces. Since the perimeter of a square of side length L is considerably smaller than its area for large L, the system will generate the (half) Wilson loop both by mainly constructing its perimeter with edges. More generally, we can say that large loops will always be dominantly covered by edges as opposed to surfaces, as long as $\lambda \gtrapprox \Delta$ (cf. Fig. 4.14(a)). Therefore, the numerator and denominator in Eq. (4.50) then have the same scaling behaviour. Except when surfaces are much cheaper than edges. This is the case when the matter field is considerably heavy, while the gauge field is ordered $\Delta \gg \lambda$. Then the closed loop gets filled with surfaces. The open loop is equivalently covered with surfaces, but the remaining (L dependent) line has to be covered by expensive edges (cf. Fig. 4.14(b)). Thus, the numerator decays much faster than the denominator. Central

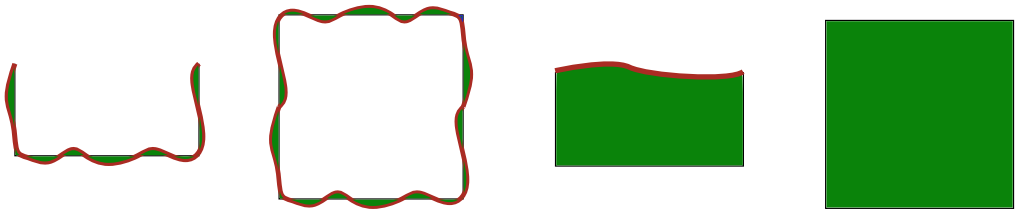

(a) (b)

Figure 4.14: Graphical evaluation of the equal-time version of the Fredenhagen-Marcu order parameter. In (a) open and closed loop are covered mostly with edges (red) as opposed to surfaces (green). In panel (b) the closed loop is covered completely with surfaces, while for the open loop there have to be edges introduced that close the loop.

to these scaling behaviours is the necessity of matter flow (edges) in the generation of the half Wilson loop. In conclusion, we have that

$$\lim_{L\to\infty} R(L) = \begin{cases} 0 & \Delta \gg \lambda \\ const & \text{else} \end{cases} . \tag{4.51}$$

Either the numerator decays faster or the scaling is equal up to a constant. By taking the $\lambda \to 0$ limit, we can rewrite Eq. (4.45) as

$$H = -\Delta \sum_i \prod_{\square} \sigma^z - \frac{1}{\Delta} \sum_{<ij>} \sigma^x_{ij} - \frac{1}{\lambda} \sum_i \prod_{+} \sigma^x \,, \tag{4.52}$$

where we replaced $\tau^x_i = \prod_{+} \sigma^x$ via the gauge constraint. If also $\Delta \to \infty$, we find an emergent toric code, which we know from the previous chapter to come with deconfined external charges. Using this we can infer

$$\lim_{L\to\infty} R(L) = \begin{cases} 0 & \text{deconfined} \\ const & \text{confined} \end{cases} . \tag{4.53}$$

This connection can be made more explicit by considering the original Fredenhagen-Marcu order parameter. As we will see, it can be related to confinement and deconfinement of the dynamical matter charges.

Fredenhagen-Marcu operator

The original Fredenhagen-Marcu order parameter is equivalent to the one discussed above, except that a spatial direction is exchanged for the imaginary time direction (cf. Fig. 4.13(b)). We construct the operator formulation along the lines of Ref. [22]. We assume that the two matter spins τ_s and $\tau_{s'}$ lie at the same time slice, which we set to $\tau = 0$. Choosing the temporal gauge and performing the imaginary time propagation

analogously to Eq. (4.33), we find that

$$W_{1/2}(L,\mathcal{T}) = \langle G|\, \tau_s^z(0)\tau_{s'}^z(0)\ S(L,-\mathcal{T}/2)\,|G\rangle\ . \tag{4.54}$$

The gauge flux generated from charges at s and anti-charge at s' gets introduced at time $-\mathcal{T}/2$ and the respective charges are created at time zero. Using a unit velocity v, we choose $v\mathcal{T} = L_\tau = L$ such that the loop only has L dependence. For the Wilson loop we have

$$\begin{aligned} W(L) &= \langle G|\, S(L,\mathcal{T}/2)\ \ S(L,-\mathcal{T}/2)\,|G\rangle \\ &= \langle G|\, S(L,\mathcal{T}/2)\tau_s^z(0)\tau_{s'}^z(0)\ \ \tau_s^z(0)\tau_{s'}^z(0)S(L,-\mathcal{T}/2)\,|G\rangle\ . \end{aligned} \tag{4.55}$$

We explicitly add and remove the matter charges for convenience. We define a state where we added a matter charge and anti-charge, that are a distance L apart, to the ground state as

$$|S(L)\rangle = \tau_s^z(0)\tau_{s'}^z(0)\ S(L,-\mathcal{T}/2)\,|G\rangle\ . \tag{4.56}$$

If we assume the distance to go to infinity, we can focus on the matter charge and neglect the anti-charge at infinity. Thus, the state $|S(L\to\infty)\rangle$ can be interpreted as a free charge state. Applying the reformulation to the (half) Wilson loop gives

$$W_{1/2}(L) = \langle G|S(L)\rangle \qquad \text{and} \qquad W(L) = \langle S(L)|S(L)\rangle\ . \tag{4.57}$$

The Fredenhagen-Marcu operatoris rewritten to

$$R(L) = \frac{W_{1/2}(L)}{\sqrt{W(L)}} = \frac{\langle G|S(L)\rangle}{\sqrt{\langle S(L)|S(L)\rangle}}\,, \tag{4.58}$$

i.e., the overlap between the ground state and the normalised charge anti-charge state. Taking the $L\to\infty$ limit indicates a phase containing free (deconfined) charge states $|S(L\to\infty)\rangle$ only if $R(L)$ decays to zero. Since there the state is orthogonal to the ground state. If in turn there is a finite overlap, the state $|S(L)\rangle$ would decay into the ground state [16, 22]. Therefore, we write

$$\lim_{L\to\infty} R(L) = \begin{cases} 0 & \text{deconfined} \\ const & \text{confined} \end{cases}\ . \tag{4.59}$$

This diagnostic was first proposed in Ref. [16] to test whether a theory contains free or confined quarks. The general idea is that if the potential is confining, no free quarks can exist, as for a large distance L between the quark anti-quark pair, the energy would be infinite. Thus, it is high enough for each quark to decay into hadrons, provided those are part of the theory. From a quark perspective, this would leave behind the ground state.

This is exactly captured by the overlap between $|S(L)\rangle$ and $|G\rangle$. The normalisation is necessary as the confining potential leads to infinite energy in the system for $L \to \infty$ if we would only consider the quark anti-quark state.

Evaluation

For evaluation purposes, the equal-time version of the Fredenhagen-Marcu operator is preferred since the calculations can again be performed with time independent perturbation theory. The calculations are not given explicitly. For a small but finite λ, we find that

$$R(L) \approx \begin{cases} \exp\left\{-\left|\ln\left(\frac{\lambda}{2}\right)\right|L\right\} & \Delta \gg \Delta_c \\ \frac{\left[\frac{\lambda^2}{4}\right]^{2L}}{\sqrt{\left[\frac{\lambda^2}{4}\right]^{4L}+\left[\frac{\Delta^2}{8}\right]^{L^2}}} & \Delta \ll \Delta_c \end{cases} . \tag{4.60}$$

For $\Delta \gg \Delta_c$ we obtain an exponential decay depending on L, the distance between the charge anti-charge pair. Thus the numerator of $R(L)$ decays faster than the denominator. This can be understood from Fig. 4.14(b). In this phase, the gauge fields are ordered yielding a perimeter decay of closed loops. To bridge the gap of the open loop, we initially have to annihilate the charge with the anti-charge over a distance L. The latter is exponentially suppressed for a strongly fluctuating matter field (λ small). If however the gauge fields strongly fluctuate as well, $\Delta \ll \Delta_c$, large open and closed loops are generated through matter charges flowing along their perimeter. This is visualised in Fig. 4.14(a) and can be seen in Eq. (4.60) since for large L, the perimeter decay dominates the denominator. Thus, the scaling behaviour of numerator and denominator are equal for $\Delta \ll \Delta_c$. Taking the limit yields

$$\lim_{L\to\infty} R(L) = \begin{cases} 0 & \Delta \gg \Delta_c \\ 1 & \Delta \ll \Delta_c \end{cases} . \tag{4.61}$$

Proving that the equal-time version distinguishes the deconfined phase hosting the toric code for $\Delta \gg \Delta_c$ from the confined phase with $\Delta \ll \Delta_c$ as in Fig. 4.12.

This finalises our analysis of order parameters in lattice gauge theories. We first saw that the Wilson loop detects topological ordering in a pure gauge theory, the (2+1)D quantum Ising gauge model, and that is related to the potential between static external charges. By introducing dynamical matter to the system we have to adapt the order parameter accordingly. The proper choice is the Fredenhagen-Marcu order parameter, which singles out the mechanism leading to a perimeter decay of the Wilson loop and can be related to the existence of free (deconfined) charges. Both operators are best calculated in their equal-time operator formulation,where the results can be obtained using time independent perturbation theory.

4.3 Evaluation of the order parameter

After familiarising ourselves with order parameters of lattice gauge theories and the realisation that the equal time version of the Fredenhagen-Marcu order parameter can detect the deconfinement/confinement transition in models containing dynamical matter, we use this knowledge on the Majorana toric code. First, we revisit the Hamiltonian

$$\begin{aligned} H_{MTC} &= H_C + H_J + H_M \,, \\ &= 4E_C \sum_i n_i^2 - E_J \sum_{<i,j>} \cos\left(\phi_i - \phi_j\right) - E_M \sum_{<i,j>} \sigma_{ij}^z \cos\left(\frac{\phi_i - \phi_j}{2}\right) \,, \end{aligned} \tag{4.62}$$

$$\text{with} \quad Q_i = \mathrm{e}^{2\pi i n_i} \prod_+ \sigma^x \,. \tag{4.63}$$

The number operator of Cooper pair charges is n_i and the conjugate variable to ϕ_i. The σ^z and σ^x are Pauli operators. In comparison to the theory of Ising gauge coupled to Ising matter in Eq. (4.45) and (4.46), we observe that the gauge field does not obtain direct dynamic. This is inferred from the absence of a term proportional to σ^x in Eq. (4.62). By constructing the inverse of the mapping between the MZMs and the spins in Eq. (3.15) for individual operators instead of bonds with a Jordan-Wigner transformation (cf. Ref. [13]), one can deduce that a single σ^x would be a highly non-local operator in terms of Majorana zero modes. This we will not do explicitly in this work. We further note that the U(1) matter field cannot couple to the $\mathbb{Z}_2$ gauge field as straightforward as the $\mathbb{Z}_2$ matter fields did in Eq. (4.45). From Eq. (4.62), we see that in this case it is only the parity of the U(1) DOF that couples to the gauge field in H_M and in the gauge constraint. The latter induces indirect dynamics to the gauge field through the matter. The term $H_C + H_M$ is a generalisation of the matter terms in the theory of Ising gauge and Ising matter. The charging term disorders the phase variables, whilst H_M describes nearest neighbour coupling of single charges through the gauge DOF between them. The remaining term H_J has no analogy in the pure Ising theory. It describes a charge two nearest neighbour coupling independent of the gauge field. From the last chapter, we know that it is the gauge field that is responsible for the confinement/deconfinement transition. This suggests, that H_J by itself does not lead to a topological transition. We define such a transition to be separating two topologically distinct phases. This absence of a topological transition due to H_J is indeed what we will observe with the Fredenhagen-Marcu order parameter. Instead, the transition is a purely matter driven XY-type. In the $E_M = 0$ limit this is studied for example in Refs. [42, 43].

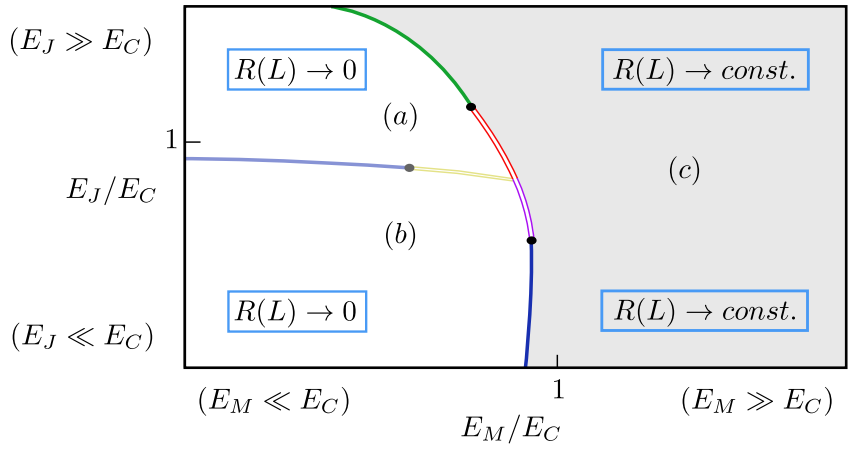

Figure 4.15: Phase diagram of the Majorana toric code (cf. Eq. (4.62)), for constant charging energy E_C. The expectation value of the equal-time Fredenhagen-Marcu operator $R(L)$ is depicted explicitly in the different phases. The phases (a) and (b) are both deconfined/topological as $R(L)$ decays to zero for large L. In contrast to that, the phase (c) is confined/non-topological, where $R(L)$ tends to a constant.

After shedding light on the similarities and differences of the MTC lattice gauge model and the previously studied Ising theory, we take a closer look at the formulation of the Fredenhagen-Marcu operator for the model at hand. We focus on the equal-time operator formulation, as it is the simplest to calculate. Adapting the matter field to be a U(1) DOF we find

$$R(L) = \frac{W_{1/2}(L)}{\sqrt{W(L)}}\,, \tag{4.64}$$

where

$$W(L) = \langle G| \prod\nolimits_{l\in\mathcal{C}} \sigma_l^z \, |G\rangle \ , \tag{4.65}$$

$$W_{1/2}(L) = \langle G| \, d_s^\dagger \prod\nolimits_{l\in\mathcal{C}_{1/2}} \sigma_l^z \ d_{s'} \, |G\rangle \ . \tag{4.66}$$

The operators $d^{(\dagger)}$ are the annihilation (creation) operators of single charges defined in Sec. 3.3. In the following, we will evaluate this operator with time independent perturbation theory in the different limiting regimes of the lattice gauge theory in Eq. (4.62). This results in Fig. 4.15.

Both the charge-2e superconductor (a) as well as the Mott insulator (b) are a deconfined/topological phase, since we find $R(L) \to 0$ in the limit $L \to \infty$. This is in accordance with the existence of the toric code in both phases [11, 14]. It also indicates that the XY-type transition separating these phases is purely matter based and not a topological transition. The charge-e superconducting phase (c) is confined/non-topological and we find $R(L) \to const.$ In total, this proves that the Fredenhagen-Marcu operator

is the correct order parameter to determine the topological signature of the phases in the Majorana toric code, which can be written as a lattice gauge theory with dynamical matter. Furthermore, we will derive from the equal-time formulation that it is the condensation of open loops that drives the transition into a non-topological phase, which corresponds to free flowing single charges. Subsequently, we work our way through the different regimes of Fig. 4.15 and calculate the above-mentioned scaling behaviours.

4.3.1 Dominant charging energy

We start by analysing the case of dominant charging energy $E_C \gg E_J, E_M$. In the phase diagram in Fig. 4.15 this is phase (b). From a charge perspective the system behaves as a Mott insulator. As in Sec. 4.1.1, the unperturbed Hamiltonian is then given by

$$H_0 = 4E_C \sum_i n_i^2 \,. \tag{4.67}$$

Thus, the ground state is charge-less. From the previous Brillouin-Wigner calculation, we know that for $E_M \neq 0$ the ground state degeneracy reduces to the four-fold topological one. In light of this we limit our calculation to

$$|G\rangle = w \sum_{s\in\mathcal{S}} |s\rangle \;, \tag{4.68}$$

the equal weight w superposition of all closed loop configurations $\mathcal{S}$, introduced in Sec. 2.1. Furthermore, we there established that the ground state degeneracy persists in low enough orders of perturbation theory. Therefore, we perform the calculation only for a single candidate ground state. In zeroth order perturbation theory, this yields

$$W(L) = \langle G| \prod\nolimits_{l\in\mathcal{C}} \sigma_l^z \, |G\rangle = 1 \,, \tag{4.69}$$

$$W_{1/2}(L) = \langle G| \, d_s^\dagger \prod\nolimits_{l\in\mathcal{C}_{1/2}} \sigma_l^z \; d_{s'} \, |G\rangle = 0 \,, \tag{4.70}$$

since the ground state contains closed but not open loops, as long as the perturbation is neglected. The perturbative term is

$$V = E_M V_M + E_J V_J = -\frac{E_M}{2} \sum_{<i,j>} \sigma_{ij}^z \left(d_i^\dagger d_j + d_i d_j^\dagger \right) - \frac{E_J}{2} \sum_{<i,j>} \left({d_i^\dagger}^2 d_j^2 + d_i^2 {d_j^\dagger}^2 \right) . \tag{4.71}$$

Taking V into account we obtain for the ground state to first order

$$\begin{aligned} N' \left|G'\right\rangle &= |G\rangle - E_M \sum_{|n\rangle\neq|G\rangle} \frac{|n\rangle\langle n|}{E_0 - E_n} V_M |G\rangle - E_J \sum_{|m\rangle\neq|G\rangle} \frac{|m\rangle\langle m|}{E_0 - E_m} V_J |G\rangle \\ &= |G\rangle - \frac{E_M}{2} \sum_{<i,j>} \sigma_{ij}^z \left(d_i^\dagger d_j + d_i d_j^\dagger\right) \frac{1}{-2\cdot E_C} |G\rangle \\ &\quad - \frac{E_J}{2} \sum_{<i,j>} \left(d_i^{\dagger 2} d_j^2 + d_i^2 d_j^{\dagger 2}\right) \frac{1}{-2\cdot 4E_C} |G\rangle \\ &= |G\rangle + \frac{1}{4}\frac{E_M}{E_C} \sum_{<i,j>} \sigma_{ij}^z \left(d_i^\dagger d_j + d_i d_j^\dagger\right) |G\rangle \\ &\quad + \frac{1}{16}\frac{E_J}{E_C} \sum_{<i,j>} \left(d_i^{\dagger 2} d_j^2 + d_i^2 d_j^{\dagger 2}\right) |G\rangle \\ &= |G\rangle + |G_1\rangle + |G_2\rangle \ . \end{aligned} \tag{4.72}$$

We define N' to be the normalisation factor. The sums run over the eigenstates $|n\rangle$ of the unperturbed Hamiltonian H_0 and E_n is their associated (unperturbed) energy. In the second equality, we inserted the explicit form of the perturbation and the energy differences between $|n\rangle$ and $|G\rangle$ are calculated. For the second term, the Majorana term, the two single charge creation/annihilation operators each lead to an $n_i^2 = 1/4$ on the respective island and thus result in an energy change of $2\cdot E_C$. This is the charging energy of two single charges. For the third term, the Josephson term, we analogously obtain $E_m - E_0 = 2\cdot 4E_C$, the charging energy of two cooper pairs. With this perturbative ground state one can now calculate the expectation value of the (half) Wilson loop, both again to first order. In the following, we denote the state with respect to which we calculate the expectation value of the Wilson loop explicitly by redefining $W(L) = \langle G|W(L)|G\rangle$. As the mixed terms vanish, this yields

$$\begin{aligned} N'^2 \left\langle G'\right|W(L)\left|G'\right\rangle = \ & \langle G|W(L)|G\rangle + \langle G_1|W(L)|G_1\rangle + \langle G_2|W(L)|G_2\rangle + 0 \\ = 1 + & \left[\frac{1}{4}\frac{E_M}{E_C}\right]^2 \sum_{<i,j>}\sum_{<k,l>} \langle G|\, \sigma_{ij}^z \left(d_i^\dagger d_j + d_i d_j^\dagger\right) \\ & \cdot \left(\prod\nolimits_{r\in C} \sigma_r^z\right) \sigma_{kl}^z \left(d_k^\dagger d_l + d_k d_l^\dagger\right) |G\rangle \\ & + \left[\frac{1}{16}\frac{E_J}{E_C}\right]^2 \sum_{<i,j>}\sum_{<k,l>} \langle G|\left(d_i^{\dagger 2} d_j^2 + d_i^2 d_j^{\dagger 2}\right) \\ & \cdot \left(\prod\nolimits_{r\in C} \sigma_r^z\right) \left(d_k^{\dagger 2} d_l^2 + d_k^2 d_l^{\dagger 2}\right) |G\rangle \\ = 1 + & 2N \left[\frac{1}{4}\frac{E_M}{E_C}\right]^2 + 2N \left[\frac{1}{16}\frac{E_J}{E_C}\right]^2 . \end{aligned} \tag{4.73}$$

For the first term we use the result from our analysis of the unperturbed ground state. For the remaining terms it is important to note that the creation/annihilation operators

commute with the Pauli operators and that the perturbations are Hermitian. In the second term, the Majorana term, one finds that it only gives a finite contribution for $i = k$ and $j = l$. Thus, it only yields a finite result if the charge transfer occurs on the same link. In that case, the creation/annihilation as well as the Pauli operators cancel out. This happens for $2N$ terms of the sum, where N is the number of nodes in the system. Each of those terms gives the unperturbed expectation value of the Wilson loop. For the third term, the Josephson term, we analogously find those $2N$ summands, but with different prefactors.
Most importantly we note that the expectation value for the Wilson loop is finite to zeroth order already. If we now perform the same analysis for the half Wilson loop with a length L larger than two links, we find again that the mixed terms vanish and

$$\begin{aligned} N'^2 \left\langle G' \middle| W_{1/2}(L) \middle| G' \right\rangle &= \langle G|W_{1/2}(L)|G\rangle + \langle G_1|W_{1/2}(L)|G_1\rangle + \langle G_2|W_{1/2}(L)|G_2\rangle \\ &= 0 + \left[\frac{1}{4}\frac{E_M}{E_C}\right]^2 \sum_{<i,j>} \sum_{<k,l>} \langle G| \sigma^z_{ij} \left(d_i^\dagger d_j + d_i d_j^\dagger\right) \\ &\qquad \cdot d_s^\dagger d_{s'} \left(\prod\nolimits_{r\in C_{1/2}} \sigma_r^z\right) \sigma^z_{kl} \left(d_k^\dagger d_l + d_k d_l^\dagger\right) |G\rangle \\ &\quad + \left[\frac{1}{16}\frac{E_J}{E_C}\right]^2 \sum_{<i,j>} \sum_{<k,l>} \langle G| \left(d_i^{\dagger 2} d_j^2 + d_i^2 d_j^{\dagger 2}\right) \\ &\qquad \cdot d_s^\dagger d_{s'} \left(\prod\nolimits_{r\in C_{1/2}} \sigma_r^z\right) \left(d_k^{\dagger 2} d_l^2 + d_k^2 d_l^{\dagger 2}\right) |G\rangle \\ &= 0\,. \end{aligned} \tag{4.74}$$

The first term is again the unperturbed expectation value. An open loop of length $L > 2$ has a zero expectation value in first order perturbation theory. However, from Eq. (4.74) we are in a position to generalise to even higher orders. It can be readily seen that the excitations due to the Josephson term, the third term, cannot yield a contribution even in higher orders of perturbation theory, since the Pauli operators σ^z can never be cancelled or form a closed contour. The second term yields a finite contribution if the open loop $C_{1/2}$ is bridged by consecutive single electron transfers. One can infer that even for mixed terms in higher orders, the lowest order contribution is still given by the pure single charge tunnelling. Those are at least of order $\mathcal{O}([E_M/(4E_C)]^L)$. Now we are in a position to calculate the expectation value of the Fredenhagen-Marcu operator to leading order in the perturbation theory. With the ground state $|G^*\rangle$ and normalisation N^* of at least $\mathcal{O}(L/2)$ in the perturbation, this reads

$$R(L) = \frac{\langle G^*|W_{1/2}(L)|G^*\rangle}{\sqrt{\langle G^*|W(L)|G^*\rangle} N^*} \approx \frac{\left[\frac{1}{4}\frac{E_M}{E_C}\right]^L}{1\cdot 1} = \mathrm{e}^{-\ln\left(4\frac{E_C}{E_M}\right)L} \quad \overset{L\to\infty}{\longrightarrow} \quad 0\,. \tag{4.75}$$

The Wilson loop as well as the normalisation are approximated to leading order as 1. Thus, the expectation value of the Fredenhagen-Marcu operator vanishes for $L \to \infty$ in the regime of dominant charging energy $E_C \gg E_J, E_M$. This situation is sketched in Fig. 4.14(b), where the gap of size L has to be bridged. The closing of this gap, which is linked to the transfer of single charges, is suppressed for dominant charging energy. For this parameter setting we are in a deconfined phase. Due to the system being placed on a torus, it has a topological order. The latter is given by the four-fold degeneracy of the ground state encoded in the parity of the non-contractible closed loops as discussed in Sec. 2.1. These findings are in accordance with the effective toric code Hamiltonian in Sec. 4.1. In the following, we repeat this treatment for different parameter regimes.

4.3.2 Dominant Josephson energy

In this section, we investigate the signature of topological ordering of the model in Eq. (4.62) in the limit of dominant Josephson energy E_J. We aim to reproduce the effective breakdown of the U(1) to $\mathbb{Z}_2$ matter, suggested by Ref. [11] and the field theory in Ref. [12]. This breakdown is denoted for dominant E_J by the pure Ising transition (green line) in Fig. 4.15. Furthermore, we show that the charge-$2e$ superconducting phase (a) is deconfined, whilst the charge-e superconducting phase (c) is confined, assuming large E_J.

Effective Ising theory

We start by analysing the $E_J = \infty$ limit of the Hamilton in Eq. (4.62). Under this condition, the phase differences $\phi_i - \phi_j$ between the superconducting islands are fixed.

$$\phi_i - \phi_j = 2\pi m_{ij}\,, \qquad \text{where} \quad m_{ij} \in \mathbb{Z} \qquad \forall\, i,j\,. \tag{4.76}$$

Now we set one arbitrary but fixed phase to $\phi_0 = 0$. Then we have

$$\phi_i = 2\pi m_i\,, \qquad \text{where} \quad m_i \in \mathbb{Z} \qquad \forall\, i\,. \tag{4.77}$$

Inserting this into the exponentials, we obtain

$$\mathrm{e}^{\pm i\phi_i} = 1 \qquad \text{and} \qquad \mathrm{e}^{\pm i\phi_i/2} \in \{-1, 1\}\,. \tag{4.78}$$

This suggests that in the regime of large Josephson coupling the U(1) matter field is effectively described by $\mathbb{Z}_2$ matter. In other words, the parity of the U(1) matter is the important degree of freedom. To display this more clearly, the following operator mapping is considered

$$\mathrm{e}^{\pm i\phi_i/2} \;\to\; \tau_i^z \qquad \text{and} \qquad \mathrm{e}^{2\pi i n_i} \;\to\; \tau_i^x\,. \tag{4.79}$$

The latter identification is chosen to satisfy the Pauli algebra as stated in Eq. (3.12). To gain some insight in not only the upper line of the phase diagram in Fig. 4.15, but a finite regime below, we relax the limiting condition to $E_J \to \infty$. Meaning large, but finite Josephson coupling. Using Eq. (4.79) the gauge transformation can be written as

$$Q_i = \tau_i^x \prod_+ \sigma^x \,. \tag{4.80}$$

Compared to Eq. (4.63), no spontaneous breaking of this local symmetry occurred. We merely introduced a more explicit operator formulation for the parity of the U(1) matter DOF. Moving on to the single charge transfer, we can straightforwardly rewrite it as

$$H_M = -E_M \sum_{<i,j>} \tau_i^z \sigma_{ij}^z \tau_j^z \,. \tag{4.81}$$

The remaining task is the translation of the charging term H_C in Eq. (4.62) into the effective Ising picture. Here, we follow an idea outlined for a 1D system in Ref. [44]. The charge term induces fluctuations around the fixed phase values, that lead to oscillations around the rest values and phase slips by 2π. The oscillations alter the eigenvalues of the Hamiltonian, but do not lead to phase transitions, so that those terms are neglected in the following discussion. In Ref. [11] the phase-slips can effectively be described using the semi-classical WKB method [45]. In their work, the phases are fixed due to the coupling of each island to a common ground superconductor. This simplifies the calculations since the slips occur relative to the ground superconductor separately on single islands decoupled from the remaining network. In the case under consideration, where the Josephson coupling is between nearest neighbouring islands, a phase slip is a non-local process involving all phases of the network. Since we are only interested in the qualitative properties of the phases, we approximate the slips to be still decoupled. The charging term is then approximated as

$$4E_C \sum_i n_i^2 \quad \to \quad \Delta \sum_i \tau_i^x \,. \tag{4.82}$$

Here τ_i^x can be seen to represent a phase slip by 2π at site i. The prefactor Δ can be associated with the tunnelling amplitude of ϕ by $\pm 2\pi$ under the above assumption of independent slips (cf. Fig. 4.16).

The dominant coupling dependence of Δ then follows to be $\Delta \propto \mathrm{e}^{-\sqrt{E_J/E_C}}$. Thus, we completed the transition to an effective $\mathbb{Z}_2$ model Hamiltonian and find

$$H = \Delta \sum_i \tau_i^x - E_M \sum_{<i,j>} \tau_i^z \sigma_{ij}^z \tau_j^z \,, \tag{4.83}$$

$$\text{with} \quad Q_i = \tau_i^x \prod_+ \sigma^x \,. \tag{4.84}$$

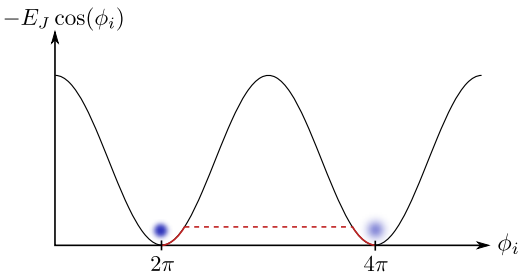

Figure 4.16: Sketch of the tunnelling process that is considered to calculate the amplitude of the 2π phase slips. The phase value ϕ_i (blue) is washed out around the minimanl value due the charging term. This enables tunnelling by 2π to the adjacent minimum. The respective amplitude can be determined by a semi-classical calculation along the red curve.

These are the matter terms of the theory of Ising gauge coupled to Ising matter, investigated in Sec. 4.2.2. The gauge invariant Hamiltonian description in Eq. (4.83) is evaluated in the following for the regimes of weak and strong Majorana coupling E_M. However, before we dive into the specific calculations, let us rewrite the effective Ising model to the Ising gauge model discussed in Sec. 4.2.1, connecting to the system considered in Ref. [11]. The first step is to realise that by choosing a gauge, we can fix the matter DOF to be in the $+1$ eigenstate of the τ_i^z. Applying this so called London gauge results in

$$H' = \Delta \sum_i \tau_i^x - E_M \sum_{<i,j>} \sigma_{ij}^z \,. \tag{4.85}$$

Furthermore, using the gauge constraint, we can express the τ^x in terms of the σ^x such that

$$H' = \Delta \sum_i \prod_+ \sigma^x - E_M \sum_{<i,j>} \sigma_{ij}^z \,. \tag{4.86}$$

In a last step we perform a basis rotation ($x \leftrightarrow z$) and switch from the direct to the dual lattice. The latter leads to an interchange of plaquette and star operators ($\square \leftrightarrow +$), as the two dimensional square lattice is self dual. We then arrive at

$$H' = \Delta \sum_i \prod_\square \sigma^z - E_M \sum_{<i,j>} \sigma_{ij}^x \,, \tag{4.87}$$

the (2+1)D Ising gauge model discussed in Sec. 4.2.1. The local gauge symmetry that remains is $\tilde{Q}_i = \prod_+ \sigma^x$. It is the local plaquette symmetry discussed in Sec. 3.2 after the basis rotation and going to the dual lattice. The model in Eq. (4.87) connects to that of Ref. [11]. In particular, we explicitly show that the phase transition in Fig. 4.15 for dominant Josephson coupling E_J belongs to the (2+1)D-Ising universality class. We know already that the order parameter of the system in Eq. (4.87) is the Wilson loop and it distinguishes between a topological/deconfined phase for $\Delta \gg E_M$ and a non-topological/confined phase for $\Delta \ll E_M$.

Our goal is to prove the existence of an order parameter that works throughout the entire phase diagram independent of specific gauge choices. To this end, we return to the gauge invariant formulation in Eq. (4.83) and compute the equal-time Fredenhagen-Marcu op-

erator in different parameter regimes using time independent perturbation theory. For that to work, we have to adapt the half Wilson loop for the effective Ising description of the matter fields to

$$W_{1/2}(L) = \langle G|\, d_s^\dagger \prod\nolimits_{l\in\mathcal{C}_{1/2}} \sigma_l^z \; d_{s'}\, |G\rangle \;\longrightarrow\; \langle G|\, \tau_s^z \prod\nolimits_{l\in\mathcal{C}_{1/2}} \sigma_l^z \; \tau_{s'}^z\, |G\rangle \;. \tag{4.88}$$

With this we move on to the perturbative calculations.

Weak Majorana coupling

For weak Majorana coupling, we are in the charge-2e superconducting phase (a) of the phase diagram (cf. Fig. 4.15), *i.e.*, $E_J \gg E_C \gg E_M$. For the effective Ising formulation this means $\Delta \gg E_M$. The unperturbed Hamiltonian as well as the perturbation are given as

$$H_0 = \Delta \sum_i \tau_i^x \qquad \text{and} \qquad V = E_M V_M = -E_M \sum_{<i,j>} \tau_i^z \sigma_{ij}^z \tau_j^z \,. \tag{4.89}$$

Therefore, the unperturbed ground state is in the -1 eigenstate of all τ_i^x, assuming that $\Delta > 0$. Analogously to the case of dominant charging energy, we find that the gauge transformation reduces to $Q_i = \prod_+ \sigma^x$ and the ground state becomes

$$|G\rangle = w \sum_{s\in\mathcal{S}} |s, \tau_i^x = -1\rangle \;=\; w \sum_{s\in\mathcal{S}} |s\rangle \;. \tag{4.90}$$

This is the equal weight superposition of all closed loop configurations, introduced in Sec. 2.1. The unperturbed ground state expectation value for a (half) Wilson loop is then again

$$W(L) = \langle G| \prod\nolimits_{l\in\mathcal{C}} \sigma_l^z\, |G\rangle = 1 \,, \tag{4.91}$$

$$W_{1/2}(L) = \langle G|\, \tau_s^z \prod\nolimits_{l\in\mathcal{C}_{1/2}} \sigma_l^z \; \tau_{s'}^z\, |G\rangle = 0 \,. \tag{4.92}$$

To evaluate the operators away from $E_M = 0$, perturbation theory is used which in first order yields

$$\begin{aligned} N'\,|G'\rangle &= |G\rangle - E_M \sum_{|n\rangle\neq|G\rangle} \frac{|n\rangle\langle n|}{E_0 - E_n} V_M\, |G\rangle \\ &= |G\rangle - \frac{E_M}{-2\Delta\cdot 2} \sum_{<i,j>} \tau_i^z \sigma_{ij}^z \tau_j^z\, |G\rangle \\ &= |G\rangle + \frac{1}{4}\frac{E_M}{\Delta} \sum_{<i,j>} \tau_i^z \sigma_{ij}^z \tau_j^z\, |G\rangle \\ &= |G\rangle + |G_1\rangle \;. \end{aligned} \tag{4.93}$$

The energy difference in the second summand is obtained by the two matter DOF that are flipped into the $+1$ eigenstate of τ_i^x, each contributing 2Δ. Comparing Eq. (4.93) to (4.72), we note that the perturbations $|G_1\rangle$ only differ in the formulation of the matter DOF, whilst the charge-two perturbation is absent. As the expectation value of the Fredenhagen-Marcu operator to leading order was determined from $|G_1\rangle$, we find completely analogously to Sec. 4.3.1 that

$$R(L) = \frac{\langle G^*|W_{1/2}(L)|G^*\rangle}{\sqrt{\langle G^*|W(L)|G^*\rangle N^*}} \approx \frac{\left[\frac{1}{4}\frac{E_M}{\Delta}\right]^L}{1\cdot 1} = \mathrm{e}^{-\ln\left(4\frac{\Delta}{E_M}\right)L} \overset{L\to\infty}{\longrightarrow} 0\,. \tag{4.94}$$

Here, we defined $|G^*\rangle$ to be the perturbative ground state to $\mathcal{O}\big(V^{L/2}\big)$, with normalisation factor N^*. Thus, the charge-$2e$ superconducting phase (a) in Fig. 4.15 is a deconfined/topological phase similar to the Mott insulator phase (b) and in agreement with the emergence of a toric code phase as shown in Ref. [11].

Strong Majorana coupling

Moving on to the limit of $E_C \ll E_M$, *i.e.* $\Delta \ll E_M$ in terms of the effective couplings, the unperturbed Hamiltonian and perturbation follow to be

$$H_0 = -E_M \sum_{<i,j>} \tau_i^z \sigma_{ij}^z \tau_j^z \qquad \text{and} \qquad V = \Delta \sum_i \tau_i^x\,, \tag{4.95}$$

with the gauge constraint

$$Q_i = \tau_i^x \prod_+ \sigma^x\,. \tag{4.96}$$

From a charge perspective, this limiting region belongs to the charge-e superconducting phase (c) in Fig. 4.15. To order to obtain the ground state formulation of the unperturbed model, we revisit the procedure in Sec. 2.1, where we determined the gauge invariant ground state of the toric code. Analogously, we assume to be in the x-basis of both τ and σ. Determining the valid node configurations due to Eq. (4.96), we realise that in addition to the diagrams in Fig. 2.2, open ends are allowed if the matter DOF on the node itself is also in the -1 eigenstate of τ_i^x (cf. Fig. 4.17).
In other words, the introduction of the matter DOF allows, besides the closed loops of flipped gauge DOF discussed earlier, open loops with flipped matter DOF at the endpoints. The candidate ground state is therefore a superposition of all open loop states

$$|\tilde{G}\rangle = \sum_{m\in\mathcal{M}} w_m\,|m\rangle\,. \tag{4.97}$$

The set $\mathcal{M}$ denotes all valid open loop configurations. Closed loops are here treated as a special case of open loops with coinciding endpoints and thus contained in the sum.

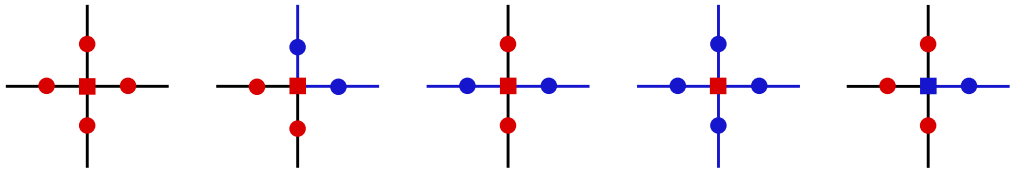

Figure 4.17: Allowed node configurations that satisfy $\tau_i^x \prod_+ \sigma^x = 1$. We focus on a specific node i, where the adjacent gauge DOF (circles) as well as the matter DOF (squares) are displayed in the x-basis. The colors red/blue indicate the gauge/matter σ_{ij}/τ_i to be in the $+1/-1$ eigenstate of σ_{ij}^x/τ_i^x. To be valid, the configuration needs to contain an even number of -1 eigenstates. To obtain the complete set, the four (two, four) possible rotations of the second (third, fifth) graph have to be considered as well.

Additionally, the ground state has to be in the $+1$ eigenstate of all $\tau_i^z \sigma_{ij}^z \tau_j^z$, which replace the plaquette operators used in the construction of the toric code ground state. For the state to be invariant under a flip of the variables along a link, we have to fix the weights in the superposition to be equal

$$|G\rangle = w \sum_{m \in \mathcal{M}} |m\rangle \;=\; \prod_{<i,j>} \frac{1}{\sqrt{2}} \left(1 + \tau_i^z \sigma_{ij}^z \tau_j^z\right) |0\rangle \;. \tag{4.98}$$

We also gave the explicit form of the ground state, where N is the number of nodes in the system and $|0\rangle$ is defined as the state where all DOF are in the $+1$ eigenstate of σ_{ij}^x and τ_i^x, respectively. In the following, we will also refer to the ground state as open loop condensate. Even though the procedure was the same, there is a major difference between Eq. (4.98) and Eq. (4.90). While the latter is four-fold degenerate due to the parity of non-contractible loops, the first one is not degenerate. In the open loop condensate, even as well as odd numbers of NC loops have to be present with equal weight since the construction using $\tau_i^z \sigma_{ij}^z \tau_j^z$ does not leave the parity of NC loops invariant. The parity can already be changed in a single application of it, for example by opening a NC loop. This means that at least in the unperturbed case, the phase is non-topological. There is no space of topologically different degenerate ground states separated by an energy gap from the orthogonal space. This is reflected also in the calculation of the (half) Wilson loop. There we obtain

$$W(L) = \langle G| \prod\nolimits_{l \in \mathcal{C}} \sigma_l^z \, |G\rangle = 1 \,, \tag{4.99}$$

$$W_{1/2}(L) = \langle G| \, \tau_s^z \, \prod\nolimits_{l \in \mathcal{C}_{1/2}} \sigma_l^z \; \tau_{s'}^z \, |G\rangle = 1 \,. \tag{4.100}$$

Here $R(L)$ takes a constant value for $L \to \infty$. To calculate the Fredenhagen-Marcu order

parameter in the perturbed case, we compute the first order perturbative ground state.

$$\begin{aligned} N' \left|G'\right\rangle &= \left|G\right\rangle + \Delta \sum_{|n\rangle \neq |G\rangle} \frac{|n\rangle\langle n|}{E_0 - E_n} \sum_i \tau_i^x \left|G\right\rangle \\ &= \left|G\right\rangle + \frac{\Delta}{-2E_M \cdot 4} \sum_i \tau_i^x \left|G\right\rangle \\ &= \left|G\right\rangle \underbrace{-\frac{1}{8}\frac{\Delta}{E_M}}_{=:\,\alpha} \sum_i \tau_i^x \left|G\right\rangle \\ &= \left|G\right\rangle + \left|G_1\right\rangle \,. \end{aligned} \tag{4.101}$$

We define the constant α to simplify the notation. Since we are interested in the ground state expectation value of $R(L)$ for the limit of an infinite lattice we can, to a reasonable degree, approximate higher order corrections to the ground state as independent flips of matter DOF. Under this assumption of locally separate perturbations, we find for the ground state at order $N_{\max}$

$$\begin{aligned} N^* \left|G^*\right\rangle &\approx \left|G\right\rangle + \alpha \sum_i \tau_i^x \left|G\right\rangle + \frac{1}{2!}\, \alpha^2 \Big(\sum_i \tau_i^x\Big)^2 \left|G\right\rangle + \dots \\ &\approx \left|G\right\rangle + \sum_{n=1}^{N_{\max}} \frac{1}{n!}\, \alpha^n \Big(\sum_i \tau_i^x\Big)^n \left|G\right\rangle \,. \end{aligned} \tag{4.102}$$

At n-th order, we thus assume n independent flips to occur, where the $n!$ is necessary to avoid double counting. The normalisation is then calculated to

$$N^{*2} = \langle G|G\rangle + \langle G| \sum_{n=1}^{N_{\max}} \frac{1}{n!}\, \alpha^n \Big(\sum_i \tau_i^x\Big)^n \cdot \sum_{m=1}^{N_{\max}} \frac{1}{m!}\, \alpha^m \Big(\sum_j \tau_j^x\Big)^m \left|G\right\rangle \,. \tag{4.103}$$

Under the assumption of independent flips, the mixed order contributions have to vanish, as otherwise at least one τ_s^x does not square out. The latter leads to a vanishing expectation value since

$$\begin{aligned} \langle G|\, \tau_s^x \left|G\right\rangle &= \langle 0| \prod_{<i,j>} \frac{1}{\sqrt{2}} \left(1 + \tau_i^z \sigma_{ij}^z \tau_j^z\right)\ \tau_s^x\ \frac{1}{\sqrt{2}} \prod_{<k,l>} \left(1 + \tau_k^z \sigma_{kl}^z \tau_l^z\right) |0\rangle \\ &= \frac{1}{4^N} \langle 0|\, \tau_s^x \prod_{\substack{<i,j> \\ s \notin <i,j>}} \left(1 + \tau_i^z \sigma_{ij}^z \tau_j^z\right)^2 \prod_{\substack{<i,j> \\ s \in <i,j>}} \underbrace{\left(1 - \tau_i^z \sigma_{ij}^z \tau_j^z\right)\left(1 + \tau_i^z \sigma_{ij}^z \tau_j^z\right)}_{=\,0} |0\rangle = 0\,. \end{aligned} \tag{4.104}$$

Commuting the τ_s^x through the left product flips the sign on links containing the node s. Combined with the right product, those contributions give zero. In particular, this means that the two sums in the calculation of the normalisation in Eq. (4.103) simplify

with a Kronecker delta δ_{nm} to

$$\begin{aligned} N^{*2} &= \underbrace{\langle G|G\rangle}_{=\,1} + \sum_{n=1}^{N_{\max}} \frac{1}{n!^2}\, \alpha^{2n} \langle G| \Big(\sum_i \tau_i^x\Big)^n \cdot \Big(\sum_j \tau_j^x\Big)^n |G\rangle \\ &= 1 + \sum_{n=1}^{N_{\max}} \frac{1}{n!}\, \alpha^{2n} \Big(\sum_i\Big)^n \underbrace{\langle G|G\rangle}_{=\,1} \\ &= \sum_{n=0}^{N_{\max}} \frac{1}{n!}\, (\alpha^2 N)^n \;\approx\; \mathrm{e}^{\alpha^2 N} \end{aligned} \tag{4.105}$$

In the first equality, we used the fact that there are $n!$ ways to arrange the sums over j such that all τ_i^x square out. The empty sums run over all nodes resulting in the total number of nodes N. In the last step, we added the remaining terms from $N_{\max}$ to infinity, which is a negligible difference for large enough $N_{\max}$. Moving on to the expectation value of the Wilson loop, we obtain to first order with Eq. (4.101)

$$\begin{aligned} N'^2 \left\langle G'\middle|W(L)\middle|G'\right\rangle &= \langle G|W(L)|G\rangle + \langle G_1|W(L)|G_1\rangle \\ &= 1 + \sum_{i,j} \alpha^2 \langle G|\, \tau_i^x \prod\nolimits_{l\in\mathcal{C}} \sigma_l^z\; \tau_j^x\, |G\rangle \\ &= 1 + \sum_i \alpha^2 \langle G| \prod\nolimits_{l\in\mathcal{C}} \sigma_l^z\, |G\rangle \\ &= 1 + \alpha^2 N\,. \end{aligned} \tag{4.106}$$

Since the τ^x commute with the σ^z, we again obtain a Kronecker delta because the τ^x have to square out to result in a finite contribution. Thus, we repeat the above higher order calculation for the normalisation factor for the Wilson loop to find

$$N^{*2} \langle G^*|W(L)|G^*\rangle \;\approx\; \mathrm{e}^{\alpha^2 N}\,. \tag{4.107}$$

In contrast to that, the half Wilson loop expectation value yields to first order

$$\begin{aligned} N'^2 \left\langle G'\middle|W_{1/2}(L)\middle|G'\right\rangle &= \langle G|W_{1/2}(L)|G\rangle + \langle G_1|W_{1/2}(L)|G_1\rangle \\ &= 1 + \sum_{i,j} \alpha^2 \langle G|\, \tau_i^x\; \tau_s^z \tau_{s'}^z \prod\nolimits_{l\in\mathcal{C}_{1/2}} \sigma_l^z\; \tau_j^x\, |G\rangle \\ &= 1 + \alpha^2\, [(N-2)-2] \langle G|\, \tau_s^z \tau_{s'}^z \prod\nolimits_{l\in\mathcal{C}_{1/2}} \sigma_l^z\, |G\rangle \\ &= 1 + \alpha^2 (N-4)\,. \end{aligned} \tag{4.108}$$

In total $N-2$ of the τ_j^x commute with τ_s^z and $\tau_{s'}^z$. In two terms the τ operators anticommute so that the expectation value differs from the Wilson loop. Assuming

independent perturbations analogously to Eq. (4.107) results in

$$N^{*2}\,\langle G^*|W_{1/2}(L)|G^*\rangle \;\approx\; \mathrm{e}^{\alpha^2(N-4)}\,. \tag{4.109}$$

Collecting Eq. (4.105), (4.107) and (4.109), we obtain for the Fredenhagen-Marcu operator

$$\begin{aligned} R(L) &= \frac{\langle G^*|W_{1/2}(L)|G^*\rangle}{\sqrt{\langle G^*|W(L)|G^*\rangle}} = \frac{N^{*2}\,\langle G^*|W_{1/2}(L)|G^*\rangle}{N^*\sqrt{N^{*2}\,\langle G^*|W(L)|G^*\rangle}} \\ &\approx \frac{\mathrm{e}^{\alpha^2(N-4)}}{\mathrm{e}^{(\alpha^2 N)/2}\,.\,\mathrm{e}^{(\alpha^2 N)/2}} = \mathrm{e}^{-4\alpha^2}\,. \end{aligned} \tag{4.110}$$

Resubstitution of the constant gives

$$R(L) = \mathrm{e}^{-\frac{1}{16}\left(\frac{\Delta}{E_M}\right)^2} \quad \overset{L\to\infty}{\longrightarrow} \quad const\,. \tag{4.111}$$

Thus, the system is in a confined phase for $E_M, E_J \gg E_C$, in accordance with the above observation that the unperturbed ground state is non-degenerate. For the charge-e superconducting phase (c) in Fig. 4.15, we therefore conclude through the Fredenhagen-Marcu operator that it is non-topological due to the condensation of open loops.

Sign sensitivity

As we know from the symmetry considerations in Sec. 3.2 and the effective Hamiltonian calculation in Sec. 4.1.3, the system is not invariant under the change of sign of the Josephson coupling E_J. So before moving on to the remaining regime of dominant Majorana coupling E_M, we briefly analyse the sensitivity of the effective $\mathbb{Z}_2$ formulation of the MTC model under the assumption of $E_J < 0$. Taking the $E_J \to -\infty$ limit of the full Hamiltonian in Eq. (4.62) results in fixed phase differences

$$\phi_i - \phi_j = \pi + 2\pi m_{ij}\,, \qquad \text{where} \quad m_{ij} \in \mathbb{Z} \qquad \forall\; i,j\,. \tag{4.112}$$

Inserting this into the single charge transfer H_M, we find

$$H_M = E_M \sum_{<i,j>} \sigma_{ij}^z \cos\!\left(\frac{\phi_i - \phi_j}{2}\right) = 0\,, \qquad \text{since} \qquad \cos\!\left(\frac{\pi}{2} + \pi m_{ij}\right) = 0\,. \tag{4.113}$$

For dominant but negative Josephson coupling the single electron transfer is suppressed. Previously, we saw that a small single electron tunnelling rate E_M is necessary to realise the toric code ground state, whilst for large E_M the topological property is destroyed. Introducing large, negative E_J could thus be a means to obtain a topological phase even for large Majorana coupling E_M. This insight seems worthwhile to be investigated closely in future projects. With this we finalised our analysis for dominant Josephson energy.

4.3.3 Dominant Majorana coupling

We complete our analysis of topological ordering by considering the limit of dominant Majorana coupling. For simplicity, we assume $E_J = 0$ and take the limit $E_M \gg E_C$. This is the charge-e superconducting phase (c) in Fig. 4.15, but for zero Josephson coupling. For $E_M \to \infty$ the single electron transfer yields

$$\sigma_{ij}^z \cos\left(\frac{\phi_i - \phi_j}{2}\right) = 1 \qquad \forall \ < i,j > \ . \tag{4.114}$$

As the gauge field does not have direct dynamic, we assume it to be in a configuration $\{\sigma_{ij}\}$. Depending on the σ_{ij}^z eigenstate they are in, we find

$$\sigma_{ij}^z = 1: \quad \frac{\phi_i - \phi_j}{2} = 2\pi m_{ij}\,, \qquad \text{where} \quad m_{ij} \in \mathbb{Z} \tag{4.115}$$

$$\sigma_{ij}^z = -1: \quad \frac{\phi_i - \phi_j}{2} = \pi + 2\pi m_{ij}\,, \qquad \text{where} \quad m_{ij} \in \mathbb{Z}\,. \tag{4.116}$$

Restricting ourselves again to the interval $\phi_i \in [0, 4\pi)$ this gives

$$\phi_i - \phi_j = 0/2\pi\,, \qquad \text{for} \qquad \sigma_{ij}^z = 1/-1\,. \tag{4.117}$$

In particular, these two phase differences agree with the values in Eq. (4.76) so that we apply the same reformulation in terms of $\mathbb{Z}_2$ DOF to obtain

$$H_M = -E_M \sum_{<i,j>} \tau_i^z \sigma_{ij}^z \tau_j^z\,. \tag{4.118}$$

The charging term H_C introduces fluctuations of the phase variables, that are represented as terms $\propto \tau_i^x$. Which yields

$$H = \Delta' \sum_i \tau_i^x - E_M \sum_{<i,j>} \tau_i^z \sigma_{ij}^z \tau_j^z\,. \tag{4.119}$$

To estimate the coupling strength Δ' of this term, we calculate the tunnelling amplitude of a 4π tunnelling of the phase variable ϕ_i in the potential $V = -E_M \cos(\phi_i/2)$ with the WKB method. Here, we again assume a tunnelling to occur on a single node separate from the neighbouring phases to find a qualitative description of $\Delta'^2 \propto \mathrm{e}^{-\sqrt{E_M/E_C}}$, following the treatment in Sec. 4.3.2. This process, however, is of second order in the fundamental fluctuation that we introduced to the Hamiltonian. Thus, the fluctuation strength is determined by the square root of the calculated tunnelling amplitude. Comparing Eq. (4.119) to Eq. (4.83), we note that they only differ in the coupling constants Δ and Δ', respectively. This is a strong indication for the absence of an additional phase boundary within the charge-e superconducting phase, in agreement with the field theory results from Ref. [12]. The perturbative calculations for $E_M \ll \Delta'$ can be performed as

in Sec. 4.3.2 yielding

$$R(L) = \mathrm{e}^{-\frac{1}{16}\left(\frac{\Delta'}{E_M}\right)^2} \quad \overset{L\to\infty}{\longrightarrow} \quad const\,. \tag{4.120}$$

This proves that throughout the phase (c) in Fig. 4.15 the Fredenhagen-Marcu operator $R(L)$ takes a finite value even for $L \to \infty$, diagnosing a confined phase.

With this, we evaluated the Fredenhagen-Marcu operator in all possible limiting regimes of the phase diagram and proved the claimed topological signatures in Fig. 4.15. Thus, from a gauge field perspective the charge-$2e$ superconducting (a) and the Mott insulator phase (b) are deconfined/topological, separated by a pure matter transition, while the charge-e superconducting phase (c) is confined/non-topological. The mechanism that drives the system into a non-topological phase is the condensation of open loops. From a charge perspective, those are generated by free flowing single charges, as present in the charge-e superconductor.

Chapter 5

Conclusion and Outlook

This thesis investigated the topological ordering in the Majorana toric code. After a short motivation in Chapter 1, we began in Chapter 2 with an introduction to the toric code and Majorana zero modes. We understood the toric code to be a prime example of a system with topological ordering with its four-fold degenerate topologically protected ground state being a candidate platform for quantum memory. Thereafter, we explicitly observed the emergence of Majorana zero modes from the Kitaev chain [26], making it possible to encode a qubit in a non-local fermionic mode.

Consecutively, in Ch. 3 we constructed a two dimensional square lattice of superconducting islands carrying four Majorana zero modes [10, 13] resulting in the Majorana toric code model. The previously known charge signatures and phase transitions are discussed, where we saw that for constant charging energy, the system can be in a charge-$2e$ superconducting, a Mott insulator and a charge-e superconducting phase [10]. Two features particularly stood out. The transition between the different superconducting phases is of the (2+1)D-Ising type and both the charge-e superconductor and the Mott insulator effectively realise the aforementioned toric code. This posed the main question for the thesis: How can one detect the topological ordering in the Majorana toric code? To shed light on the topological ordering of the system, we performed a mapping of the microscopic model onto the lattice gauge theory of U(1) matter parity coupled to $\mathbb{Z}_2$ gauge, inspired by Ref. [36]. Particularly, we transformed pairs of MZM into spin d.o.f. on the links of the lattice.

This model was then further analysed in Chapter 4. We started off by performing a perturbative calculation for the effective Hamiltonian in the Mott insulator phase to see the emergence of the toric code. In contrast to previous works [11, 14], we explicitly considered the Josephson tunnelling between adjacent superconducting islands and found that the inter island Cooper pair transfer stabilises the ground state space if the tunnelling rate is assumed to be small.

Subsequently, we continued with an introduction of lattice gauge theorys and their respective order parameters. Using the quantum Ising gauge model as an example, we learned about the importance of non-locality of the order parameter. The Wilson loop, linked to the potential between static external charges, was calculated in different parameter regimes in agreement with the literature [22]. It correctly diagnosed the transition between a confined and a deconfined phase. The equal-time formulation thereby turned out to be the easiest to calculate. Introducing dynamical matter to the system, the Wilson loop is no longer a good order parameter of the theory [41]. However, in the Ising gauge coupled to Ising matter theory, we showed that the Fredenhagen-Marcu operator can be utilised to distinguish the deconfined and confined phase, as already stated in Ref. [22]. This operator could be connected to the existence of free charges in the system [16] and again was most efficiently calculated in the equal-time formulation.

In the last section, we evaluated the Fredenhagen-Marcu operator in the lattice model derived in Ch. 3. We found it to detect the topological ordering in the charge-$2e$ superconducting and Mott insulator phase as well as the absence of this ordering in the charge-e superconducting phase. Furthermore, we identified the transition into the non-topological regime to be driven by the condensation of open loops. In the charge perspective, those are represented by free flowing electrons, in accordance with the charge-e superconductor. During the calculations, we reduced the Majorana toric code model into an effective (2+1)D-Ising gauge model for dominant Josephson coupling. This explains that the transition between the two superconducting phases is of Ising type.

All in all, we successfully met the challenge of diagnosing the topological ordering in the model of the Majorana toric code by mapping it onto a lattice gauge model. This enabled the use of the Fredenhagen-Marcu order parameter that linked the mechanism leading to the topological phase transition to the condensation of open loops, *i.e.*, free flowing single electrons. A recurring theme during the calculations was the dependence of the system on the sign of the Josephson coupling. Especially the case of dominant, but negative coupling could lead to a remarkably stable topological phase. This could be the basis of future projects around the Majorana toric code. Since we assumed four Majorana zero modes to be present independent of their specific realisation, the question of the optimal microscopic setup with emergent MZM is still to be answered. Thus, even though we made progress in the understanding of the topological order of the system, there is still a lot to explore on the road to a practical quantum storage device.

Appendices

A From Majoranas to spins

In this section, we describe the duality transformation given in Eq. (3.15) based on the bond algebraic approach from Refs. [35, 36]. First, we define $\mathcal{L}$ as the set of all nearest neighbour bonds, $\mathcal{I}$ as the set of islands and the operator $P_i = -\gamma^i_{a,1}\gamma^i_{a,2}\gamma^i_{b,1}\gamma^i_{b,2}$ to compactify the notation. The set of bonds forming the bond algebra is then given by

$$i\gamma^k\gamma^l\,, \quad \forall\ (k,l) \in \mathcal{L} \qquad \text{and} \qquad P_i\,, \quad \forall\ i \in \mathcal{I}\,. \tag{A.1}$$

Making use of the Clifford algebra (cf. Sec. 2.2) one can show that the bond algebra $\mathcal{A}$ contains the intensive relations, *i.e.*, independent of the lattice size,

I) $(i\gamma^k\gamma^l)^2 = P_j^2 = \mathbf{1}\,, \qquad \forall\ (k,l) \in \mathcal{L}\,, \forall\ j \in \mathcal{I}\,,$

II) $\left\{P_k, i\gamma^k\gamma^l\right\} = \left\{P_l, i\gamma^k\gamma^l\right\} = 0\,, \qquad \forall\ (k,l) \in \mathcal{L}\,,$

III) all remaining bond combinations commute.

For periodic boundary conditions, there is one extensive, *i.e.*, lattice size dependent, relation left

IV) $\prod\limits_{i\in\mathcal{I}} P_i = \alpha \prod\limits_{(k,l)\in\mathcal{L}} i\gamma^k\gamma^l\ ,$

where $\alpha = \pm 1$ accounts for the different orderings of the Majorana operators on both sides of the equation. As the MZMs are their own anti-particle, we can globally redefine occupied modes as unoccupied and vice versa without changing the spectrum. The extensive relation considers this global $\mathbb{Z}_2$ symmetry of the Majoranas. We want to reproduce the same bond algebra $\mathcal{A}$ with alternative bonds, where there is a spin-1/2 degree of freedom placed on the links between two island (cf. Fig. 3.5). This DOF is represented by the Pauli operators $\sigma^z_{ij}, \sigma^y_{ij}, \sigma^x_{ij}$ obeying the Pauli algebra (cf. Sec. 2.1). The size of the Hilbert spaces agree. There are two fermionic modes per island which can be occupied or not in case of the original bonds and two links per island containing a spin-1/2 DOF which can be up or down in the alternative bond description. The new

set of bonds is defined as

$$\sigma_{ij}^z\,, \qquad \forall\ (i,j)\in\mathcal{L} \qquad \text{and} \qquad \tilde{P}_i = \prod_{+_i} \sigma^x := \prod_{j:(i,j)\in\mathcal{L}} \sigma_{ij}^x\,, \quad \forall\ i\in\mathcal{I}\,, \tag{A.2}$$

so that $\tilde{P}_i$ is given by the product of σ^x of all four links emanating from island i. With the Pauli algebra it can be verified that the alternative bonds satisfy the intensive relations

I) $(\sigma_{ij}^z)^2 = \tilde{P}_k^2 = \mathbf{1}\,, \qquad \forall\ (i,j)\in\mathcal{L}\,, \forall\ k\in\mathcal{I}\,,$

II) $\left\{\tilde{P}_i, \sigma_{ij}^z\right\} = \left\{\tilde{P}_j, \sigma_{ij}^z\right\} = 0\,, \qquad \forall\ (i,j)\in\mathcal{L}\ ,$

III) all remaining bond combinations commute.

In order to fulfil the extensive relation, we choose one arbitrary but fixed island, say $i=0$ and set $\tilde{P}_0 = \prod_{+_0}\sigma^x \cdot (\alpha \prod_{(i,j)\in\mathcal{L}} \sigma_{ij}^z)$. With this choice, the intensive relations still hold, as the additional pre factor commutes with all remaining bonds and we obtain

IV) $\prod_{i\in\mathcal{I}} \tilde{P}_i = \alpha \prod_{(i,j)\in\mathcal{L}} \sigma_{ij}^z\,,$

since all σ^x square out. Now that the Hilbert space sizes are equal and both the intensive as well as the extensive relations are satisfied, we can write down the new model description Eq. (3.16). Both Hamiltonians are linked by a unitary transformation, see Ref. [36]. This mapping can also be obtained from Jordan-Wigner transformation followed by a duality mapping, similar to Ref. [13].

B Expansion of Brillouin-Wigner perturbation theory

In this section, we have a closer look at the expansion of the self-consistent equation for the effective Hamiltonian in Brillouin-Wigner perturbation theory. We omit the tilde in the definition of V and G again for simplicity. The first step is the identification of all fourth, fifth and sixth order terms in the effective Hamiltonian that lead to non-constant contributions. We start by noting that no linear term exists in the expansion as a single application of V to a charge less ground state creates charges on neighbouring nodes, which is not part of the ground state space. Thus, if we set $E_0 = 0$,

$$H_{\text{eff}} = -V_{-+}G_0(E)\sum_{k=0}^{\infty}\left(V_{++}G_0(E)\right)^k V_{+-}\,, \tag{B.3}$$

is at least of second order in the perturbation and an energy expansion is of the form

$$E = \delta E^{(2)} + \delta E^{(3)} + \delta E^{(4)} + \mathcal{O}\big(V^5\big)\,. \tag{B.4}$$

Since we restrict ourselves to terms up to order six and the effective Hamiltonian is of second order, the energy expansion can be terminated after fourth order. Taking into

account the results from Ref. [11, 14], we can for our purposes also drop the third order term in this expansion. It cannot yield a non-constant contribution of at most order six. To obtain a plaquette term, *i.e.*, smallest cycle on the lattice, there has to occur at least one factor proportional to V^4 before a projection to the ground state space is applied. Therefore, we limit ourselves in the energy expansion to

$$E = \delta E^{(2)} + \delta E^{(4)} = \delta E\,. \tag{B.5}$$

The energy enters the effective Hamiltonian via the Green's functions. Those are approximated with the operator identity

$$\frac{1}{X-Y} = \frac{1}{X} + \frac{1}{X} Y \frac{1}{X-Y} \tag{B.6}$$

to

$$\begin{aligned} G_0(E) &= \frac{1}{H_{0+} - \delta E} = \frac{1}{H_{0+}} + \frac{1}{H_{0+}}\ \delta E\ \frac{1}{H_{0+} - \delta E} \\ &= \frac{1}{H_{0+}} + \frac{1}{H_{0+}}\ \delta E\ \frac{1}{H_{0+}} + \frac{1}{H_{0+}}\ \delta E\ \frac{1}{H_{0+}}\ \delta E\ \frac{1}{H_{0+} - \delta E} \\ &= \frac{1}{H_{0+}} + \frac{1}{H_{0+}}\ \delta E\ \frac{1}{H_{0+}} + \frac{1}{H_{0+}}\ \delta E\ \frac{1}{H_{0+}}\ \delta E\ \frac{1}{H_{0+}} + \mathcal{O}\big(V^6\big)\,. \end{aligned} \tag{B.7}$$

Inserting Eq. (B.5), we get up to fourth order

$$\begin{aligned} G_0(E) = \frac{1}{H_{0+}} + \frac{1}{H_{0+}}\ \delta E^{(2)}\ \frac{1}{H_{0+}} + \frac{1}{H_{0+}}\ \delta E^{(4)}\ \frac{1}{H_{0+}} + \\ + \frac{1}{H_{0+}}\ \delta E^{(2)}\ \frac{1}{H_{0+}}\ \delta E^{(2)}\ \frac{1}{H_{0+}} + \mathcal{O}\big(V^6\big)\,, \end{aligned} \tag{B.8}$$

where the last summand can be neglected as it cannot generate a plaquette term below order eight in the perturbation. For our purpose it therefore suffices to approximate the Green's function by

$$G_0(E) = \frac{1}{H_{0+}} + \frac{1}{H_{0+}}\ \delta E^{(2)}\ \frac{1}{H_{0+}} + \frac{1}{H_{0+}}\ \delta E^{(4)}\ \frac{1}{H_{0+}}\,. \tag{B.9}$$

To identify the relevant terms for the effective Hamiltonian, we will separately analyse different values of k in Eq. (B.3).

$$\begin{aligned} H_{\text{eff}}^{(k=0)} &= -V_{-+} G_0(E) V_{+-} = -V_{-+} \left[\frac{1}{H_{0+}} + \frac{1}{H_{0+}}\ \delta E^{(2)}\ \frac{1}{H_{0+}} + \frac{1}{H_{0+}}\ \delta E^{(4)}\ \frac{1}{H_{0+}} \right] V_{+-} \\ &= const - V_{-+} \frac{1}{H_{0+}}\ \delta E^{(4)}\ \frac{1}{H_{0+}} V_{+-} \\ &= const - \delta E^{(4)} V_{-+} G_0(0)^2 V_{+-}\,, \end{aligned} \tag{B.10}$$

where the first two terms only yield constants. For the terms $k \geq 1$ we can truncate the energy expansion after second order.

$$\begin{aligned}
H_{\text{eff}}^{(k=1)} &= -V_{-+}G_0(E)V_{++}G_0(E)V_{+-} \\
&= -V_{-+}\left[\frac{1}{H_{0+}} + \frac{1}{H_{0+}}\,\delta E^{(2)}\,\frac{1}{H_{0+}}\right]V_{++}\left[\frac{1}{H_{0+}} + \frac{1}{H_{0+}}\,\delta E^{(2)}\,\frac{1}{H_{0+}}\right]V_{+-} \\
&= -V_{-+}G_0(0)V_{++}G_0(0)V_{+-} - \left[\delta E^{(2)}\right]^2 V_{-+}G_0(0)^2V_{++}G_0(0)^2V_{+-} \\
&\quad - \delta E^{(2)}\left[V_{-+}G_0(0)^2V_{++}G_0(0)V_{+-} + V_{-+}G_0(0)V_{++}G_0(0)^2V_{+-}\right] \\
&= const
\end{aligned} \tag{B.11}$$

For $k = 1$ no term up to sixth order contains a connected fourth order term that enables a plaquette contribution to arise.

$$\begin{aligned}
H_{\text{eff}}^{(k=2)} &= -V_{-+}\left[G_0(0) + \delta E^{(2)}G_0(0)^2\right]V_{++}\left[G_0(0) + \delta E^{(2)}G_0(0)^2\right] \\
&\quad \cdot V_{++}\left[G_0(0) + \delta E^{(2)}G_0(0)^2\right]V_{+-} \\
&= \underbrace{-V_{-+}G_0(0)V_{++}G_0(0)V_{++}G_0(0)V_{+-}}_{= H_{\text{eff}}^{(M)}} \\
&\quad - \delta E^{(2)}V_{-+}G_0(0)\Big[G_0(0)V_{++}G_0(0)V_{++} + V_{++}G_0(0)^2V_{++} \\
&\qquad\qquad + V_{++}G_0(0)V_{++}G_0(0)\Big]G_0(0)V_{+-} + \mathcal{O}\big(V^8\big) \\
&= H_{\text{eff}}^{(M)} - \delta E^{(2)}V_{-+}G_0(0)M^2G_0(0)V_{+-} + \mathcal{O}\big(V^8\big)\,,
\end{aligned} \tag{B.12}$$

where M^2 is defined such that the last equality holds. We rewrite it with

$$\begin{aligned}
V_{++}G_0(0)V_{++}G_0(0) = [V_{++}G_0(0)V_{++}G_0(0)]^\dagger &= G_0(0)^\dagger V_{++}^\dagger G_0(0)^\dagger V_{++}^\dagger \\
&= G_0(0)V_{++}G_0(0)V_{++}
\end{aligned} \tag{B.13}$$

to find

$$M^2 = 2V_{++}G_0(0)V_{++}G_0(0) + V_{++}G_0(0)^2V_{++}\,, \tag{B.14}$$

since $G_0(0)$ and V_{++} are hermitian. For $k \geq 3$ we approximate $G_0(E) = G_0(E_0) = G_0(0)$.

$$H_{\text{eff}}^{(k=3)} = -V_{-+}G_0(0)\left[V_{++}G_0(0)\right]^3 V_{+-} \tag{B.15}$$

$$H_{\text{eff}}^{(k=4)} = -V_{-+}G_0(0)\left[V_{++}G_0(0)\right]^4 V_{+-} \tag{B.16}$$

We neglect terms for $k \geq 5$ as those only generate terms $\mathcal{O}(V^7)$. Collecting the results for different orders of k, we find

$$\begin{aligned} H_{\text{eff}} &= H_{\text{eff}}^{(k=0)} + H_{\text{eff}}^{(k=2)} + H_{\text{eff}}^{(k=3)} + H_{\text{eff}}^{(k=4)} \\ &= const + H_{\text{eff}}^{(M)} - \delta E^{(4)} V_{-+} G_0(0)^2 V_{+-} - \delta E^{(2)} V_{-+} G_0(0) M^2 G_0(0) V_{+-} \\ &\quad - V_{-+} G_0(0) \left[V_{++} G_0(0)\right]^3 V_{+-} - V_{-+} G_0(0) \left[V_{++} G_0(0)\right]^4 V_{+-} \,. \end{aligned} \tag{B.17}$$

Rearranging the expression into different orders of the perturbation V yields

$$H_{\text{eff}}^{(4)} = -V_{-+} G_0(0) V_{++} G_0(0) V_{++} G_0(0) V_{+-} \tag{B.18}$$

$$H_{\text{eff}}^{(5)} = -V_{-+} G_0(0) \left[V_{++} G_0(0)\right]^3 V_{+-} \tag{B.19}$$

$$\begin{aligned} H_{\text{eff}}^{(6)} &= -\delta E^{(4)} V_{-+} G_0(0)^2 V_{+-} - \delta E^{(2)} V_{-+} G_0(0) M^2 G_0(0) V_{+-} \\ &\quad - V_{-+} G_0(0) \left[V_{++} G_0(0)\right]^4 V_{+-} \,. \end{aligned} \tag{B.20}$$

These contributions are evaluated separately in Chapter 4.

C Sixth order calculation of the effective Hamiltonian

In this section, we will separately calculate the different contributions in sixth order to the effective Hamiltonian. The energy corrections δE are in general determined iteratively, such that the effective Hamiltonian cannot necessarily be written in a non-self-consistent form. In our case however, we will see that we are in a position to give such a closed form since the energy corrections are identical for all states in the ground state space. For the energy corrections we have

$$\delta E^{(4)} = \langle G | H_{\text{eff}}^{(4)} | G \rangle + const \,, \tag{C.21}$$

where $|G\rangle$ denotes an arbitrary, but fixed ground state. This term is combined with

$$V_{-+} G_0(0)^2 V_{+-} = V_{J,-+} G_0(0)^2 V_{J,+-} + V_{M,-+} G_0(0)^2 V_{M,+-} \,, \tag{C.22}$$

where mixed V_M, V_J combinations cannot bring the exited state back to the ground state such that those do not contribute.

$$\begin{aligned} V_{J,-+} G_0(0)^2 V_{J,+-} &= P_- \frac{1}{64} \frac{E_J^2}{E_C^2} \; N \; \mathbf{1} P_- = \frac{1}{64} \frac{E_J^2}{E_C^2} \; N \; \mathbf{1} \\ V_{M,-+} G_0(0)^2 V_{M,+-} &= P_- \frac{1}{4} \frac{E_M^2}{E_C^2} \; N \; \mathbf{1} P_- = \frac{1}{4} \frac{E_M^2}{E_C^2} \; N \; \mathbf{1} \end{aligned} \tag{C.23}$$

The $\mathbf{1}$ is a unity in the ground state space, such that this expression is only meaningful there. We also introduced N as the number of nodes in the system. Merging our results

in Equations (C.21) and (C.23) yields

$$-\delta E^{(4)} V_{-+} G_0(0)^2 V_{+-} = \left[\frac{5}{1024}\frac{E_M^4 E_J^2}{E_C^5} + \frac{5}{64}\frac{E_M^6}{E_C^5}\right] N \ \langle G|\sum_i \prod_{\square} \sigma^z |G\rangle \, \mathbf{1}\,, \tag{C.24}$$

where we neglected terms that do not yield the desired plaquette structure. As there is only one state dependent factor in the product we can in this case rewrite the expression in a non-iterative fashion

$$-\delta E^{(4)} V_{-+} G_0(0)^2 V_{+-} = \left[\frac{5}{1024}\frac{E_M^4 E_J^2}{E_C^5} + \frac{5}{64}\frac{E_M^6}{E_C^5}\right] N \ P_- \sum_i \prod_{\square} \sigma^z P_-\,. \tag{C.25}$$

The P_- indicates here that the expression actually is only to be evaluated for the ground state space. So we can restrict our Hilbert space and neglect the projections in the course of further calculations. Furthermore we find

$$\delta E^{(2)} = \delta E_M^{(2)} \ + \ \delta E_J^{(2)}\,, \qquad \text{with} \qquad \delta E_J^{(2)} = \langle G|V_{J,-+} G_0(0) V_{J,+-}|G\rangle\,. \tag{C.26}$$

These can be calculated to

$$\begin{aligned}
\delta E_J^{(2)} &= \langle G|V_{J,-+} G_0(0) V_{J,+-}|G\rangle = -\frac{1}{8}\frac{E_J^2}{E_C} N \langle G|\mathbf{1}|G\rangle = -\frac{1}{8}\frac{E_J^2}{E_C} N \\
\delta E_M^{(2)} &= \langle G|V_{M,-+} G_0(0) V_{M,+-}|G\rangle = -\frac{1}{2}\frac{E_M^2}{E_C} N \langle G|\mathbf{1}|G\rangle = -\frac{1}{2}\frac{E_M^2}{E_C} N\,.
\end{aligned} \tag{C.27}$$

Note that $\delta E_J^{(2)}$ and $\delta E_M^{(2)}$ are actually invariant for all states in the ground state space. Additionally we obtain

$$\begin{aligned}
V_{-+} G_0(0) M^2 G_0(0) V_{+-} &= const + V_{M,-+} G_0(0) M_M^2 G_0(0) V_{M,+-} \\
&= const + \frac{29}{64}\frac{E_M^4}{E_C^4} \ P_- \sum_i \prod_{\square} \sigma^z P_-\,.
\end{aligned} \tag{C.28}$$

Only the term involving V_M^4 can give a plaquette contribution. The remaining ones are included in the constant. Combining Equations (C.27) and (C.28) results in

$$-\delta E^{(2)} V_{-+} G_0(0) M^2 G_0(0) V_{+-} = const + \left[\frac{58}{1024}\frac{E_M^4 E_J^2}{E_C^5} + \frac{29}{128}\frac{E_M^6}{E_C^5}\right] N \ P_- \sum_i \prod_{\square} \sigma^z P_- \tag{C.29}$$

The last contribution to the effective Hamiltonian

$$-\, V_{-+} G_0(0) \left[V_{++} G_0(0)\right]^4 V_{+-} \tag{C.30}$$

can be split into multiple parts. First the Cooper pair or additional single electron can go back and forth on a link that is part of the plaquette, second it can move on a link

sharing one node with the plaquette and third it can move on a disconnected link. Two Cooper pairs can hop on different links of the plaquette, partially cancelled by single electron hoppings analogously to the fifth order contribution. All of those lead to a plaquette contribution and the calculations yield

$$\begin{aligned}
&[-V_{-+}G_0(0)\,[V_{++}G_0(0)]^4\,V_{+-}]_{\text{plaquette}} \\
&\quad = const - \left[\frac{11}{32}+\frac{353}{216}+\frac{39}{128}(N-6)\right]\frac{E_M^6}{E_C^5}\sum_i\prod_{\square}\sigma^z \\
&\qquad - \left[\frac{45415}{225792}+\frac{656053}{23708288}+\frac{123022}{521525}+\frac{63}{1024}(N-6)\right]\frac{E_M^4E_J^2}{E_C^5}\sum_i\prod_{\square}\sigma^z \\
&\quad = -\left[\frac{259}{1728}+\frac{39}{128}N\right]\frac{E_M^6}{E_C^5}\sum_i\prod_{\square}\sigma^z \\
&\qquad - 0,09556\frac{E_M^4E_J^2}{E_C^5}\sum_i\prod_{\square}\sigma^z - \frac{63}{1024}N\,\frac{E_M^4E_J^2}{E_C^5}\sum_i\prod_{\square}\sigma^z\,. \qquad \text{(C.31)}
\end{aligned}$$

Combining this result with Equations (C.25) and (C.29), the extensive N dependent terms cancel to give

$$H_{\text{eff}}^{(6,1)} = -\left[\frac{259}{1728}\frac{E_M^6}{E_C^5}+0,09556\frac{E_M^4E_J^2}{E_C^5}\right]\sum_i\prod_{\square}\sigma^z\,. \qquad \text{(C.32)}$$

Besides the plaquette contribution, we find a term involving adjacent plaquettes with

$$H_{\text{eff}}^{(6,2)} = -\frac{63}{256}\frac{E_M^6}{E_C^5}\sum_i\Big(\prod_{\square\square}\sigma^z+\prod_{\substack{\square\\\square}}\sigma^z\Big)\,. \qquad \text{(C.33)}$$

The implications of these terms are discussed in Sec. 4.1.4.

D The Anderson-Higgs mechanism

In this section, we analyse the symmetry breaking mechanism that leads to a Higgs phase. We there realise why the Higgs mechanism should not be referred to as a spontaneous symmetry breaking of a local gauge symmetry. The system we consider is the same as in Section 4.2.2. For convenience it is again depicted in Fig. D.1.

There are $\mathbb{Z}_2$ gauge fields σ_{ij} placed on the links of a two dimensional square lattice and $\mathbb{Z}_2$ DOF located on the nodes. Thus, the matter fields have a $\mathbb{Z}_2$ charge with which they couple to the gauge fields. The full Hamiltonian of this system is the lattice gauge theory

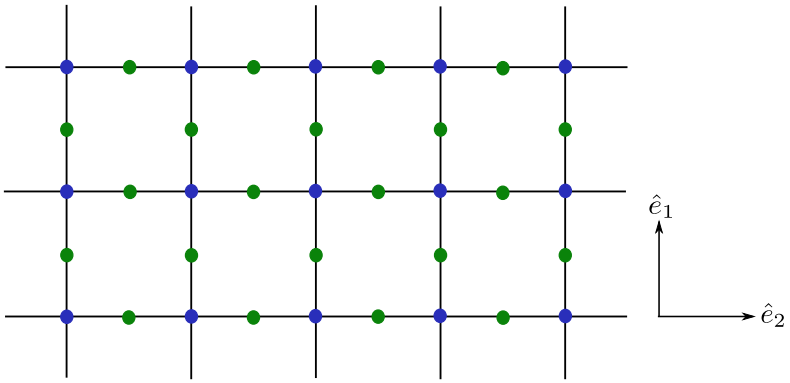

Figure D.1: Sketch of the two dimensional square lattice, with $\mathbb{Z}_2$ gauge DOF σ_{ij} (green dots) placed centrally on the links and $\mathbb{Z}_2$ matter fields τ_i (blue dots) on the nodes. This system can realise a $\mathbb{Z}_2$ lattice gauge theory with $\mathbb{Z}_2$ matter (Higgs) fields.

of Ising gauge coupled to Ising matter [20] again as in Section 4.2.2.

$$H = -\Delta \sum_i \prod_\square \sigma^z - \frac{1}{\Delta} \sum_{<i,j>} \sigma^x_{ij} \\ - \lambda \sum_{<i,j>} \tau^z_i \sigma^z_{ij} \tau^z_j - \frac{1}{\lambda} \sum_i \tau^x_i \,, \tag{D.34}$$

$$\text{with} \quad Q_i \,|\text{phys}\rangle = |\text{phys}\rangle \,, \qquad \text{where} \quad Q_i = \tau^x_i \prod_+ \sigma^x \,. \tag{D.35}$$

For a discussion of the different terms see Sec. 4.2. The local symmetry in Eq. (D.35) satisfies Elitzur's theorem and can thus not be spontaneously broken [40].

The phase diagram of this model was explored in Ref. [41] and found to contain a Higgs phase. We define a Higgs phase to be present if the scalar matter field τ_i, also referred to as the Higgs field, obtains a non-vanishing ground state expectation value $m_i{}' = \langle G'|\tau^z_i|G'\rangle$. The question now arises, how the local operator can have a non-zero expectation m'_i, if there is the local gauge symmetry in Eq. (D.35). It is often concluded that the Higgs mechanism spontaneously breaks this local gauge symmetry, which we know from Elitzur's theorem to be impossible.

To solve this problem we reproduce explicitly the existence of a Higgs phase in the model in Eq. (D.34).[1] Initially, we realise that the local gauge symmetry also results in a global $\mathbb{Z}_2$ gauge symmetry

$$\mathcal{Q} = \prod_i Q_i = \prod_i \tau^x_i \,. \tag{D.36}$$

[1] The treatment outlined here was inspired by a talk of Jörg Schmalian at the DPG Summer School 2018 on "Gauge Theory and Topological Quantum Matter".

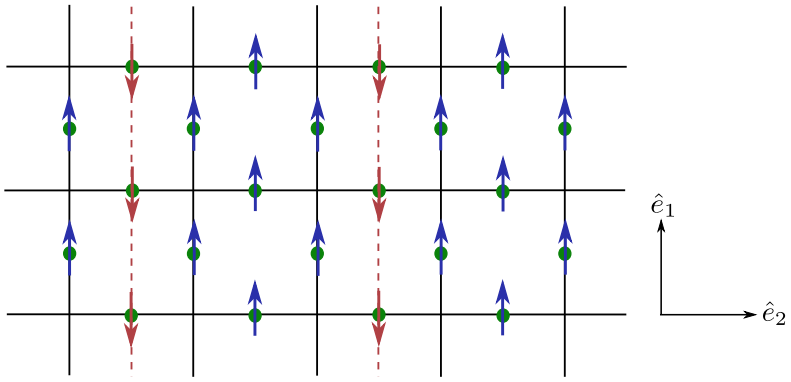

Figure D.2: Schematic of the two dimensional square lattice with spin DOF on the links. The spins in $\hat{e}_1$-direction are gauged into the $+1$ eigenstate of σ^z_{ij} and plaquettes cannot be frustrated. This has the effect that only closed lines on the dual lattice (red dashed lines) possibly are in the -1 eigenstate (red arrows).

Taking the $\Delta \to \infty$ limit of Eq. (D.34), we find

$$H' = -\lambda \sum_{<i,j>} \tau^z_i \sigma^z_{ij} \tau^z_j - \frac{1}{\lambda} \sum_i \tau^x_i \,, \tag{D.37}$$

$$\text{with} \qquad Q_i = \tau^x_i \prod_+ \sigma^x \,. \tag{D.38}$$

Additionaly, there is the constraint $\prod_\square \sigma^z = 1$, *i.e.*, no plaquette is frustrated. In combination with the gauge constraint one finds that it is possible to choose a gauge for the system such that all σ_{ij} are in the $+1$ eigenstate of σ^z_{ij}. The easiest way to see this is to first choose a gauge, where $\sigma^z_{ij} = 1$ only for the links in $\hat{e}_1$-direction. This can be done despite a specific parameter choice. The fact that no frustrated plaquettes can appear then only allows for spins on closed lines on the dual lattice to be in the $\sigma^z_{ij} = -1$ state. This situation is sketched in Fig. D.2, where only the gauge fields are explicitly depicted for clarity.

These closed lines in turn can then be gauged away using Eq. (D.35). After applying this gauge choice, the model is given by

$$H' = -\lambda \sum_{<i,j>} \tau^z_i \tau^z_j - \frac{1}{\lambda} \sum_i \tau^x_i \,. \tag{D.39}$$

This is the quantum Ising model known from Sec. 4.2.1, which only remains with the global gauge symmetry $\mathcal{Q}$. The ground state $|G'\rangle$ of this model breaks this global symmetry spontaneously for the case of $\lambda \to \infty$. Thus, we find ourselves in the Higgs phase with $m'_i = \langle G'|\tau^z_i|G'\rangle \neq 0$. This ground state $|G'\rangle$ does not respect the gauge symmetry in Eq. (D.35), but neither is it expected to. It is the ground state of H' in Eq. (D.39), which is only valid under a specific gauge choice of H in Eq. (D.34). The local gauge symmetry was not broken spontaneously at any point, only the global gauge symmetry

$\mathcal{Q}$. To obtain the ground state of H, which has to be gauge invariant, one can take the equal weight superposition of all the possible gauge transformations applied to the ground state $|G'\rangle$. This yields

$$|G\rangle = \prod_i \frac{1}{\sqrt{2}} (1 + Q_i) |G'\rangle \ , \quad \text{with} \quad Q_i = \tau_i^x \prod_+ \sigma^x \, . \tag{D.40}$$

Notably, the constraint that there are no frustrations present, is only obtained in the $\Delta = \infty$ limit. In Ref. [41], however, it is shown that this phase exists also for large but finite values of Δ.

In conclusion, we found that in a specific gauge choice, the charged matter field, *i.e.*, Higgs field, obtains a non-vanishing ground state expectation value. In that case it spontaneously breaks the global $\mathbb{Z}_2$ gauge symmetry. Elitzur's theorem is never violated. To obtain the ground state of the system with local gauge symmetry, one has to take the equal weight superposition of all possible local gauge transformations applied to the solution of the gauge fixed model. This procedure analogously can be generalised for different gauge fields or matter charges, for example in superconductivity.

E Isotropy of the Majorana toric code

In this section the equivalence of the three dimensional classical model with the action

$$S_{cl} = -J \sum_{\mu,\nu} \sigma^z_{\mu,\mu+\hat{e}_\nu} \cos\left(\frac{\phi_\mu - \phi_{\mu+\hat{e}_\nu}}{2}\right) - K \sum_{\mu,\nu} \cos\left(\phi_\mu - \phi_{\mu+\boldsymbol{e}_\nu}\right) \tag{E.41}$$

to the model of the Majorana toric code is shown. The treatment is structured analogous to the mapping of the three dimensional Ising gauge model in Ref. [21]. The index μ runs over all lattice sites in a three dimensional square lattice. The vectors $\hat{e}_\nu$ run over the three conventional basis vectors of the lattice. We choose one arbitrary direction to be the imaginary time direction. Notably, the description in Eq. (E.41) is isotropic, such that every choice of temporal direction is equivalent. Latin indices will in the following denote the summation only over the spatial dimensions. The first step is the introduction of temporal coupling constants J_τ, K_τ.

$$\begin{aligned} S_{cl} = &-J_\tau \sum_{\mu} \sigma^z_{\mu,\mu+\hat{e}_\tau} \cos\left(\frac{\phi_\mu - \phi_{\mu+\hat{e}_\tau}}{2}\right) - K_\tau \sum_{\mu} \cos\left(\phi_\mu - \phi_{\mu+\hat{e}_\tau}\right) \\ &- J \sum_{\mu,j} \sigma^z_{\mu,\mu+\hat{e}_j} \cos\left(\frac{\phi_\mu - \phi_{\mu+\hat{e}_j}}{2}\right) - K \sum_{\mu,j} \cos\left(\phi_\mu - \phi_{\mu+\hat{e}_j}\right) \end{aligned} \tag{E.42}$$

It is important to note that the system has a local symmetry. It is invariant under a flip of all spins emanating from a site μ, while one simultaneously rotates $\phi \to \phi + 2\pi$. This

can be readily seen as

$$\begin{aligned} \sigma^z_{\mu,\mu+\hat{e}_\nu} \cos\left(\frac{\phi_\mu - \phi_{\mu+\hat{e}_\nu}}{2}\right) \quad &\longrightarrow \quad -\sigma^z_{\mu,\mu+\hat{e}_\nu} \cos\left(\frac{\phi_\mu - \phi_{\mu+\hat{e}_\nu}}{2} + \pi\right) \\ &= \sigma^z_{\mu,\mu+\hat{e}_\nu} \cos\left(\frac{\phi_\mu - \phi_{\mu+\hat{e}_\nu}}{2}\right) \end{aligned}$$

$$\begin{aligned} \text{and} \qquad \cos\left(\phi_\mu - \phi_{\mu+\hat{e}_\nu}\right) \quad &\longrightarrow \quad \cos\left(\phi_\mu - \phi_{\mu+\hat{e}_\nu} + 2\pi\right) \\ &= \cos\left(\phi_\mu - \phi_{\mu+\hat{e}_\nu}\right) . \end{aligned} \tag{E.43}$$

It is just another way to phrase the gauge constraint that has to be imposed on the system. We can therefore choose the temporal gauge, where $\sigma^z_{\mu,\mu+\hat{e}_\tau} = 1$. Inserting the gauge choice and rewriting the action up to a constant gives

$$\begin{aligned} S_{cl} = J_\tau \sum_\mu \left[1 - \cos\left(\frac{\phi_\mu - \phi_{\mu+\hat{e}_\tau}}{2}\right)\right] + K_\tau \sum_\mu \left[1 - \cos\left(\phi_\mu - \phi_{\mu+\hat{e}_\tau}\right)\right] \\ - J \sum_{\mu,j} \sigma^z_{\mu,\mu+\hat{e}_j} \cos\left(\frac{\phi_\mu - \phi_{\mu+\hat{e}_j}}{2}\right) - K \sum_{\mu,j} \cos\left(\phi_\mu - \phi_{\mu+\hat{e}_j}\right) . \end{aligned} \tag{E.44}$$

Furthermore, we set $J_\tau = 4K_\tau$, where the four is only included for convenience. Then if we take the anisotropic limit $K_\tau \to \infty$, the ϕ_μ can be assumed to vary only slowly in time direction, which allows for the approximations

$$\begin{aligned} 1 - \cos\left(\frac{\phi_\mu - \phi_{\mu+\hat{e}_\tau}}{2}\right) &\approx \frac{1}{2}\left(\frac{\phi_\mu - \phi_{\mu+\hat{e}_\tau}}{2}\right)^2 \\ &= \frac{1}{8}\left(\phi_\mu - \phi_{\mu+\hat{e}_\tau}\right)^2 \\ &\approx \frac{1}{8}\tau^2 \left(\partial_\tau \phi_\mu\right)^2 \\ \text{and analogously} \qquad 1 - \cos\left(\phi_\mu - \phi_{\mu+\hat{e}_\tau}\right) &\approx \frac{1}{2}\tau^2 \left(\partial_\tau \phi_\mu\right)^2 , \end{aligned} \tag{E.45}$$

where τ denotes the lattice spacing in time direction. Furthermore we can identify

$$\sum_{\mu,j} \quad \longrightarrow \quad \int \mathrm{d}\tau' \frac{1}{\tau} \sum_{i,j} \tag{E.46}$$

The summation now runs exclusively over the spatial lattice at a given time step. With that we can write

$$\begin{aligned} S_{cl} = \int \mathrm{d}\tau' \Bigg[& 4K_\tau \tau \frac{1}{8} \sum_i \left(\partial_\tau \phi_i\right)^2 + K_\tau \tau \frac{1}{2} \sum_i \left(\partial_\tau \phi_i\right)^2 \\ & - J \frac{1}{\tau} \sum_{i,j} \sigma^z_{i,i+\hat{e}_j} \cos\left(\frac{\phi_i - \phi_{i+\hat{e}_j}}{2}\right) - K \frac{1}{\tau} \sum_{i,j} \cos\left(\phi_i - \phi_{i+\hat{e}_j}\right) \Bigg] \\ = \int \mathrm{d}\tau' \Bigg[& K_\tau \tau \sum_i \left(\partial_\tau \phi_i\right)^2 - J \frac{1}{\tau} \sum_{i,j} \sigma^z_{i,i+\hat{e}_j} \cos\left(\frac{\phi_i - \phi_{i+\hat{e}_j}}{2}\right) \\ & - K \frac{1}{\tau} \sum_{i,j} \cos\left(\phi_i - \phi_{i+\hat{e}_j}\right) \Bigg] . \end{aligned} \tag{E.47}$$

Additionally, we define appropriate constants such that the continuum limit can be taken in a well defined manner. So for $\tau \to 0$ we set

$$K_\tau = \frac{4E_C}{\tau} \to \infty \quad , \quad J = \tau E_M \to 0 \quad , \quad K = \tau E_J \to 0 \,, \tag{E.48}$$

with E_C, E_M, E_J being constants. We introduce the conjugate momentum n_i to the phase variables ϕ_j as

$$[n_i, \phi_j] = i\delta_{ij} \,. \tag{E.49}$$

Where n_i, ϕ_j are now operators. This yields

$$S_{cl} = \int \mathrm{d}\tau' \left[4E_C \sum_i n_i^2 - E_M \sum_{i,j} \sigma^z_{i,i+\hat{e}_j} \cos\left(\frac{\phi_i - \phi_{i+\hat{e}_j}}{2}\right) - E_J \sum_{i,j} \cos\left(\phi_i - \phi_{i+\hat{e}_j}\right) \right] , \tag{E.50}$$

where the transfer matrix formulation gives us the τ-continuum quantum Hamiltonian [21] for the Majorana toric code, if we return to the notation of spatial nearest neighbouring site i and j as $< i, j >$

$$H_{MTC} = 4E_C \sum_i n_i^2 - E_M \sum_{<i,j>} \sigma^z_{i,j} \cos\left(\frac{\phi_i - \phi_j}{2}\right) - E_J \sum_{<i,j>} \cos\left(\phi_i - \phi_j\right) . \tag{E.51}$$

This is the Majorana toric code model as discussed in this thesis.

Acknowledgements

First of all, I want to thank my parents for making my whole study experience possible. Without your support this would have been considerably harder. I also want to thank my sister Katharina for all the love and encouragement I received over the years.

I am deeply thankful to my partner Svenja who managed to make me smile even through the more stressful times of the last year and on whos love and support I could always count on.

Special thanks go out to my supervisors Fabian Hassler and Ananda Roy. Working with you was a pleasure. Your motivation and guidance fueled my passion for physics and made me a better scientist.

Furthermore, I am grateful to all the people at the IQI for creating this nice working environment. I want to thank Benedikt, Evangelos, Martin and Tobias for all the hours we spent in the office discussing physics and non-physics problems.

I am grateful to David DiVincenzo to be my co-supervisor and hosting the weekly group meeting. Lastly, I thank Benedikt, Fabian, Martin, Niklas, Stefan and Svenja for taking the time to proof read this thesis. Whereas I need to thank Evangelos for facilitating the fancy torus figures.

Bibliography

[1] P. W. Shor, Algorithms for quantum computation: discrete logarithms and factoring, in *Proceedings 35th Annual Symposium on Foundations of Computer Science*, pages 124–134, 1994.

[2] R. L. Rivest, A. Shamir, and L. Adleman, Commun. ACM **21**, 120 (1978).

[3] D. Loss and D. P. DiVincenzo, Phys. Rev. A **57**, 120 (1998).

[4] A. Shnirman, G. Schön, and Z. Hermon, Phys. Rev. Lett. **79**, 2371 (1997).

[5] J. Koch *et al.*, Phys. Rev. A **76**, 042319 (2007).

[6] D. Gottesman, Phys. Rev. A **54**, 1862 (1996).

[7] E. Dennis, A. Kitaev, A. Landahl, and J. Preskill, J. Math. Phys. **43**, 4452 (2002).

[8] A. Kitaev, Annals of Physics **303**, 2 (2003).

[9] P. W. Anderson, Science **177**, 393 (1972).

[10] C. Xu and L. Fu, Phys. Rev. B **81**, 134435 (2010).

[11] B. M. Terhal, F. Hassler, and D. P. DiVincenzo, Phys. Rev. Lett. **108**, 260504 (2012).

[12] A. Roy, B. M. Terhal, and F. Hassler, Phys. Rev. Lett. **119**, 180508 (2017).

[13] A. Roy and F. Hassler, Phys. Rev. B **97**, 024512 (2018).

[14] L. A. Landau *et al.*, Phys. Rev. Lett. **116**, 050501 (2016).

[15] F. J. Wegner, Journal of Mathematical Physics **12**, 2259 (1971).

[16] K. Fredenhagen and M. Marcu, Phys. Rev. Lett. **56**, 223 (1986).

[17] J. L. Park, Foundations of Physics **1**, 23 (1970).

[18] W. K. Wootters and W. H. Zurek, Nature **299**, 802 (1982).

[19] E. Knill, R. Laflamme, and W. H. Zurek, Proc. Roy. Soc. Lond. **A454**, 365 (1998).

[20] E. Fradkin, *Field Theories of Condensed Matter Physics*, Cambridge University Press, 2 edition, 2013.

[21] J. B. Kogut, Rev. Mod. Phys. **51**, 659 (1979).

[22] K. Gregor, D. A. Huse, R. Moessner, and S. L. Sondhi, New J. Phys. **13**, 025009 (2011).

[23] E. Majorana, Il Nuovo Cimento **14**, 171 (1937).

[24] M. Leijnse and K. Flensberg, Semicond. Sci. Tech. **27**, 124003 (2012).

[25] R. M. Lutchyn *et al.*, Nature Reviews Materials **3**, 52 (2018).

[26] A. Y. Kitaev, Physics-Uspekhi **44**, 131 (2001).

[27] F. Wilczek, Nature Physics **5**, 614 EP (2009).

[28] J. Alicea, Y. Oreg, G. Refael, F. von Oppen, and M. P. A. Fisher, Nature Physics **7**, 412 EP (2011).

[29] A. Stern, Nature **464**, 187 (2010).

[30] V. Mourik *et al.*, Science **336**, 1003 (2012).

[31] J. R. Williams *et al.*, Phys. Rev. Lett. **109**, 056803 (2012).

[32] L. Fu, Phys. Rev. Lett. **104**, 056402 (2010).

[33] J. Alicea, Reports on Progress in Physics **75**, 076501 (2012).

[34] A. Y. Kitaev, Russian Mathematical Surveys **52**, 1191 (1997).

[35] E. Cobanera, G. Ortiz, and Z. Nussinov, Adv. Phys. **60**, 679 (2011).

[36] Z. Nussinov, G. Ortiz, and E. Cobanera, Phys. Rev. B **86**, 085415 (2012).

[37] I. Hubac and S. Wilson, *Brillouin-Wigner Methods for Many-Body Systems*, volume 21, Springer, 2009.

[38] R. Winkler, *Spin-Orbit Coupling Effects in Two-Dimensional Electron and Hole Systems*, Springer, 2003.

[39] S. Bravyi, D. P. DiVincenzo, and D. Loss, Annals of Physics **326**, 2793 (2011).

[40] S. Elitzur, Phys. Rev. D **12**, 3978 (1975).

[41] E. Fradkin and S. H. Shenker, Phys. Rev. D **19**, 3682 (1979).

[42] M. P. A. Fisher, P. B. Weichman, G. Grinstein, and D. S. Fisher, Phys. Rev. B **40**, 546 (1989).

[43] S. Sachdev, *Quantum phase transitions*, Cambridge University Press, 2011.

[44] B. van Heck, E. Cobanera, J. Ulrich, and F. Hassler, Phys. Rev. B **89**, 165416 (2014).

[45] L. D. and E. M. Lifshitz, *Quantum Mechanics, Non-Relativistic Theory*, volume 3 of *Course of Theoretical Physics*, Pergamon Press, London, 1958.